Příloha 9.1

Cytometry Part B (Clinical Cytometry) 92B:380–389 (2017)

Original Article

Appearance of Cytomegalovirus-Specific T-Cells Predicts Fast Resolution of Viremia Post Hematopoietic Stem Cell Transplantation

Ondrej Pelak,[1,2] Jan Stuchly,[1,2] Ladislav Krol,[1,2] Petr Hubacˇek,[1] Petra Keslova,[1] Petr Sedlacˇek,[1] Renata Formankova,[1] Jan Stary,[1] Ondrej Hrusak,[1,2] and Tomas Kalina[1,2]*

[1]Department of Pediatric Hematology and Oncology, 2nd Faculty of Medicine, Charles University Prague and University Hospital Motol, V Uvalu 84, Prague, 150 06, Czech Republic

[2]CLIP–Childhood Leukemia Investigation Prague, 2nd Faculty of Medicine, Charles University Prague

Background: Cytomegalovirus (CMV) specific T-cells are known to provide long-term control of CMV reactivation, which is a frequent complication of hematopoietic stem cell transplantation. We have stud-ied 58 pediatric patients after hematopoietic stem cell transplantation who suffered from CMV reactiva-tion to reveal which functional T cell subset is best correlating with successful reactivation resolution and which protects from reactivation episode.

Methods: Detection of 30 combinatorial subsets of four types of response to ex vivo CMV stimulation (IFNg secretion, IL-2 secretion, CD40L upregulation and degranulation) that were detectable on either CD81 or CD41 T cells through flow cytometry intracellular cytokine staining was used.

Results: We found that the presence of CD81 dual positive (IFNg1 and IL-21) cells is the most accu-rate functional parameter that can predict fast resolution of CMV reactivation. Next, we show that the presence of CD81 dual positive (IFNg1 and IL-21) and CD81 IFNg1 cells provides a protective effect (a hazard risk of 0.28 (confidence interval 0.18 – 0.43) and 0.45 (CI 0.27 – 0.75), respectively) and the presence of corticotherapy increases the risk of reactivation (HR 2.47 (CI 1.82-3.36)). Thus, a patient without corticotherapy and with both of the critical T cell subsets present has a cumulative 19.6 times lower risk of developing CMV reactivation than a patient on corticotherapy and without CD81 dual positive (IFNg1 and IL-21) or CD81 IFNg1 cells.

Conclusions: We have established parameters of CMV specific functional response ex vivo that can be used in assisting clinical management of patients with CMV reactivation. Vc **2015 International Clinical Cytometry Society**

Key terms: cytomegalovirus; bone marrow transplantation; T-cells; immune reconstitution; flow cytometry

How to cite this article: Pelak O, Stuchly J, Krol L, Hubacˇek P, Keslova P, Sedlacˇek, P, Formankova R, Stary J, Hrusak O and Kalina T. Appearance of Cytomegalovirus-Specific T-Cells Predicts Fast Resolution of Viremia Post Hematopoietic Stem Cell Transplantation. Cytometry Part B 2017; 92B: 380–389.

INTRODUCTION

Viral infections after allogeneic hematopoietic stem cell transplantation (HSCT) are currently one of the major causes of morbidity and mortality. Cytomegalovirus (CMV) reactivation is a common infectious complication in secondary immunodeficient patients due to impaired T-cell mediated immunity (1), and progression to CMV disease is often fatal. Therefore, sensitive screening meth-ods were established for monitoring the CMV viral load in patients after HSCT (2,3) to enable timely pre-emptive antiviral treatment, before the onset of CMV disease.

Additional Supporting Information may be found in the online version of this article.

*Correspondence to: Tomas Kalina, Department of Pediatric Hematology and Oncology, 2nd Faculty of Medicine, Charles University Prague and University Hospital Motol, V Uvalu 84, 150 06 Prague 5, Czech Republic. E-mail: tomas.kalina@lfmotol.cuni.cz. T.K. was supported as an “ISAC Scholar” by International Society for Advancement of Cytometry. Grant sponsor: Czech Science Foundation (Grant number: 13-22777S). Grant sponsor: GAUK 376214.

Received 19 October 2015; Revised 11 November 2015; Accepted 1 December 2015

Published online 8 December 2015 in Wiley Online Library (wileyonlinelibrary.com).

DOI: 10.1002/cyto.b.21348

However, pre-emptive treatment leads to overtreatment of patients with spontaneous ability to control CMV reactivation by reconstituting CMV specific T-cells (4). Such an overtreatment can have negative sequels. First, antiviral drugs have significant marrow (ganciclovir, valganciclovir and cidofovir) and renal (foscarnet and cidofovir) toxicities (5,6). Second, ganciclovir can exhibit a T-cell proliferation suppressive effect (7). Third, evidence exists showing that viremia induces a CMV specific T-cell response that can potentiate beneficial anti-leukemia effects (8–10) and enhance T-cell reconstitution (11). Ideally, therapeutic interventions should ensure that patients with a risk of progression towards CMV disease are given antiviral treatment, patients with poor response are directed for T-cell therapy, and patients with adequate spontaneous CMV response are not burdened with unnecessary antivirotics and their side effects. This approach requires knowledge about the protective potential of patients' anti-CMV cellular response together with the kinetics of the CMV viral load. Controversy exists about the role of CD4 (12) versus CD8 T-cells [evidenced by observational (13–15) and also adoptive transfer studies (16–18)] in protection from CMV reactivation. Some studies show that both CD4 and CD8 T-cells must be present (19). We (13) and Lilleri (20) have shown that CD8 T-cells producing both IFNg and IL-2 in response to ex vivo CMV antigen stimulation are found in the majority of CMV reactivation controlling patients, whereas they are missing in CMV non-controlling patients. Other studies investigated the presence of CMV multimer positive CD8 T-cells, as detected by MHC multimer staining (21,22), or IFNg producing T-cells (14,15) and found a correlation with protection from CMV reactivation. Graft versus host disease and/or its treatment has negative impacts on the CMV control (19,23). Recently, the kinetic interplay between CMV DNAemia and CMV specific T-cells was investigated, showing that kinetic relationships, rather than static values at fixed time points, may offer a better tool for outcome prediction (24,25).

Here, we summarize our findings of 6 years of CMV specific T cells functional testing in a pediatric cohort of patients, where only limited data are available so far. First, we aim at finding the most accurate and specific prediction of short-lasting reactivation, among measured CD81 and CD41 CMV specific T cells, that would not necessitate antivirotic treatment beyond pre-emptive ganciclovir. Second, we investigate whether the thus defined CMV specific T cell subsets responsible for short duration of reactivation also contribute to prevention of CMV reactivation during the post-transplant period in a multivariate Cox regression hazard risk model.

METHODS

Patients

Fifty eight patients (undergoing 60 transplants) who experienced CMV reactivation after allogeneic HSCT (of a total of 230 patients transplanted between January 2008 and August 2014) aged 0–19 years were included in the study. Twenty one patients were reported on in our previous study, albeit with different endpoint(13). The conditioning regimens and GvHD prophylaxis were different according to the diagnosis, age, and the treatment protocols (Table 1). Ethical approval for this study was obtained from the University Hospital Motol Institutional Review Board. All patients provided informed con-sent according to the Helsinki Declaration.

Table 1
Patients' Characteristics

Patients followed after HSCT	230
Patients (unique transplants) with repeated CMV reactivation under study	58 (60)
Age median (range)	8.6 (0.2 2 19.9)
Gender	
Male	37 (63.8%)
Female	21 (36.2%)
CMV serostatus:	
Recipient CMV-seropositive/ Donor CMV-seronegative	34 (56.7%)
Recipient CMV-seropositive/ Donor CMV-seropositive	22 (36.7%)
Recipient CMV-seronegative/ Donor CMV-seronegative	1 (1.7%)
Recipient CMV-seronegative/ Donor CMV-seropositive	3 (5.0%)
Disease	
Acute lymphoblastic leukemia	14 (24.1%)
Acute myelogenous leukemia	9 (16.7%)
Myelodysplastic syndrome	11 (19.0%)
Other	24 (41.7%)
Donor type	
Matched related	6 (10.0%)
Matched unrelated	49 (81.7%)
Mismatch unrelated	5 (8.3%)
Stem cell source	
BM	29 (48.3%)
PBSC	25 (41.7%)
Umbilical blood	6 (10.0%)
Conditioning regimen	
Myeloablative	39 (65.0.%)
Non-myeloablative	21 (35.0%)
Acute GVHD incidence	
Grades I-II	29 (48.3%)
Grades III-IV	5 (8.3%)
Chronic GVHD incidence	
Limited	6 (10.0%)
Extensive	17 (28.3%)

Conditioning

In vivo T-cell depletion by rabbit anti-human thymocyte globulin or alemtuzumab monoclonal antibody were used in most unrelated HSCT. Patients were nursed in high efficiency particulate air (HEPA)-filtered rooms. All blood products were irradiated and leukocyte depleted. Pneumocystis jiroveci pneumonitis prophylaxis (trimetoprim-sulfometoxazol) was used in all patients until 1 year after HSCT. Antifungal prophylaxis was administered during the periods of cytopenia until hematological engraftment. Acyclovir or valacyclovir was used until 1 year after transplant. All prophylactic drugs were administered longer in the case of GvHD requiring systemic immunosuppressive therapy. No selective intestinal decontamination was used routinely. Intravenous immunoglobulin (IVIG) at a dose of

200 mg/kg was infused every 1–2 weeks until full recov-ery of humoral immunity.

CMV Monitoring and Pre-emptive Therapy

Monitoring of the CMV viral loads in the whole blood was performed on a weekly basis using real-time quantitative PCR. The viral loads were normalized to 10,000 human genomic equivalents obtained by quantification of the albumin gene(3,26). PCR monitoring was started on day 1 7 after HSCT and was performed weekly until 3 months after HSCT. Afterwards it was performed every 2–3 weeks until 6 months after transplant and once a month until 1 year after transplant thereafter. The moni-toring scheme was intensified individually during reacti-vation or during continuous high immunosuppressive therapy in cases of GvHD. Pre-emptive therapy with ganciclovir was started (after myeloid engraftment) whenever the normalized viral load exceeded 100 copies or at lower viremia in patients with symptoms suggestive of CMV disease.

Patients were treated with i.v. ganciclovir (5 mg/kg twice a day) for 2 weeks. A maintenance dose of i.v. ganciclovir (5 mg/kg/day) or p.o. valganciclovir (900 mg/m^2/day) was administered for an additional 1–2 weeks. Pre-emptive therapy was discontinued after a negative PCR result or a decrease in the viral load below 100 copies and no further increase in a 2-week follow-up period. Foscarnet i.v. (60 mg/kg twice a day) was added to the therapy schedule or was used to replace ganciclovir or valganciclovir when the viral load continued to be clinically significant beyond the third week of treatment or when a significant increase of the viral load was documented during the administration of the full dose of ganciclovir. Foscarnet was used as the first-line pre-emptive therapy during the period of aplasia in the first weeks after transplant. Resistance to ganciclovir was tested in patients who failed to respond to therapy with i.v. ganciclovir.

GvHD Prophylaxis and Treatment

After allo-HSCT, all the patients were administered cyclo-sporine A (CsA) usually in combination with methotrexate or mycophenolatemofetil as a prophylaxis of acute GvHD (aGvHD). The drug doses were reduced after the second or third month after transplantation with respect to chimer-ism status, disease status, and any evidence of aGvHD. Patients with aGvHD were treated with methylpredniso-lone (1–2 mg/kg/day). Samples for CMV specific T-cell functional tests taken in periods when prednisone was administered were analyzed separately and coded “GC”.

Definitions of “Slow-Responding” CMV Viremia and “Well-Responding” CMV Viremia

A CMV viremia lasting for up to 14 days on pre-emptive ganciclovir treatment followed by maintenance treatment discontinuation within 2 weeks was regarded as “well-responding” viremia (with no recurrence of viremia dur-ing maintenance).The CMV viremia lasting for >14 days was regarded as “slow-responding” viremia. We character-ized each reactivation episode by median response in each functional subset. In “slow-responding” viremia episodes we evaluated only first 28 days of CMV viremia for the prediction of “slow-response” similar to “well-responding” since longer duration means “slow-response” by definition. CMV viremia period was defined as a time period starting when the normalized viral load exceeded 100 copies for the first time and ending when it exceeded 100 copies for the last time.

Flow Cytometry

Blood samples were obtained at defined time-points: Day 30, Day 60, Day 90, and Day 180 and at any point when CMV DNAemia raised above the threshold. For all patients, we performed at least 3 flow cytometry measurments of CMV specific T-cells to allow for CMV specific T-cell dynam-ics assessment. Nine milliliters of EDTA anticoagulated fresh peripheral blood was collected, PBMCs were obtained using Ficoll-Paque (Pharmacia, Uppsala, Sweden), resuspended in 10 mL of complete RPMI 1640 media (RPMI 1640 supplemented with 10% heat-inactivated FBS, 100 U/mL penicillin, 100 lg/mL streptomycin sulfate and 1.7 mM sodium glutamate) and rested over night at 378C. The next morning, costimulatory antibodies (CD28/ CD49d, 1 lg/mL, Cat. No. 347690, BD Biosciences, San Jose, CA) and CD107a Alexa488 (Cat. No. A4-671-T100, Exbio Praha, Prague, Czech Republic), along with 3 million cells aliquoted at 100 lL, were added to each well on 96-well plate containing a cocktail of 1 lg/mL of pp65 and IE-1 CMV overlapping peptides and 20 lg/mL whole CMV lysate. Both an unstimulated (without CMV peptides and whole CMV lysate) and a positive control (anti-CD3, Cat. No. 12–202-C100, 10 lg/mL, Exbio) wells were included in each assay. After 2 h incubation in 378C brefeldin A (10 lg/ mL, Sigma-Aldrich, St Louis, MO) was added to each well and stimulation continued for another 4 h at 378C. Follow-ing incubation, 2 lL of 0.1 M EDTA (Sigma-Aldrich) and LIVE/DEAD Violet Viability Dye (Cat. No. L34955, Invitro-gen, Carlsbad, CA) were added along with antibodies to CD14 Pacific Blue (Cat. No. PB-293-T100, Exbio), CD20 Pacific Blue (Cat. No. PB-414-T100, Exbio) and CD8 Hori-zon V500 (Cat. No. 560774, BD Biosciences). After 20-min incubation in dark cells were washed with PBS containing 2 mM EDTA and permeabilized and fixed using FACS lysing solution/FACS Perm 2 (BD Biosciences) according to the manufacturers instructions. Following fixation and perme-abilization, cells were resuspended in 50 lL of PBS contain-ing 1% BSA (Sigma-Aldrich) and stained for 30 min with CD3 PerCP-Cy5.5 (Cat No. T9-514-T100, Exbio), CD4 ECD (Cat.No. 6604727, Immunotech, Marseille, France), CD154 PE (Cat. No. IM2216U, Immunotech), IFNg PE Cy7 (Cat. No. 25–7319-82, eBioscience, San Diego, CA) and IL2 APC (Cat.No. 17–7029-82, eBioscience). Cells were then washed once in PBS with 1% BSA.

The whole content of each well was acquired on LSR ‡ cytometer (BD Immunocytometry Systems, San Jose, CA). Data analysis was performed using FlowJo version 9.7.6 (TreeStar, Ashland, OR). Initial gating used a for-ward scatter area (FCS-A) versus side scatter (SSC-A) plot to select lymphocytes. Events were then gated on CD3,

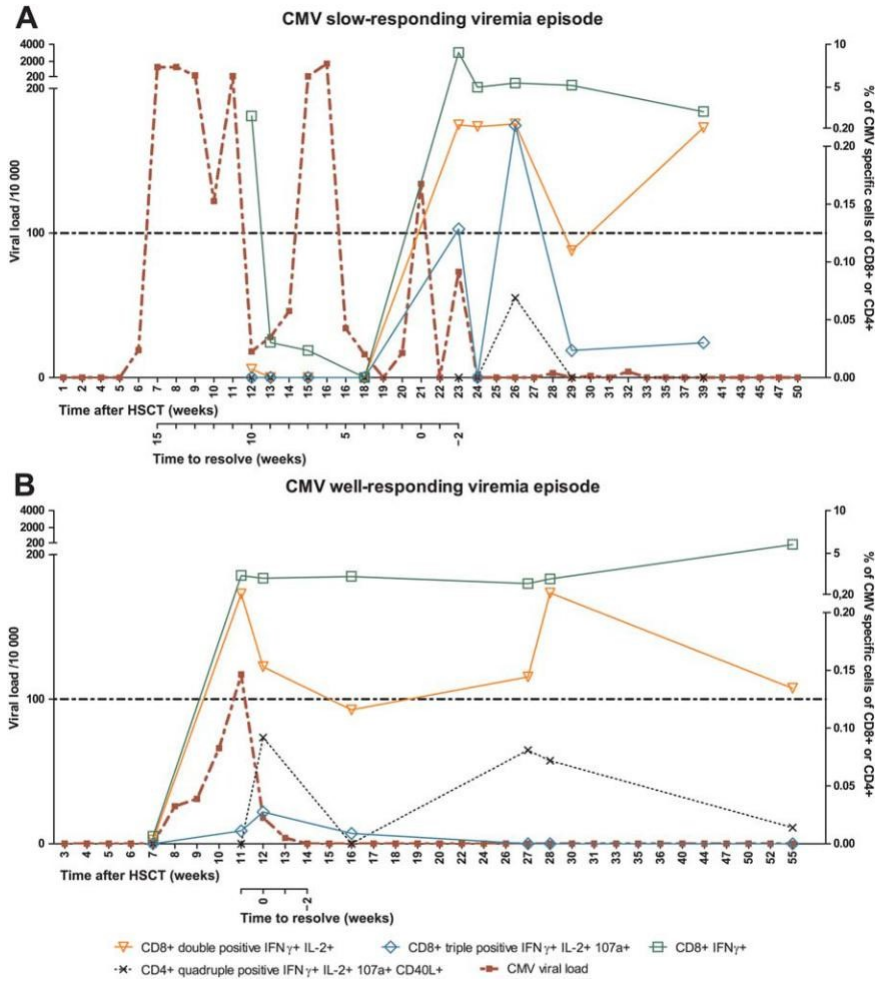

FIG. 1. CMV reactivation patterns in patients post HSCT. Time course of CMV DNAemia, specific CD81Tcell subsets (IFNg1 and any other function1, dual positive IFNg1 IL-21, triple positive IFNg1 IL-21 CD107a1) and a CD41 quadruple positive IFNg1 IL-21 CD107a1 CD40L1 T cell subset in representative cases of Slow-responding (A) and Well-responding (B) patients. The left axis shows the viral load (normalized to 10 000 human genomic equivalents), the threshold for the pre-emptive treatment at 100 copies is shown by dotted line. The right axis shows the percentage of various T cell subsets of the total CD81 or CD41 T cells respectively. The X axis shows the time needed to complete CMV clearance. [Color figure can be viewed in the online issue, which is available at wileyonlinelibrary.com.]

excluding CD14, CD20 Pacific Blue, and LIVE/DEAD Violet Viability dye (DUMP channel) stained events to remove dead cells and to reduce background. Events were further gated on FCS-A versus forward scatter height (FCS-H) to remove doublets. Following identification of CD41 and CD81 T cells, a gate was made for each respective function (production of IFNg, IL-2 and expression of CD107a and CD154). Median of 92434 CD81 and 31361 CD41 T cells was acquired. We have excluded 32 samples with <10,000 CD31 events recorded out of 363 total. Consider-ing a CV of our determination of 20% acceptable, we can accept minimum size of a positive subset at 25 events, which translates to a theoretical sensitivity threshold of 0.027% for CD81 T cell subsets and 0.08% for CD41 T cells (for the median of the acquired events).

Statistical Methods

We have calculated accuracy and specificity of predicting well-responding CMV viremia and found the most accurate threshold for each functional CMV specific T cell subset (30 gated combinatorial functionalities of IFNg, IL-2, CD107a and CD154 on CD81 and CD41 T cells). Accuracy was calculated as number of cases ("well-responding" above threshold 1 "slow-responding" below threshold)/(all reactivations) (calculation known as "Rand index")(27), while specificity was ("slow-responding" below threshold)/(all "slow-responding"). We sought the threshold with maximum accuracy and with ability to identify well-responding reactivation episodes with specificity of at least 80% for each functional subset (all data points were tested as thresholds).

The statistical significance of the slow responding and well-responding patients was determined by Mann-Whitney test (GraphPad Software, La Jolla, CA). Hazard risk of CMV reactivation was determined by Cox's proportional hazard model with time-dependent covariates and robust sandwich variance estimator. Variables were incorporated in to the model by stepwise use of Akaike

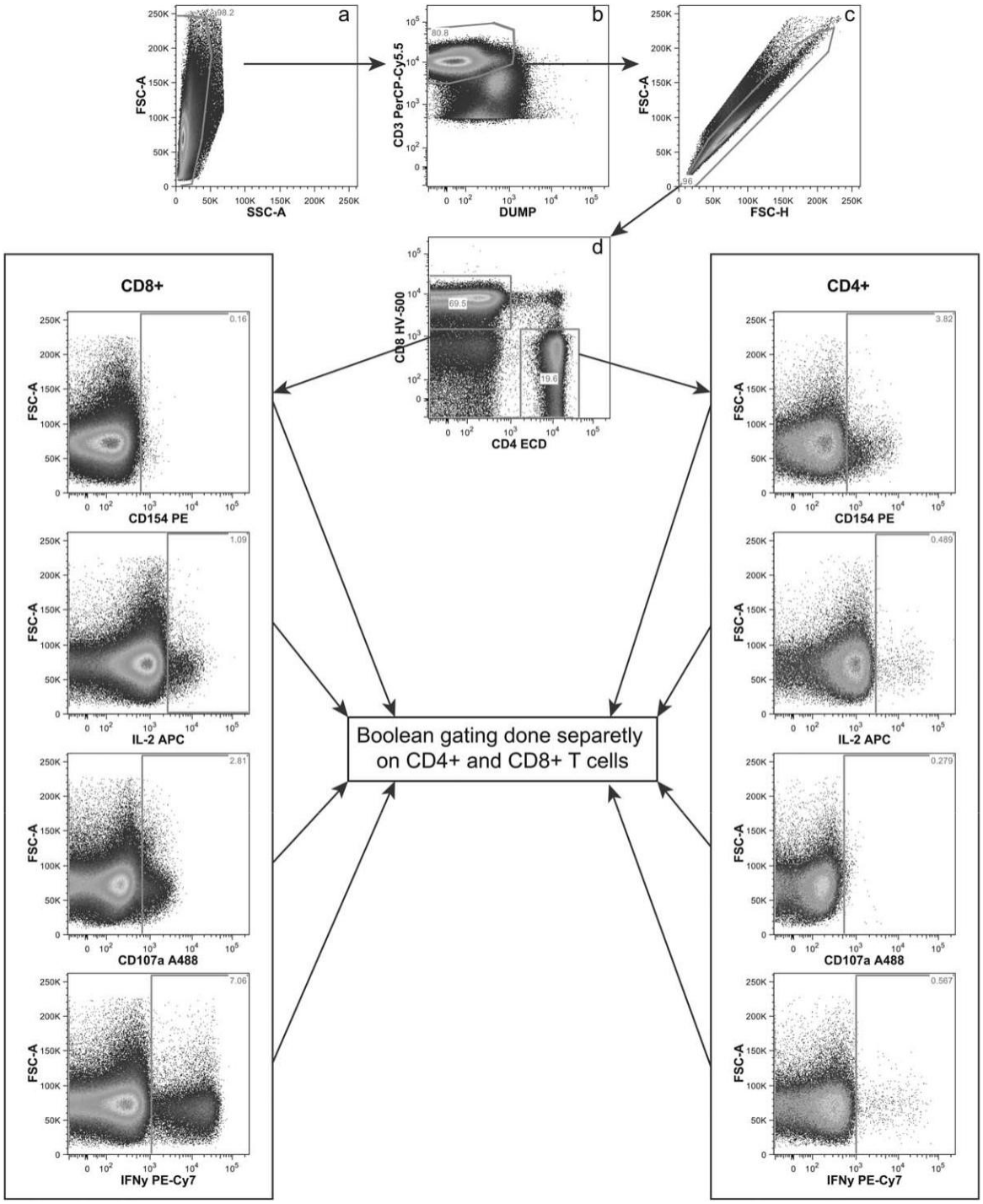

FIG. 2. Representative gating strategy. Typical gating sequence determining every functional T cell subset responding to CMV antigen stimulation. Initial gating of total events included the lymphocytes gate (a), followed by the selection for live T cells (ViViD- CD14- CD20- CD31) (b), singlet cell gate (c), and CD41 or CD81 T cells (d). The total frequency of CMV specific CD154, CD107a expressing, and IFNg or IL-2 producing CD41 and CD81 T cells is gated as shown. Boolean gating analysis of selected populations separately categorizes each cell based on its functionality or quality with respect to the positivity in the observed marker. Each responding cell is assigned to 1 of 15 possible combinations of IFNg, IL-2, CD107a, or CD154 separately done for CD41 and CD81 T cells. Well-responding patient to CMV antigen stimulation is shown.

information criterion and analysis of deviance was used to assess their significance. Only variables improving the model significantly were incorporated. The analysis and regression diagnostics were performed using tools implemented in R-package version 1.1–7, http://CRAN.R-project.org/package 5 lme4 (mixed effect models) and

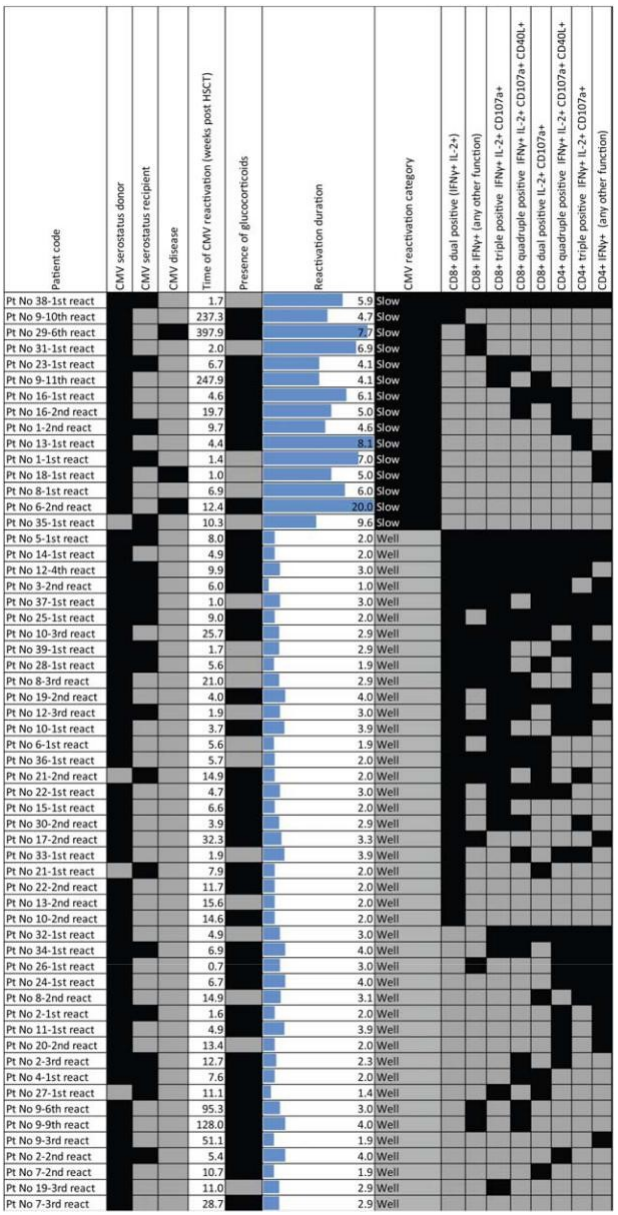

FIG. 3. Summary of Patients characteristics used for determination of accuracy and specificity of T cell functional subsets in classifying well-responding period. We summarized patients characteristics for each CMV reactivation episode. Black rectangles stand for positive occurrence of the respective attribute. [Color figure can be viewed in the online issue, which is available at wileyonlinelibrary.com.]

https://cran.r-project.org/web/packages/survival (Cox's proportional hazard model).

RESULTS

Merit of Various T Cell Subsets in CMV Clearance

Patients after bone marrow transplantation suffer from CMV reactivations. According to the length of CMV reactivation period we defined "slow-responding" reactivation (>2 weeks, Fig. 1A) and "well-responding" reactivation (up to 2 weeks, Fig. 1B). Since controversy exists in the value of various functional T cell subsets for CMV viremia clearance, we investigated which of the functional subsets (a combination of secretion of IFNg, IL-2, degranulation of CD107a or expression of CD40L (CD154) by either CD81 or CD41 T cells, Fig. 2) can optimally distinguish the slow versus well responding viremia episodes (see defini-tions in the Methods). Within our cohort (Fig. 3), the best accuracy (65%) with specificity 86.7% was achieved by a subset of dual positive CD81 T cells producing both IFNg and IL-2, and also by a triple positive subset (IFNg, IL-2 and degranulation, accuracy 60.3%, specificity 80%). CD81 T cells responding with all four functions followed with the accuracy of 55.2%. When we looked just at the CD81 T cells producing IFNg without any further distinction (a population corresponding to CD81 IFNg produc-ing T cells in some other studies) they were only 48.3% accurate at an optimal threshold of 1.75%, which is three orders of magnitude higher than the multifunctional subsets mentioned above. CD41 T cells displayed accuracy of 50–57%, where the best specificity (86.7%) was found in CD41 triple positive (IFNg1 IL-21 CD107a1) cells. CD41 quadruple positive cells (IFNg1 IL-21 CD107a1 CD40L1) and CD41 IFNg1 cells presented with specific-ity of 80%. We summarized all functional subsets with accuracy over 50% and sensitivity over 80% in Table 2 and show all corresponding ROC curves in Supporting Infor-mation Figure 1. Of note, other criteria including all responding CD41 T cells or all responding CD81 T cells (of any functionality) did not reach that level of accuracy. Thus, we conclude that ex-vivo functional response to CMV antigen can be used to accurately assess well-responding reactivation episode and that the most accu-rate parameter are dual positive CD81 T cells producing IFNg and IL-2. Indeed, patients with slow-responding vire-mia had significantly lower percentages of the functionally responding T cell subsets than well-responding patients (Fig. 4). When functional response in slow-responding versus well-responding patients was plotted against time, it became obvious that CMV specific T cells appear only when viremia reaches resolution (Supporting Information Fig. 2).

CMV Viremia Episode Prediction

Next, we investigated whether the functional T cell sub-sets that predicted viremia duration were also relevant for viremia incidence and what was the role of corticoid ther-apy for GvHD. In order to determine the relative contribu-tion of the presence of particular CMV specific functional T cell subset and corticoid treatment on the development of CMV reactivation, we have used Cox's proportional hazard model with time-dependent covariates and robust sandwich variant estimator (28). Since no correlation between the functional populations in question and vire-mia and time after the last transplantation, respectively was detected (linear mixed effect model), we used piecewise constant interpolation between measurement points. Based on the accuracy data, we have pre-selected the functional subsets best predicting good response to antivi-rals (CD81 dual positive IFNg1 IL-21 and CD81 triple

Table 2
Accuracy and Specificity of T Cell Functional Subsets in Classifying Well-Responding Period

Parameter	Threshold	Slow-responding (cases)	Well-responding (cases)	Accuracy	Specificity
CD81 dual positive IFNg1 IL-21				65.5%	86.7%
	<5 0.004%	13	18		
	> 0.004%	2	25		
CD81 triple positive IFNg1 IL-21 CD107a1				60.3%	80.0%
	5 0%	12	20		
	> 0%	3	23		
CD81 quadruple positive IFNg1 IL-21 CD107a1 CD40L1				55.2%	80.0%
	<5 0.0005%	12	23		
	> 0.0005%	3	20		
CD81 dual positive IL-21 CD107a1				53.4%	80.0%
	5 0%	12	24		
	> 0%	3	19		
CD81 IFNg1 (any other function)				48.3%	80.0%
	<5 1.75%	12	27		
	> 1.75%	3	16		
CD41 quadruple positive IFNg1 IL-21 CD107a1 CD40L1				56.9%	80.0%
	<5 0.007%	12	22		
	> 0.007%	3	21		
CD41 triple positive IFNg1 IL-21 CD107a1				56.9%	86.7%
	<5 0.06%	13	23		
	> 0.06%	2	20		
CD41 IFNg1 (any other function)				51.7%	80.0%
	<5 0.595%	12	25		
	> 0.595%	3	18		

We summarized the T cell subsets with accuracy over 50% and sensitivity over 80% (and CD81 IFNg1).

positive IFNg1 IL-21 CD107a1 and CD41 quadruple positive IFNg1 IL-21 CD107a 1 CD40L1) and the most commonly used CD8 and CD4 functional parameter (CD81 IFNg1 and CD41 IFNg1) together with the corticoid treatment parameter. Each parameter was used as categori-cal variable (cells detected above threshold as in Table 2). To include time course into the model and to exploit the fact that we have made 1850 functional tests in our patients (229 events of reactivation), we evaluated separately time periods from one functional investigation up to the follow-ing test, which allowed us to investigate 1850 periods in the model. Cox's proportional hazard model showed that only the presence of CD81 dual positive IFNg1 IL-21 and CD81 IFNg1 and a lack of corticoid treatment signifi-cantly and nonredundantly contributed to the reduced risk of reactivation in a given period (Table 3 and Supporting Information Fig. 3).

DISCUSSION

This is the largest pediatric study testing the func-tional response to CMV antigens in patients post Hema-topoietic Stem Cell Transplantation, with the ambition to develop a clinically useful test. CMV specific T cells are depleted during HSCT, which creates the opportu-nity for CMV virus reactivation (29) has clearly shown that CMV seropositive recipients benefit from CMV sero-positive grafts, by having less reactivation periods and less antiviral treatment. This effect correlated with the higher number of CMV specific T-cells prior to the first CMV reactivation, while no differences were observed after the first reactivation. It was previously suggested that effector CD8 T-cells travel in the bloodstream to act immediately against CMV, whereas effector-memory cells reside in lymph nodes (30) and circulate at lower levels but are essential for long-term reactivation control. Key controversial questions in the literature concern the T-cell subtype to be monitored (CD4 or CD8) and the function to be followed (IFNg production or a combina-tion of functions including or not IFNg production). We have used large data set of measurements in patients with post HSCT reactivation to find the most accurate functional response and threshold for the prediction of the outcome of the pre-emptive treatment. We show in Table 2, that monitoring of several functional T cell sub-sets can yield an accurate prediction of reactivation out-come, although CD81 dual positive IFNg1IL-21 were the most accurate. Negative and positive predictive values are comparable with studies by Gimenez (31) and Tormo (32). Surprisingly, the optimal thresholds for considering a patient immune protected, are close to the theoretical limit of detection for most of the functional subsets in our assays [requirement for at least 25 positive events was similar to that of Minimal residual disease detection in leukemia (33,34)]. Yet, we find no CMV responding cells in 40–50% of patients resolving their reactivation very well. Thus, the efficient immune response might be secluded out of the bloodstream. An exception to this rule are CD81 IFNg producing cells, which are most accurate at a high threshold of 1.75% of CD81 T cells. This finding is in line with our previous study where we found that this functional subset appears as a "first-line effector", while reactivation control is found in patients

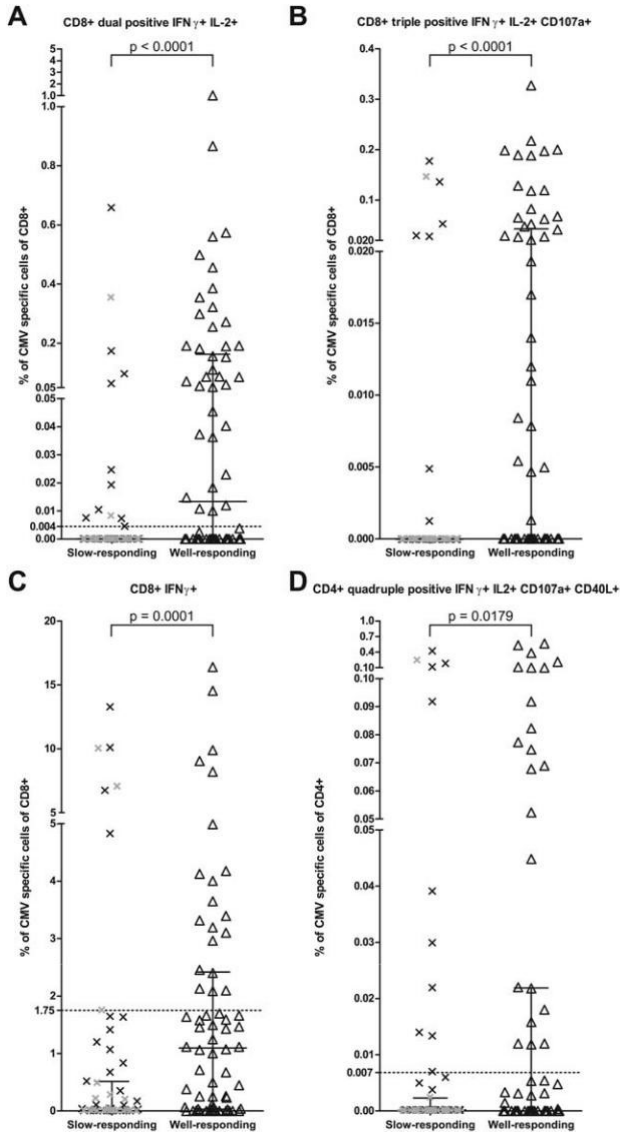

FIG. 4. Different cytokine production during CMV reactivation epi-sode in Well-responding and Slow-responding patients. The Percentage of CD81 (A, B, C) or CD41 (D) T cells responding to *in vitro* CMV stimulation with a specific combination of cytokine production (IFNg and/or IL-2) and/or CD40L and/or CD107a expression assessed in Slow- and Well-responding patients. All included cytometry assess-ments of Slow-responding (*n* 5 58, in grey are assessments taken more than 4 weeks before CMV clearance) and Well-responding (*n* 5 67) patients are shown. *P* values of Mann-Whitney test is shown. Medians with interquartile range and thresholds for optimal distinction between Slow-responders and Well-responders (dotted line) are depicted. (See Supporting Information Fig. 2 for information on time of investigation in relation to reactivation resolution.

where CD8 1 IFNg1 IL-21 dual positive "master effector" cells are detectable (13). In addition, both CD81 dual positive (IFNg1 IL-21) and CD81 IFNg1 cells were found to be a significant, nonredundant (additive) protec-tive parameter in CMV reactivation development. This finding is in line with the intricate evolution of short-term and long-term effector functions in CD8 T cells and their eventual exhaustion (35,36), which is mirrored in their capacity to respond in single or poly functional manner (37).

From the assay design perspective, monofunctional CD8 1 IFNg1 cells pose an easier target, as they are detectable at much higher levels (most accurate cut-off is 1,75%), however their accuracy is slightly inferior to that of CD81 IFNg 1 IL21, which provide accuracy of 65% (compared to 48%of monofunctional cells). Further-more, in the hazard risk model, where additive effect of multiple readouts can be evaluated, both subsets con-tribute and thus should be measured simultaneously to gain maximum predictive information. While we could not determine the threshold as a number of functional cells per microliter (we did not collect absolute T-cell counts at the beginning of our study), for the most accu-rate parameter (CD81 IFNg1 IL-21 dual positive), we observed rather qualitative relationship to immune response (detectable or undetectable).

Although relatively laborious, this functional test can be performed in a single multicolor tube and it should be manageable to perform once a week for the trans-plant patients (sample draw, density gradient separation within 24 h (38) and resting in media on one day, anti-gen stimulation, staining, and data acquisition the next day). To ensure sensitivity to low numbers of specific T-cells, we process 6–9 mL total blood. Based on our data we suggest that following IFNg and IL-2 on CD8 T cells is essential and the presence of any number of dual positive cells is a hallmark of viremia resolution. Implementation of functional studies in a multi-laboratory setting is cumbersome, however multiple measures to improve pre-analytical phase with lyophilized reagents (39), standardized flow cytometry settings (40), auto-mated data analysis (41), or employing a central labora-tory (42) has been published.

Glucocorticoid (GC) treatment is an important con-founding factor in T-cell response evaluation. GC adminis-tration is a risk factor for CMV DNAemia development, however our analysis shows that it is a risk factor inde-pendent of the CMV specific response. To our surprise CMV specific functional T cells were present in some patients treated with GC; however, they were not able to protect the patient from CMV reactivation. Our study

Table 3
Hazard Ratio Contribution for CMV Viremia Development Post-Transplant

Factor	Hazard ratio	Lower CI	Upper CI	*P* values
CD81 dual positive IFNg1 IL-21 present	0.28	0.18	0.43	<1 e-05
CD81 IFNg1 (any other function)	0.45	0.27	0.75	0.002
Corticoids present	2.47	1.82	3.36	<1 e-05

Hazard ratio below 1 means a protective factor and above 1 means a risk factor.

also highlights the appropriate timing of the test, which should be performed at the time of CMV DNAemia to provide information on the functional T-cells reconstitu-tion and whether reactivation resolution is underway. Discrimination of short versus prolonged viremia episode is also a very powerful tool for timing of the pre-emptive therapy. Tan et al. (43) has shown that initiation of pre-emptive therapy even at lower CMV viral load levels was associated with decreased risk of prolonged viremia. Application of our approach to their study would allow exclusion of patients who are going to resolve reactiva-tion spontaneously from the initiation of pre-emptive therapy. This strategy would lead to decreased number of unnecessarily treated episodes of CMV viremia that may be resolved spontaneously. In addition, since antigenemia has been reported to stimulate efficient CMV protective immunity (23,44), allowing spontaneous resolution may benefit the quality of developing immune response.

Two large transplant centers calculated the cost of CMV reactivation treatment at 34000 USD in pediatric patients (45) or 58,000 to 74,000 USD in adults (46). From the clinical management point of view, there are three types of interventions: watch and wait for spontaneous resolution, pre-emptive treatment of each reactivation, and CMV specific T-cell administration (experimental). Attempts to direct therapy based on specific T-cell assessment were published (19,47), where presence of CMV specific T-cells at immune reconstitution in the absence of corticotherapy allowed for CMV viremia resolution without treatment.

We developed a sensitive monitoring tool that predicts whether the viremia would resolve within next 2 weeks after T-cell response assessment. In accordance with accepted protocols, we suggest monitoring CMV viremia weekly in patients shortly after transplantation. When an increase above the threshold is observed, CMV specific T-cells assessment should be performed. When CMV specific response is detected (dual positive (IFNg1 IL-21) or single positive (IFNg1) CD8 cells), CMV DNAemia will likely be resolved in two weeks by the action of T-cells. The proposed cessation of antiviral therapy should be tested in a prospective study. Another use of CMV specific T cells assessment is in predicting of CMV reacti-vation episode. Post-transplant patients with detectable dual or single positive CMV specific CD81 T cells who are free of corticosteroid therapy have 19.6 times lower risk of developing CMV reactivation and thus might be put on a less intensive viremia monitoring scheme.

ACKNOWLEDGMENTS

T.K. was supported as an “ISAC Scholar”. CLIP cytometry laboratory received infrastructural support from CZ.2.16/3.1.00/21540. The authors thank to Daniel Thurner€ for superior technical assistance.

CONFLICT OF INTEREST

Authors declare no conflict of interest.

LITERATURE CITED

1 Hebart H, Einsele H. Clinical aspects of CMV infection after stem cell transplantation. Hum Immunol 2004;65:432–436..

1 Limaye AP, Huang M, Leisenring W, Stensland L, Corey L, Boeckh M. Cytomegalovirus (CMV) DNA load in plasma for the diagnosis of CMV disease before engraftment in hematopoietic stem-cell trans-plant recipients. J Infect Dis 2001;183:377–382.

1 Tanaka N, Kimura H, Iida K, Saito Y, Tsuge I, Yoshimi A, Matsuyama T, Morishima T. Quantitative analysis of cytomegalovirus load using a real-time PCR assay. J Med Virol 2000;60: 455–462.

1 Boeckh M, Leisenring W, Riddell SR, Bowden RA, Huang M, Myerson D, Stevens-Ayers T, Flowers MED, Cunningham T, Corey L. Late cytomegalovirus disease and mortality in recipients of alloge-neic hematopoietic stem cell transplants: Importance of viral load and T-cell immunity. Blood 2003;101:407–414.

1 Boeckh M. Complications, diagnosis, management, and prevention of CMV infections: Current and future. Hematology 2011;2011:305– 309.

1 Sellar RS, Peggs KS. Therapeutic strategies for the prevention and treatment of cytomegalovirus infection. Expert Opin Biol Ther 2012;12:1161–1172.

1 Battiwalla M, Wu Y, Bajwa RPS, Radovic M, Almyroudis NG, Segal BH, Wallace PK, Nakamura R, Padmanabhan S, Hahn T, et al. Ganci-clovir inhibits lymphocyte proliferation by impairing DNA synthesis. Biol Blood Marrow Transplant 2007;13:765–770.

1 Behrendt CE, Rosenthal J, Bolotin E, Nakamura R, Zaia J, Forman SJ. Donor and recipient CMV serostatus and outcome of pediatric allogeneic HSCT for acute leukemia in the era of CMV-preemptive therapy. Biol Blood Marrow Transplant 2009;15:54–60.

1 Green ML, Leisenring WM, Xie H, Walter RB, Mielcarek M, Sandmaier BM, Riddell SR, Boeckh M. CMV reactivation after alloge-neic HCT and relapse risk: Evidence for early protection in acute myeloid leukemia. Blood 2013;122:1316–1324.

1 Elmaagacli AH, Steckel NK, Hegerfeldt Y, Koldehoff M, Ditschkowski M, Christoph S, Gromke T, Ross RS, Beelen DW. Early cytomegalovirus replication after allogeneic stem cell transplanta-tion is associated with a dramatically reduced relapse risk in acute myeloid leukemia patients: Evidence for a putative virus-versus-leukemia effect. Biol Blood Marrow Transplant 2011;17:S161.

1 Lugthart G, van Ostaijen-Ten Dam MM, Jol-van der Zijde CM, van Holten TC, Kester MGD, Heemskerk MHM, Bredius RGM, van Tol MJD, Lankester AC. Early cytomegalovirus reactivation leaves a spe-cific and dynamic imprint on the reconstituting T cell compartment long-term after hematopoietic stem cell transplantation. Biol. Blood Marrow Transplant 2014;20:655–661.

1 Hoegh-Petersen M, Roa L, Liu Y, Zhou F, Ugarte-Torres A, Louie P, Fonseca K, Khan F, Russell JA, Storek J. Low cytomegalovirus-specific T-cell counts at reactivation are associated with progression to high-level viremia or disease in seropositive recipients of hemato-poietic cell grafts from seropositive but not seronegative donors. Cytotherapy 2012;14:194–204.

1 Krol L, Stuchly J, Hubac˘ek P, Keslova P, Sedlac˘ek P, Stary J, Hrusak O, Kalina T. Signature profiles of CMV-specific T-cells in patients with CMV reactivation after hematopoietic SCT. Bone Marrow Transplant 2011;46:1089–1098.

1 Eid AJ, Brown RA, Hogan WJ, Lahr BD, Eckel-Passow JE, Litzow MR, Razonable RR. Kinetics of interferon-gamma producing cytomegalovirus (CMV)-specific CD41 and CD81 T lymphocytes and the risk of subsequent CMV viremia after allogeneic hematopoietic stem cell transplantation. Transpl Infect Dis 2009;11:519–528.

1 Guerin V, Dalle JH, Pedron B, Ouachee-Chardin M, Yakouben K, Baruchel A, Sterkers G. Cellular immune parameters associated with spontaneous control of CMV in children who underwent transplan-tation. Bone Marrow Transplant 2010;45:442–449.

1 Micklethwaite KP, Clancy L, Sandher U, Hansen AM, Blyth E, Antonenas V, Sartor MM, Bradstock KF, Gottlieb DJ. Prophylactic infusion of cytomegalovirus-specific cytotoxic T lymphocytes stimulated with Ad5f35pp65 gene-modified dendritic cells after allogeneic hemopoietic stem cell transplantation. Blood 2008;112:3974–3981.

1 Feuchtinger T, Opherk K, Bethge WA, Topp MS, Schuster FR, Weissinger EM, Mohty M, Or R, Maschan M, Schumm M, et al. Adoptive transfer of pp65-specific T cells for the treatment of chemorefractory cytomegalovirus disease or reactivation after haploidentical and matched unrelated stem cell transplantation. Blood 2010;116:4360–4367.

1 Schmitt A, Tonn T, Busch DH, Grigoleit GU, Einsele H, Odendahl M, Germeroth L, Ringhoffer M, Ringhoffer S, Wiesneth M, et al.

Adoptive transfer and selective reconstitution of streptamer-selected cytomegalovirus-specific CD81 T cells leads to virus clearance in patients after allogeneic peripheral blood stem cell transplantation. Transfusion 2011;51:591–599.

(ii) Lilleri D, Gerna G, Zelini P, Chiesa A, Rognoni V, Mastronuzzi A, Giorgiani G, Zecca M, Locatelli F. Monitoring of human cytomegalo-virus and virus-specific T-cell response in young patients receiving allogeneic hematopoietic stem cell transplantation. PLoS One 2012; 7:e41648.

(iii) Lilleri D, Fornara C, Chiesa A, Caldera D, Alessandrino EP, Gerna G. Human cytomegalovirus-specific CD41 and CD81 T-cell reconstitu-tion in adult allogeneic hematopoietic stem cell transplant recipi-ents and immune control of viral infection. Haematologica 2008;93: 248–256.

(iv) Tario JD, Chen GL, Hahn TE, PFurlage RL, Zhang Y, Brix L, Halgreen C, Jacobsen K, McCarthy PL, Wallace PK. Dextramer reagents are effective tools for quantifying CMV antigen-specific T cells from peripheral blood samples. Cytometry B Clin Cytom 2015; 88:6–20.

(v) Gratama JW, Boeckh M, Nakamura R, Cornelissen JJ, Brooimans RA, Zaia JA, Forman SJ, Gaal K, Bray KR, Gasior GH, et al. Immune mon-itoring with iTAg MHC Tetramers for prediction of recurrent or per-sistent cytomegalovirus infection or disease in allogeneic hemato-poietic stem cell transplant recipients: A prospective multicenter study. Blood 2010;116:1655–1662.

(vi) Hakki M, Riddell SR, Storek J, Carter RA, Stevens-Ayers T, Sudour P, White K, Corey L, Boeckh M. Immune reconstitution to cytomegalo-virus after allogeneic hematopoietic stem cell transplantation: Impact of host factors, drug therapy, and subclinical reactivation. Blood 2003;102:3060–3067.

(vii) Tormo N, Solano C, Benet I, Clari Ma, Nieto J, de la Camara R, Lopez J, Lopez-Aldeguer N, Hernandez-Boluda JC, Remigia MJ, et al. Lack of prompt expansion of cytomegalovirus pp65 and IE-1-specific IFNgamma CD81 and CD41 T cells is associated with ris-ing levels of pp65 antigenemia and DNAemia during pre-emptive therapy in allogeneic hematopoietic stem cell transplant recipients. Bone Marrow Transplant 2010;45:543–549.

(viii) Tormo N, Solano C, Benet I, Nieto J, de la Camara R, Lopez J, Garcia-Noblejas A, Munoz~-Cobo B, Costa E, Clari MA, et al. Reconsti-tution of CMV pp65 and IE-1-specific IFN-g CD8(1) and CD4(1) T-cell responses affording protection from CMV DNAemia following allogeneic hematopoietic SCT. Bone Marrow Transplant 2011;46: 1437–1443.

(ix) Hubacek P, Virgili A, Ward KN, Pohlreich D, Keslova P, Goldova B, Markova M, Zajac M, Cinek O, Nacheva EP, et al. HHV-6 DNA throughout the tissues of two stem cell transplant patients with chromosomally integrated HHV-6 and fatal CMV pneumonitis. Br J Haematol 2009;145:394–398.

(x) Rand WM. Objective criteria for the evaluation of clustering meth-ods. J Am Stat Assoc 1971;66:846–850.

(xi) Andersen PK, Gill RD. Cox's regression model for counting proc-esses, a large sample study,. Ann Stat 1982;10:1100–1120.

(xii) Zhou W, Longmate J, Lacey SF, Palmer JM, Gallez-Hawkins G, Thao L, Spielberger R, Nakamura R, Forman SJ, Zaia JA, et al. Impact of donor CMV status on viral infection and reconstitution of multifunc-tion CMV-specific T cells in CMV-positive transplant recipients. Blood 2009;113:6465–6476.

(xiii) Remmerswaal EBM, Havenith SHC, Idu MM, Van Leeuwen EMM, Van Donselaar KAMI, Ten Brinke A, Van Der Bom-Baylon N, Bemelman FJ, Van Lier RAW, Ten Berge IJM. Human virus-specific effector-type T cells accumulate in blood but not in lymph nodes. Blood 2012;119:1702–1712.

(xiv) Gimenez E, Munoz~-Cobo B, Solano C, Amat P, de la Camara R, Nieto J, Lopez J, Remigia MJ, Garcia-Noblejas A, Navarro D. Functional pat-terns of cytomegalovirus (CMV) pp65 and immediate early-1-specific CD8 ^{1} T cells that are associated with protection from and control of CMV DNAemia after allogeneic stem cell transplantation. Transpl Infect Dis 2015;17:361–370.

(xv) Tormo N, Solano C, Benet I, Nieto J, de la Camara R, Garcia-Noblejas A, Clari MA, Chilet M, Lopez J, Hernandez-Boluda JC, et al. Kinetics of cytomegalovirus (CMV) pp65 and IE-1-specific IFN-gamma CD81 and CD41 T cells during episodes of viral DNAemia in allogeneic stem cell transplant recipients: Potential implications for the management of active CMV infection. J Med Virol 2010;82: 1208–1215.

× Rawstron AC, Bottcher€ S, Letestu R, Villamor N, Fazi C, Kartsios H, de Tute RM, Shingles J, Ritgen M, Moreno C, et al. Improving effi-ciency and sensitivity: European Research Initiative in CLL (ERIC) update on the international harmonised approach for flow cytomet-ric residual disease monitoring in CLL. Leukemia 2012;142–149.

× Wood BL. Principles of minimal residual disease detection for hema-topoietic neoplasms by flow cytometry. Cytometry B Clin Cytom 2016;90:47–53.

× Kaech SM, Cui W. Transcriptional control of effector and memory CD81 T cell differentiation. Nat Rev Immunol 2012;12:749–761.

× Kahan SM, Wherry EJ, Zajac AJ. T cell exhaustion during persistent viral infections. Virology 2015:1–14.

× Casazza JP, Betts MR, Price Da, Precopio ML, Ruff LE, Brenchley JM, Hill BJ, Roederer M, Douek DC, Koup R. Acquisition of direct antivi-ral effector functions by CMV-specific CD41 T lymphocytes with cellular maturation. J Exp Med 2006;203:2865–2877.

× Sadler R, Bateman EAL, Heath V, Patel SY, Schwingshackl PP, Cullinane AC, Ayers L, Ferry BL. Establishment of a healthy human range for the whole blood "OX40" assay for the detection of antigen-specific CD41 T cells by flow cytometry. Cytom Part B Clin Cytom 2014;86:350–361.

× Villanova F, Di Meglio P, Inokuma M, Aghaeepour N, Perucha E, Mollon J, Nomura L, Hernandez-Fuentes M, Cope A, Prevost AT, et al. Integration of lyoplate based flow cytometry and computa-tional analysis for standardized immunological biomarker discovery. PLoS One 2013;8.

× Kalina T, Flores-Montero J, van der Velden VHJ, Martin-Ayuso M, Bottcher€ S, Ritgen M, Almeida J, Lhermitte L, Asnafi V, Mendonc¸a A, et al. EuroFlow standardization of flow cytometer instrument set-tings and immunophenotyping protocols,. Leukemia 2012;26:1986– 2010.

× Mcneil LK, Price L, Britten CM, Jaimes M, Maecker H, Odunsi K, Matsuzaki J, Staats JS, Thorpe J, Yuan J, et al. A harmonized approach to intracellular cytokine staining gating: Results from an international multiconsortia proficiency panel conducted by the Cancer Immunotherapy Consortium (CIC/CRI). Cytom Part A 2013; 83:728–738.

× Maecker HT, McCoy JP, Amos M, Elliott J, Gaigalas A, Wang L, Aranda R, Banchereau J, Boshoff C, Braun J, et al. A model for har-monizing flow cytometry in clinical trials. Nat Immunol 2010;11: 975–978.

× Tan SK, Waggoner JJ, Pinsky BA. Cytomegalovirus load at treatment initiation is predictive of time to resolution of viremia and duration of therapy in hematopoietic cell transplant recipients. J Clin Virol 2015;69:179–183.

× Li, CR, Greenberg, PD, Gilbert, MJ, Goodrich, JM, Riddell, SR. Recovery of HLA-restricted cytomegalovirus (CMV)-specific T-cell responses after allogeneic bone marrow transplant: Correlation with CMV disease and effect of ganciclovir prophylaxis. Blood 1994;83:1971–1979.

× Hiwarkar P, Gaspar HB, Gilmour K, Jagani M, Chiesa R, Bennett-Rees N, Breuer J, Rao K, Cale C, Goulden N, et al. Impact of viral reactivations in the era of pre-emptive antiviral drug therapy follow-ing allogeneic haematopoietic SCT in paediatric recipients. Bone Marrow Transplant 2013;48:803–808.

× Jain N, Lu K, Ito S, Muranski P, Hourigan CS, Haggerty J, Chokshi PD, Ramos C, Cho E, Cook L, et al. The clinical and financial burden of pre-emptive management ofcytomegalovirus disease after allogeneic stem cell transplantation-implications for preventative treatment approaches. Cytotherapy 2014;16:927–933.

× Avetisyan G, Aschan J, H€agglund H, Ringden O, Ljungman P. Evalua-tion of intervention strategy based on CMV-specific immune responses after allogeneic SCT. Bone Marrow Transplant 2007;40:865.

Cytometry Part B: Clinical Cytometry

Příloha 9.2

frontiers in Immunology

ORIGINAL RESEARCH

published: 31 October 2019
doi: 10.3389/fimmu.2019.02549

Heterologous Cytomegalovirus and Allo-Reactivity by Shared T Cell Receptor Repertoire in Kidney Transplantation

Lucia Stranavova [1†], Ondrej Pelak [2†], Michael Svaton [2], Petra Hruba [1], Eva Fronkova [2], Antonij Slavcev [3], Klara Osickova [4], Jana Maluskova [5], Petr Hubacek [6], Jiri Fronek [7], Petra Reinke [8], Hans-Dieter Volk [8], Tomas Kalina [2‡] and Ondrej Viklicky [1,4*‡]

[1] Transplant Laboratory, Institute for Clinical and Experimental Medicine, Prague, Czechia, [2] CLIP – Childhood Leukaemia Investigation Prague, Department of Paediatric Haematology and Oncology, 2nd Faculty of Medicine, Charles University Prague and University Hospital Motol, Prague, Czechia, [3] Department of Immunogenetics, Institute for Clinical and Experimental Medicine, Prague, Czechia, [4] Department of Nephrology, Transplant Centre, Institute for Clinical and Experimental Medicine, Prague, Czechia, [5] Department of Transplant Pathology, Transplant Centre, Institute for Clinical and Experimental Medicine, Prague, Czechia, [6] Department of Paediatric Haematology and Oncology, 2nd Faculty of Medicine and Motol University Hospital, Charles University, Prague, Czechia, [7] Department of Transplant Surgery, Institute for Clinical and Experimental Medicine, Prague, Czechia, [8] BIH Centre for Regenerative Therapies, Berlin Centre for Advanced Therapies, Charité University Medicine Berlin, Berlin, Germany

OPEN ACCESS

Edited by:
Hermann Einsele, Julius Maximilian University of Würzburg, Germany

Reviewed by:
Fred Falkenburg, Leiden University, Netherlands
Mirko Trilling, University of Duisburg-Essen, Germany

****Correspondence:***
Ondrej Viklicky
ondrej.viklicky@ikem.cz

[†]Shared first authorship

[‡]Shared senior authorship

Specialty section:
This article was submitted to Alloimmunity and Transplantation, a section of the journal Frontiers in Immunology

Received: 08 April 2019
Accepted: 14 October 2019
Published: 31 October 2019

Citation:
Stranavova L, Pelak O, Svaton M, Hruba P, Fronkova E, Slavcev A, Osickova K, Maluskova J, Hubacek P, Fronek J, Reinke P, Volk H-D, Kalina T and Viklicky O (2019) Heterologous Cytomegalovirus and Allo-Reactivity by Shared T Cell Receptor Repertoire in Kidney Transplantation. Front. Immunol. 10:2549. doi: 10.3389/fimmu.2019.02549

Cytomegalovirus (CMV) infection is associated with allograft rejection but the mechanisms behind are poorly defined yet. Although cross-reactivity of T cells to alloantigen and CMV has been hypothesized, direct evidence in patients is lacking. In this observational cohort study, we tested the pre-transplant effector/memory T cell response to CMV peptide pools and alloantigen in 78 living donor/recipient pairs using the interferon-gamma Enzyme-Linked ImmunoSpot (ELISPOT) assay. To prove the hypothesis of cross-reactivity, we analyzed by applying next-generation sequencing the T cell receptor ß (TCR- ß) repertoire of CMV- and alloantigen-reactive T cells enriched from peripheral pre-transplant blood of 11 CMV-seropositive and HLA class I mismatched patients. Moreover, the TCR-repertoire was also analyzed in the allograft biopsies of those patients. There was a significant association between the presence of pre-transplant CMV immediate-early protein 1 (IE-1)-specific effector/memory T cells and acute renal allograft rejection and function ($p = 0.01$). Most importantly, we revealed shared TCR-ß sequences between CMV-IE1 and donor alloantigen-reactive T cells in all pre-transplant peripheral blood samples analyzed in CMV-seropositive patients who received HLA class I mismatched grafts. Identical TCR sequences were also found in particular in post-transplant allograft biopsies of patients with concomitant CMV infection and rejection. Our data show the presence of functional, cross-reactive T cells and their clonotypes in peripheral blood and in kidney allograft tissue. It is therefore likely that CMV-donor cross-reactivity as well as CMV specific T cell elicited inflammation is involved in the processes that affect allograft outcomes.

Keywords: kidney transplantation, cytomegalovirus, ELISPOT, cross-reactivity, rejection, heterologous immunity, TCR repertoire

INTRODUCTION

Although the human cytomegalovirus (CMV) infection establishes a broad immunity which controls infection, rendering it asymptomatic in majority of immunocompetent hosts even if the CMV reactivates repeatedly following different stressors during life-time (1, 2). However, it might be associated with life-threatening complications in organ transplant recipients (3). Interestingly, it is widely acknowledged that, in addition to its direct pathogenic effects, CMV infection in organ transplant recipients is associated with more frequent acute and chronic rejection (4, 5). Although several possibilities have been proposed for those indirect negative effects, the mechanisms behind are poorly understood so far and direct proofs are missing. Persistent CMV infection elicits strong and lifelong T cell immunity that controls CMV reactivation/reinfection and prevents CMV disease by permanent dynamic interaction between the virus and the CMV-reactive T cell clones. However, CMV-reactive T cells can cause tissue damage by several mechanisms: (i) direct cytotoxic effect on CMV infected (allograft) cells, (ii) indirect bystander activation and proinflammatory milieu formation, and (iii) heterologous (cross-reactive) allorecognition (6).

The cross-reactivity of CMV-reactive effector T cells to HLA class I antigens has been discussed (7) and those cross-reactive cells were transiently found in the peripheral blood of kidney transplant recipients (8). T cell receptor (TCR) cross-reactivity has been suggested as primary means of increasing the effective size of T cell compartment, while cross-reactive memory cells have been shown to expand and activate more rapidly (9). Several mechanisms have been proposed for TCR cross-reactivity, including molecular mimicry and the ability of TCR to recognize different peptide-MHC complexes (10). Several other studies have shown the presence of cross-reactive virus-specific memory T cells and donor HLA molecules (7, 8, 11, 12). However, direct evidence of the role of heterologous TCR immunity in renal allograft rejection has not been shown so far.

Herein, we demonstrate that (i) the presence of CMV-reactive T cells pre-transplant predicts risk of acute allograft rejection, (xvi) heterologous CMV- and donor-reactive cross-reactivity TCR-ß identical T cells pre-exists in patients prior to kidney transplantation, and (iii) identical cross-reactive T cell clones are detectable in renal allograft biopsies post-transplantation. Our data support the impact of heterologous immunity to CMV-IE1 and alloantigen among pre-transplant memory T cells on allograft outcome and indicate the need of adequate control not only by immunosuppression but also efficient antiviral strategies.

Abbreviations: TCR, T cell receptor; ELISPOT, Interferon-gamma Enzyme-Linked ImmunoSpot; IE-1, CMV immediate-early protein 1; pp65, Phosphoprotein 65; CI, Confidence interval; eGFR, Estimated glomerular filtration rate; CKD-EPI, Chronic Kidney Disease Epidemiology Collaboration equation; MLR, Mixed lymphocyte reaction; PBMCs, Peripheral blood mononuclear cells; NGS, Next-generation sequencing; VZV, Varicella-zoster virus; rATG, Rabbit polyclonal antithymocyte globulin; PRA, Panel-reactive antibody; CDR3, Complementarity-determining region 3; HR, Hazard ratio; FCS, Fetal calf serum; ROC, Receiver operating characteristic curve; AUC, Area under the curve.

MATERIALS AND METHODS

Patient Characteristics

In this observational cohort study, we evaluated the role of pre-transplant CMV-specific T cell immunity in acute rejection using an ELISPOT cohort consisting of 78 living donor kidney transplant recipients and their respective donors, all of whom underwent transplant surgery in the Institute for Clinical and Experimental Medicine in Prague between the years 2014 and 2017. The demographic data of the patients are summarized in **Table 1**. The peripheral blood of both donors and recipients was drawn pre-operatively to isolate PBMCs. All patients received tacrolimus, mycophenolate mofetil, and steroids as maintenance immunosuppression, initiated 48 h before the scheduled surgery. Patients at low immunological risk [panel-reactive antibody (PRA) <20%] received the anti-CD25 monoclonal antibody basiliximab (Simulect, Novartis), while patients at higher risk received rabbit polyclonal anti-thymocyte globulin (rATG, Thymoglobulin ^{R}, Genzyme Corporation) as induction immunosuppression. CMV prophylaxis with valganciclovir (Valcyte ^{R}, Roche) was given to CMV-seronegative recipients who had received grafts from seropositive donors or to CMV-seropositive recipients who had undergone rATG induction. Fourteen out of 78 patients experienced acute rejection episodes during the 1st year after transplantation and were treated as previously reported (13). For a detailed description of the histological findings, see **Table S1**.

For the analysis of the TCR repertoire of CMV- and donor alloantigen-reactive T cells (the “cross-reactive” cohort) 11 donor/recipient pairs were selected with primary low risk and pre-transplant CMV-seropositive living donor renal allograft recipients from the years 2014 to 2016. For a summary of the demographic data of these patients, see **Table 2**. All patients received tacrolimus, mycophenolate mofetil, and steroids as maintenance immunosuppression (initiated 48 h before the scheduled surgery) and basiliximab as induction immunosuppression. All patients underwent a 3-month protocol kidney graft biopsy according to the centre’s standard practice, while case biopsies were performed to histologically verify clinically suspected acute rejection. In 5 out of 11 patients, histological proven acute rejection episodes occurred within 3 months after the operation. Histological findings are given in **Table S2**. In the case of this patient cohort and their respective living donors, peripheral blood was drawn prior to transplantation in order to isolate PBMCs and the allograft biopsy was performed, with 2–3 mm of the tissue samples stored in Ambion RNAlater ^{R} Stabilization Solution (Thermo Fisher Scientific) for future molecular evaluation.

All patients from the ELISPOT and cross-reactive cohorts as well as their respective donors gave their written informed consent to participate in the study. The local ethics committee approved the study protocol under No. G14-08-38.

IFN-γ ELISPOT Assay

In the “ELISPOT” cohort, allo- and CMV-specific T cells were assessed using the IFN-γ ELISPOT method according to recently described protocols (14, 15). Peripheral blood

TABLE 1 | Demographics of the "ELISPOT" patient cohort.

	Total	IE-1 positive	IE-1 negative	*p*
Patients (n)	78	31	47	
Recipients age (years)*	45.6 ± 13.2	49.0 ± 11.7	43.0 ± 13.7	0.032
Donor age (years)*	48.6 ± 10.9	50.0 ± 11.1	48.0 ± 10.47	0.372
Gender of recipients (M/F)	54/24	20/11	34/13	0.322
Dialysis vintage (months)#	1.7 [0; 259.2]	4.0 [0; 259.2]	0.4 [0; 85.0]	0.424
HLA mismatch*	3.5 ± 1.41	3.7 ± 1.4	3.4 ± 1.4	0.427
PRA max (%)#	0 [0; 69]	0 [0; 69]	0 [0; 36]	0.932
PRA max ≥ 20% n (%)	12 (15.4)	6 (19.4)	6 (12.8)	0.430
Retransplantation n (%)	7 (8.9)	4 (12.9)	3 (6.4)	0.324
CMV prophylaxis n (%)	37 (47.4)	14 (45.2)	23 (48.9)	0.744
Pretransplant CMV IgG serostatus				
D+/R+	52 (66.7)	26 (83.9)	26 (55.3)	0.009
D+/R–	8 (10.3)	0 (0)	8 (17.0)	0.015
D–/R–	6 (7.7)	0 (0)	6 (12.8)	0.038
D–/R+	12 (15.4)	5 (16.1)	7 (14.9)	0.882
CMV DNAemia				
PCR > 10^2 n (%)	9 (11.5)	6 (19.3)	3 (6.3)	0.079
Allo-positive ELISPOT n (%)	25 (32.1)	13 (41.9)	12 (25.5)	0.129
Induction Immunosuppression				
Basiliximab n (%)	49 (62.9)	19 (61.3)	30 (63.8)	0.151
Thymoglobulin n (%)	29 (37.1)	12 (38.7)	17 (36.2)	0.820
Rejection n (%)	14 (17.9)	11 (35.5)	3 (6.4)	0.001
eGFR 3M (mL/min)*	58.7 ± 12.6	53.2 ± 11.4	62.4 ± 12.2	0.003
eGFR 6M (mL/min)*	60.3 ± 13.7	55.0 ± 11.4	64.0 ± 13.9	0.006
eGFR 12M (mL/min)*	59.6 ± 13.5	55.5 ± 12.7	62.4 ± 13.5	0.119

#Median [min; max].
*Mean ± SD (range).

TABLE 2 | Demographics of the "cross-reactive" cohort.

Patients (*n*)	**11**
Recipients age (years)*	38.6 ± 13.7
Donor age (years)*	44.1 ± 13.4
Gender of recipients (M/F)	6/5
Dialysis vintage (months)#	3.9 [0; 25.9]
HLA mismatch*	3.7 ± 1.07
PRA max (%)#	0 [0; 13]
eGFR (mL/s)	1.25 ± 0.4
CMV prophylaxis n (%)	0 (0)
Pretransplant CMV IgG serostatus n (%)	
D+/R+	11 (100)
CMV DNAemia	
PCR > 10^2 n (%)	3 (27.2)
Induction immunosuppression	
Basiliximab n (%)	11 (100)
Rejection n (%)	5 (45.5)
eGFR 3M (mL/min)*	67.9 ± 11.2
eGFR 6M (mL/min)*	75.0 ± 25.9
eGFR 12M (mL/min)*	74.6 ± 12.2

#Median [min; max].
*Mean ± SD (range).

mononuclear cells (PBMCs) were isolated from heparinized peripheral blood samples of donors and recipients taken prior to transplantation (using standard density gradient centrifugation) and cryopreserved in liquid nitrogen as described previously (16). After thawing, PBMCs were re-suspended with complete media [RPMI 1640 supplemented with 10% heat-inactivated fetal calf serum (FCS), penicillin + streptomycin (50 U/mL) and 1.7 mM sodium glutamate] and left for 24 h at 37°C in a CO_2 incubator. Next, 3 × 10^5 recipient PBMCs were stimulated with CD3-depleted donor cells to detect allospecific T cells, and with CMV antigens [whole protein-spanning overlapping peptide pools of immediate-early protein 1 (IE-1) and phosphoprotein 65 (pp65), length of each is 15 amino acids with 11 amino acid overlap] (Miltenyi Biotec) to detect CMV-reactive T cells [using pokeweed mitogen from Autoimmune Diagnostika (AID), GmbH as a positive control]. CMV peptide pools were used in the concentration of 1 µg/mL of pp65 or IE-1. PBMCs were seeded in an ELISPOT plate and incubated for 24 h at 37°C in a CO_2 incubator. The ELISPOT kit used to detect IFN-γ-producing cells was obtained from AID. After 24 h incubation at 37°C in the CO_2 incubator, cells were removed and the ELISPOT plate processed according to the manufacturer's protocol. The resulting numbers of spots were measured semi-automatically using an ELISPOT reader (AID iSpot FluoroSpot Reader System ELR07 IFL).

Antigen Specific T Cells by Flow Cytometry and FACS Sorting

Antigen specific T cells (virus specific or donor reactive) were detected as proliferating CD8+ T cells by dye dilution technique. Eleven patients from the "cross-reactive" cohort were selected for flow cytometry sorting. Cryopreserved PBMCs from recipients and donors were thawed, suspended with complete media and left for 24 h at 37°C in a CO_2 incubator. After resting, donor PBMCs were inactivated with Mitomycin C (50 µg/1 mL) (Sigma-Aldrich) for 2 h at 37°C in a CO_2 incubator and washed twice with complete media (210 RCF/10 min). Afterwards, both recipient and donor PBMCs were labeled with the dilution dyes CellTrace™ Violet and Far Red Cell Proliferation kits (Thermo Fisher Scientific), respectively, according to the manufacturer's instructions. Labeled recipient PBMCs were aliquoted by 0.5 × 10^6 in a 96-well plate (2 mL, V-bottom, Greiner Bio-One, GmbH) with a culture medium [RPMI 1640 supplemented with 10% heat-inactivated FCS, penicillin+ streptomycin (50 U/mL), 1.7 mM sodium glutamate, 0.00036% (v/v) β-mercaptoethanol, and 10 U/mL IL-2]. CellTrace™ Violet dilution dye labeled PBMC were stimulated with the following CMV antigens: 1 µg/mL of pp65, 1 µg/mL of IE-1 (Miltenyi Biotec), or whole CMV lysate (Vidia) for 6 days. To detect alloreactive and cross-reactive T cells, inactivated donor cells (ratio 1:1) were used as a stimulus (Far Red dye labeled). Additional controls consisting of unstimulated recipient cells and recipient cells with additional IL-2 (50 U/mL) (Sigma-Aldrich) were used to eliminate bystander cell proliferation (data not shown). After 6 days of stimulation, the cells were harvested in 5 ml tubes and washed once with PBS containing 2 mM EDTA. Antigen specific cells proliferate in response to antigen and loose their dilution dye (CellTrace

Violet low cells in **Figure 2**). Washed cells were stained with CMV peptide-pentamers (Pro5 ^{R} MHC Pentamers, Proimmune) matched to the patient's HLA allele (**Table S4**) for 15 min at 4°C. Cells were washed once with PBS containing 2 mM EDTA and stained with antibodies against CD3 (anti-CD3 PC7, Beckman Coulter), CD4 (anti-CD4 ECD, Immunotech), CD8 (anti-CD8 APC-H7, BD Biosciences), and CD45 (anti-CD45 PerCP, Exbio) for 20 min at 4°C. As a subsequent step, cells were washed once with PBS and analyzed using the FACSAria^{TM} III Cell sorter (BD Biosciences). Proliferating CellTrace^{TM} Violet low cells were FACS sorted into a 50 µl elution buffer (Qiagen) (sort gate position is denoted as R1 gate in **Figure 2**). Sorted cells were then incubated in a thermo block heater at 99°C and at 500 rpm for 60 min to isolate DNA; the samples were subsequently stored at −20°C for next-generation sequencing (NGS) library preparation. FlowJo software (FlowJo, LLC) was used for flow cytometry data analysis.

To limit the possibility that cells stimulating the Allo responses contain CMV-infected cells, CMV seropositive donors' blood was examined for the presence of CMV genome by real-time quantitative PCR. DNA was extracted from whole blood using MagNA Pure Compact Nucleic Acid Isolation Kit (Roche, Basel, Switzerland), and the viral loads were normalized to 10,000 human genomic equivalents (17, 18). No CMV genome was found in those samples (**Table S3**).

Kidney Biopsies and DNA Isolation

Kidney biopsy tissue samples taken from the 3-month protocol biopsies or from case biopsies due to deterioration of kidney graft function were available in 7 out of 11 patients from the "cross-reactive" patient cohort. All biopsy tissue samples were stored in Ambion RNAlater ^{R} Stabilization Solution (Thermo Fisher Scientific) at −80°C. The tissue samples were thawed and genomic DNA isolated using the QIAamp DNA Micro Kit (Qiagen) according to the manufacturer's protocol. Isolated DNA were then stored at −20°C for NGS sequencing library preparation.

TCR-β Repertoire Sequencing Using a Next Generation Sequencing Approach

Genomic DNA isolated from FACS-sorted cells and kidney biopsies were used for sequencing library preparation. Two-step PCR was used to detect the majority of V and J segments in complementarity-determining region 3 (CDR3) of the TCR-β sequence, as described previously (19–21). The established libraries were sequenced on the IonTorrent PGM using Hi-Q 400 bp chemistry (Thermo Fisher) and data were analyzed using the Vidjil application (VIDJIL web platform) (22). Samples with analyzed reads below 1,000 or reads in which the CDR3 sequence could not be identified were discarded from further analysis. Clones from the analyzed samples with reads lower than 10 were considered a source of possible cross-contamination between barcoded samples and were thus disregarded from the analysis. Non-productive rearrangements presumably originating from the second allele were retained in the analysis as additional markers of clonotypes.

Statistical Analysis

Data were analyzed using GraphPad InStat 3 (GraphPad Software) and IBM SPSS 22 software. The normality of data distribution was tested using the Kolmogorov-Smirnov test. Since all data were shown not to correspond with standard normal distribution, only non-parametric statistical methods were used. The Mann-Whitney *U* and Chi-Square tests were used to compare the patient groups. Cox proportional hazards model were used to identify risk variables for rejection. The association of recipient, donor, and transplant parameters and immunological factors were first entered to univariate regression analyses (**Table 3**). All significant variables ($p < 0.05$) were included into final multivariate Cox model adjusted for induction treatment presenting the extent of immunological risk. Kaplan-Meier survival curves and the log-rank test were used to project rejection-free intervals and to compare groups. The Wilcoxon matched-pair signed-rank test was used to evaluate ELISPOT differences. To evaluate prediction of rejection risk on the basis of pretransplant pp65/IE-1/Allo ELISPOT receiver operating characteristic (ROC) curves and the calculation of the area under the curve (AUC) were used. Spearman's rank correlation coefficient was used to calculate correlations of pretransplant IE-1 ELISPOT and eGFR in 3, 6, and 12 months. All results with a *P*-value of <0.05 were considered statistically significant.

RESULTS

Pre-transplant Presence of CMV-Specific T Cells Predicts Acute Rejection

To evaluate the relation of pre-existing CMV-reactive and donor-alloreactive T cells and acute rejection of renal allografts, ELISPOT assays were performed in 78 consecutive patients. The design of the IFNγ-ELISPOT allows the detection only of memory/effector CD4+ and CD8+ T cells preformed *in vivo*. As expected, we observed significantly higher frequencies of pre-existing CMV-reactive than alloreactive memory/effector T

TABLE 3 | Risk factors associated with graft rejection in univariate Cox regression.

Univariate analysis variables	HR	95% CI	*p*
Recipient age (years)	1.025	0.986–1.065	0.217
Recipient gender (male)	0.332	0.074–1.484	0.149
Donor age (years)	1.028	0.981–1.079	0.247
Donor gender (male)	7.320	0.960–55.96	0.055
Retransplantaion	1.162	0.362–3.733	0.801
HLA mismatch	0.984	0.680–1.425	0.933
PRA max	1.014	0.985–1.045	0.343
Dialysis vintage (months)	1.010	1–1.024	0.055
IE-1 ELISPOT	6.790	1.89–24.36	0.003
pp65 ELISPOT	1.001	0.999–1.004	0.300
Allo ELISPOT	0.986	0.963–1.010	0.255
CMV DNAemia PCR>10^2	3.820	1.20–12.20	0.024
rATG induction treatment	2.360	0.66–8.48	0.187

Hazard ratio (HR), 95% confidence interval (CI).

cells (**Figure 1A**). Interestingly, the pre-transplant presence of a CMV-reactive response, both to IE-1 and pp65 whole protein overlapping peptide pools, had a stronger predictive power of acute rejection [IE-1 and pp65: AUC = 0.70, cut-off = 122.5 at 69.8% sensitivity and 80% specificity, 95% confidence interval (CI): 0.54–0.87; p = 0.014 and AUC = 0.59, cut-off = 332 at 63.5% sensitivity; and 53.3% specificity, 95% CI: 0.44–0.74, p = 0.27, respectively] than the donor-alloreactive ELISPOT (AUC = 0.40, cut-off = 25 at 66.7% sensitivity and 25.0% specificity, 95% CI: 0.27–0.59, p = 0.39, **Figure 1B**). Moreover, a shorter rejection-free interval was observed in patients with a positive pre-transplant IE-1 ELISPOT (**Figure 1C**).

Univariate Cox regression analysis revealed as significant risk factors of acute rejection only pretransplant positive IE-1 ELISPOT [Hazard ratio (HR) = 6.8, 95% CI: 1.89–24.36, p = 0.003] and post transplant positive CMV viral load by PCR>10^2 (HR = 3.8, 95% CI: 1.2–12.2, p = 0.024) (**Table 3**). A multivariate Cox regression analysis adjusted for ATG induction treatment and CMV PCR > 10^2 revealed only IE-1 positive ELISPOT (HR = 6.2, 95% CI: 1.67–22.3, p = 0.006) to be independent risk factor of acute rejection.

Interestingly, significant correlations were also found between pre-transplant IE-1 ELISPOTs and kidney graft function (estimated glomerular filtration rate (eGFR) using the Chronic Kidney Disease Epidemiology Collaboration (CKD-EPI) equation) at 3, 6, and 12 months (p < 0.001, p = 0.002, and p = 0.038, respectively) (**Figures 1D–F**). The demographic characteristics of patients with positive and negative IE-1 ELISPOTs are summarized in **Table 1**.

Taken together, CMV-reactive cellular immunity predicts acute rejection and short-term outcome of renal allografts.

CMV- and Alloreactive T Cells Express Shared TCR Sequences

The strong association between the pre-transplant presence of CMV-reactive T cells and rejection prompted us to investigate the possible cross-reactivity of CMV-specific T cells to donor alloantigens by search for shared TCR sequences. First, we combined the donor alloantigen MLR with CMV-peptide pentamer staining to evaluate cross-reactivity at single cell level in pre-transplant peripheral blood mononuclear cells (PBMCs) (8). In contrast to previously published studies, we

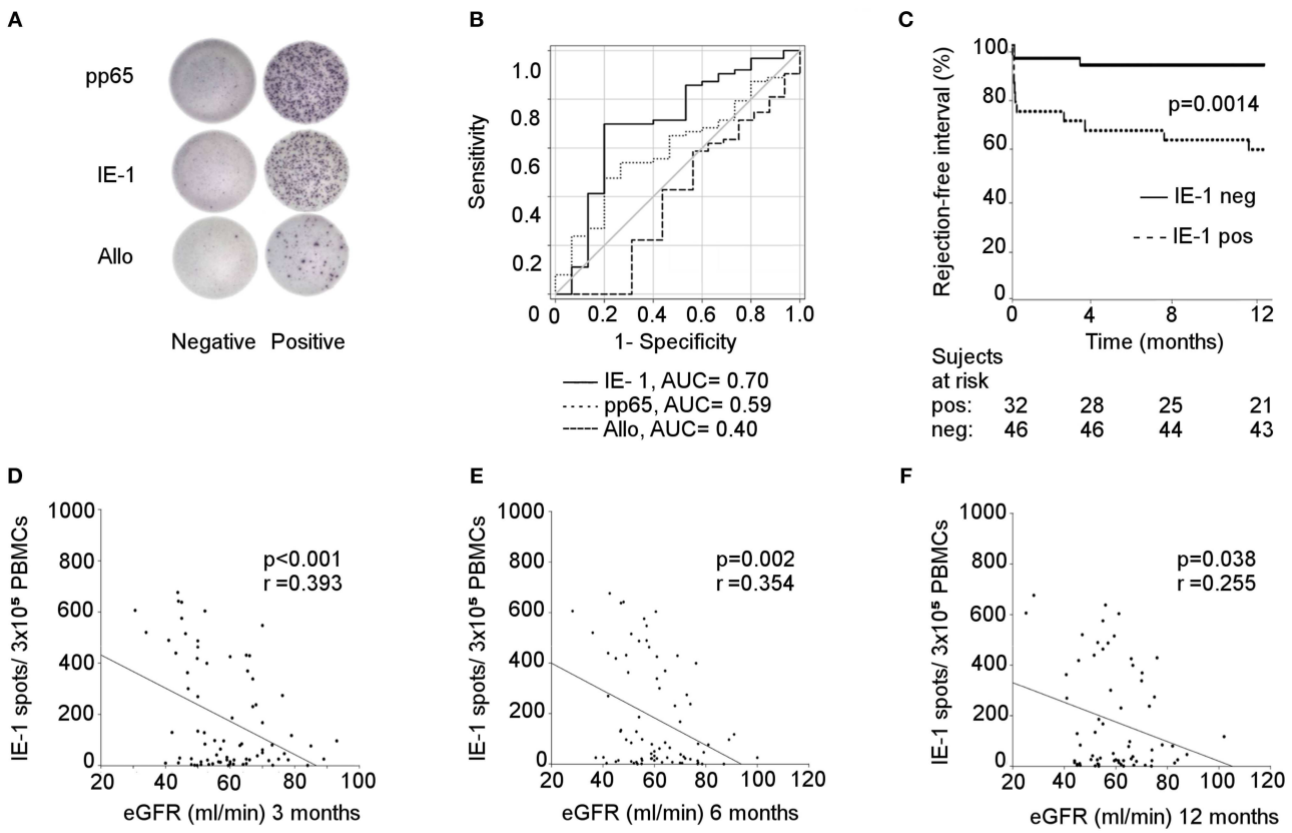

FIGURE 1 | CMV-specific (but not allospecific) ELISPOT for predicting rejection and kidney allograft function. **(A)** visualization of IFN-γ spots after stimulation with pp65/IE-1/alloantigens in positive and negative recipients; **(B)** prediction of rejection risk based on the pre-transplant pp65/IE-1/allo ELISPOT; The operating characteristic (ROC) curves and the calculation of the area under the curve (AUC) were used for this analysis; IE-1: 95% confidence interval (CI): 0.54–0.87; p = 0.014; pp65: 95% CI: 0.44–0.74, p = 0.27; Allo: 95% CI: 0.27–0.59, p = 0.39; **(C)** rejection-free intervals of patients using IE-1-positive and -negative ELISPOTs expressed as Kaplan-Meier survival curves; p = 0.0014. Correlation between a pre-transplant IE-1 ELISPOT and eGFR at 3 **(D)**, 6 **(E)**, and 12 **(F)** months were established by Spearman's rank correlation coefficient; 3M: p < 0.001; 6M: p = 0.002; 12M: p = 0.038.

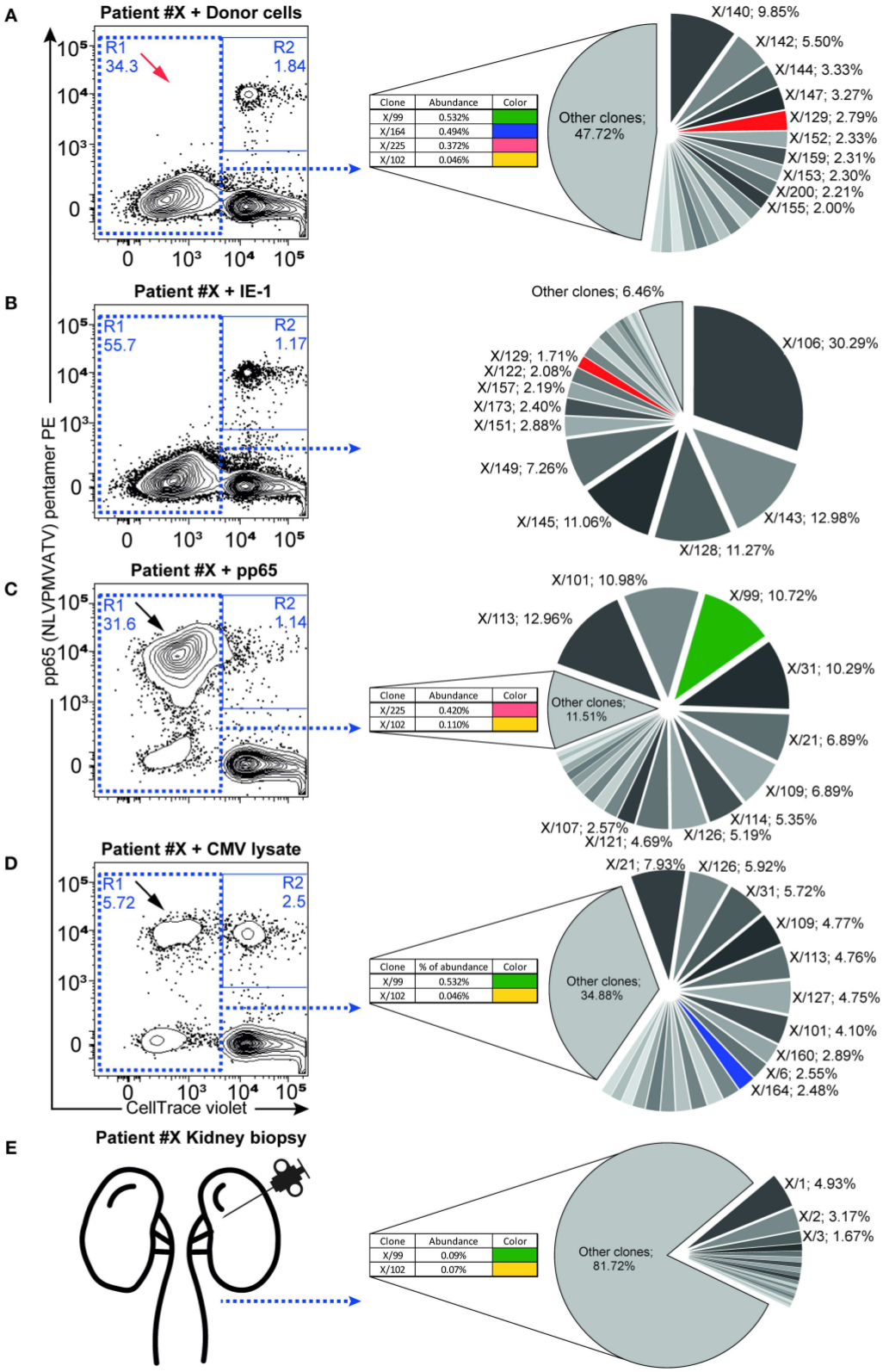

FIGURE 2 | Antigen-responding CD8$^+$ T cells containing cross-reactive TCR-β sequences. Antigen-specific responses were assessed as proliferating recipient CD8$^+$ T cells (CellTrace low cells, plots show gated CD3+CD8+ lymphocytes) after 6-days of ex-vivo culture in combination with pentamer staining for the immunodominant

(Continued)

FIGURE 2 | (pp65: NLVPMVATV-specific) TCR receptor. Flow cytometry dot plots show the proliferation response of $CD8^+$ T cells to donor cells **(A)**, IE-1 **(B)**, pp65 **(C)**, and whole CMV lysate **(D)**. Proliferating cells in R1 were FACS-sorted and used for subsequent NGS TCR-β repertoire analysis. Twenty of the most abundant TCR-β sequences are represented in the pie chart graph (right panels), while additional minor cross-reactive clones are shown in inlets. Color codes highlight the same TCR sequence clones found in the respective antigen-responding cells or in the kidney **(E)**. Black arrows highlight antigen-specific proliferating T cells recognizing the immunodominant pp65 peptide, with red arrows indicating their absence from the donor cell-elicited response. Relative clone abundance is shown next to the clone name in 10 of the most abundant clones or in the inlets. One representative patient (#X) is shown, with a complete list of responding cell fractions. The amount of sorted cells and available NGS reads are given in **Table 4**, while the cross-reactive clones found are listed in **Table S5**.

detected no T cells cross-reactive to the immunodominant pp65 CMV peptide and donor cells, as detected by the co-staining for CMV-pp65 pentamer and cell tracking dilution following proliferation to alloantigen stimulation (**Figure 2A**). However, the response to dominant epitopes (pentamer staining) is lower compared to the proliferative response to the whole CMV peptide pool as demonstrated in 10 out of 11 CMV-seropositive patients (**Figures 2B–D** and summarized in **Figure S1**). In parallel, donor alloreactive T cells were present in all patient samples (including CMV pentamer-negative ones) prior to transplantation.

To investigate whether cross-reactivity would be present among the total pool of CMV-reactive T cells, we isolated antigen-reactive T cells (either reactive to CMV peptide pool or donor PBMCs) by FACS sorting (**Figures 2A–D**) and performed NGS of TCR-β sequences (**Table 4**). In 10 out of 11 patients, we acquired a sufficient amount of reads for analysis. We hypothesize that while pentamer staining only reveals single immunodominant CD8+ T cell clones, cross-reactivity may be caused by other less-dominant TCR clones. We were able to identify hundreds of distinct TCR-ß sequences from sorted antigen-reactive T cells from all patients (median 392 [241; 491], **Table S5**). Indeed, multiple clones sharing the same unique TCR-ß sequences were found in both CMV- and donor-reactive samples (**Figure 2**, right panels) from all patients, regardless of occurrence of rejection (**Table S6**).

Our results also provide evidence that both donor cells and CMV antigens can trigger identical T cell clones for proliferation showing functional responsiveness.

Shared Cross-Reactive TCR-ß Clonotypes Are Detectable in Renal Allograft Biopsies

Next, we sought to investigate whether cross-reactive TCR-ß clonotypes would be detectable in the allografts. Allograft biopsy samples were made available for 7 patients investigated for alloreactive and CMV-specific clonotypes (see "cross-reactive" cohort described above). In the kidney biopsy samples of 6 out of 7 patients, we were able to find identical TCR-β CDR3 sequences as in the alloreactive T lymphocytes pre-transplant. For the remaining patient, only 16 clones could be analyzed from the sequencing results of the MLR tube. Therefore, cross-reactive clones could have been missed due to the lower coverage of this sequencing library. In parallel, CMV-reactive TCR-ß clonotypes were found in the biopsy samples even at higher frequencies in the same patients, with a median of 3 clones per patient and a maximum of 11 (**Table 5**). The CMV-reactive clonotypes in the kidney covered 0.5–6.4% of all TCR-β sequences (**Table 5**) found in the kidney biopsies (see individual clones in **Table S6**). Finally, in 3 out of 7 biopsy samples, we detected CMV/donor alloantigen cross-reactive clonotypes identified pre-transplant in peripheral blood (**Table 5**).

Remarkably, in agreement with the acknowledged capacity of CMV-reactive T cell clones to expand upon CMV reactivation, cumulative abundance of CMV-reactive TCR-ß sequences was the highest (6.4 and 5.1%) in the two kidney tissue samples obtained from patients (No. VIII and X) suffering from significant CMV reactivation (viral load: 935 copies/ml and 1,020 copies/ml of plasma, respectively) concomitantly with biopsy-proven cellular rejection.

In summary, CMV-reactive and alloreactive clonotypes were found in all allograft biopsies patients analyzed, and in 3 out of 7 patients, we detected cross-reactive clonotypes as defined by pre-transplant analyses. Importantly, the highest number of these cross-reactive clones was observed in the two patients with CMV reactivation and concomitant cellular rejection.

DISCUSSION

The immunity in response to previous virus infections can modify the immune response to other antigens. Although heterologous immunity can be beneficial by boosting protective responses, it can also result in severe immunopathologies (6). Here, for the first time, we provide evidence that heterologous immunity can be detected in blood and biopsies of renal allograft recipients. Firstly, we found that high frequencies of CMV-reactive effector/memory (but not of alloreactive) T cells detected pre-transplant were associated with subsequent occurrence of T cell-mediated rejection. Secondly, multiple cross-reactive T cell clones (shared TCR-ß sequences) were found in both CMV- and donor-reactive T cells enriched from pre-transplant peripheral blood samples. Finally, TCR-ß sequences of alloreactive [CMV-reactive, and cross-reactive (CMV & MLR)] clonotypes were found in renal allografts; the latter particularly in association with CMV-associated T cell mediated acute rejection. Therefore, our data demonstrate that identical clonotypes of T cells can react in response to alloantigens as well as CMV antigens. This observation might explain how CMV reactivation, especially in the case of high viral load during uncontrolled replication, boosts directly not only the CMV but also the alloimmune T cell response.

Interestingly, in contrast to the association between high levels of pre-transplant CMV memory/effector response, in our study, we found no associations between pre-transplant donor-reactive memory/effector T cell response and acute rejection. Given the standardized, validated and robust ELISPOT method applied (previously used in a large European multicentre clinical trial; see www.biodrim.eu), it is unlikely that any

TABLE 4 | Percentages of proliferating $CD8^+$ T cells (% CellTrace low), the number of sorted proliferating $CD8^+$ T cells (sorted events), and the number of reads obtained after TCR-β next generation sequencing of sorted proliferating $CD8^+$ T cells (No. of reads) in response to different stimulations.

Stimulation	Donor PBMCs cells			IE-1			pp65			CMV lysate			Kidney
Patient ID	% CellTrace low	Sorted events	No. of reads	% CellTrace low	Sorted events	No. of reads	% CellTrace low	Sorted events	No. of reads	% CellTrace low	Sorted events	No. of reads	No. of reads
I	35.5	11,142	33,778	49.6	13,014	28,014	31.2	5,258	13,246	12.3	1308	53188	16423
II	8.93	1,888	28,855	63.2	20,656	802	65.2	29,571	19,164	49.1	14738	3846	NA
III	36.1	10,516	10,804	36	3,081	56,507	16.9	933	71,615	15.6	1267	65789	12312
IV	33.6	12,458	35,175	52.6	7,945	51,790	41.5	8,673	25,332	7.5	2263	61281	NA
V	10.4	2,788	27,888	3.2	218	20,024	46.3	6,339	31,116	37.3	7534	16768	6915
VI	13.7	3,262	68,617	10.6	2,000	65,951	40.3	3,546	70,503	12.9	3194	104427	121
VII	24.3	3,428	46,562	57.4	70,911	1,702	10.1	2,901	51,597	8.3	5410	79025	20816
VIII	24.7	23,849	1,549	38.7	22,871	9,790	41.3	19,032	4,141	16.4	931	53528	20825
IX	36.5	3,731	37,273	0.1	8	0	7.75	302	33,931	2.8	200	56879	2799
X	34.3	18,084	26,346	55.7	20,473	1,898	31.6	11,140	32,570	5.7	2040	66330	19806
XI	7.7	2,289	70,817	67.9	18,835	140	NA	NA	NA	67.3	37150	143	NA

The kidney column only lists results from TCR-β next generation sequencing of isolated cells from fine needle biopsies where sorting of $CD8^+$ T cells was not possible.

TABLE 5 | CMV-, Allo-, and Cross-reactive clones identified from blood pre-transplant are found in the kidney.

Patient ID	Number of shared clones between PBMCs and kidney from kidney		
	CMV specific (% of reads from all TCR-β sequences found in the biopsy)	Alloreactive (% of reads from all TCR-β sequences found in the biopsy)	Cross-reactive (% of reads from all TCR-β sequences found in the biopsy)
I	1 (0.5%)	1 (0.4%)	0%
III	1 (0.7%)	3 (2.4%)	2 (1.8%)
V	3 (1.8%)	6 (12.6%)	2 (3%)
VII	3 (0.5%)	2 (0.6%)	0%
VIII	11 (5.1%)	0%	0%
IX	0%	2 (9.2%)	0%
X	1 (0.1%)	7 (6.4%)	1 (0.1%)

The percentage of reads from clones that were identified in the functional assay as CMV-reactive, Allo-reactive, or in both tubes as Cross-reactive clones is shown as fraction of all the TCRβ sequences found in the kidney biopsies.

methodological bias occurred. An earlier study reported that higher pre-transplant T cell alloresponse was associated with acute allograft rejection in a study where patients received non-lymphocyte-depleting induction immunosuppression (23). Contrary, in our study some 40% of patients had received rATG T cell depletive induction immunosuppression. Similarly, pre-transplant allo-T cell responses have also been shown to correlate with lower post-transplant eGFR in patients with non-depleting induction (24). Apart from the association between CMV-specific memory/effector T cells and acute rejection, we found significant correlation with lower post-transplant eGFR at three different time-points during the first post-Tx year, rendering our observations more robust. Therefore, it is likely that the T cell-depletion strategy used in about half of our patients effectively reduced the available clonal size of alloreactive memory/effector T cells to a level that could be further controlled by maintenance immunosuppression.

Interestingly, there was weaker association of CMV-pp65- vs. CMV-IE-1-reactive T cells with acute rejection in our study. This phenomenon might be explained by higher CD8+ T cell response to IE-1 than to pp65 antigens (25).

In fact, subclinical CMV reactivation is frequently detected in over 30% of kidney transplant recipients despite CMV prophylaxis (26–28). We speculate that subtle localized CMV reactivations are even more frequent and, while undetected, provide antigen stimulation to CMV-specific T cells. This is in line with observations made by authors of a previous prospective randomized trial. They found that late-onset of CMV viremia, which developed in more than half of patients despite CMV prophylaxis, is associated with poorer outcomes (29).

Although it was reported that at least 151 of the 213 predicted CMV proteins, elicited T cell responses in at least one out of 33 donors (30), we and others could show that the T cell responses to IE-1 and pp65 CMV-proteins are the most dominant ones. Therefore, we concentrated in this study on the two immunodominant CMV proteins.

Applying the previously described method for detecting cross-reactive T cells based on MLR-reactivity combined with peptide-pentamer staining, was not effective in our scenario to detect cross-reactive T cells (7, 8, 31). One reason for this might be the use of unbiased PBMC samples with a scarcity of cross-reactive cells. In fact, as our access to patient material was limited by ethical reasons, we used only 5×10^5 T lymphocytes for functional stimulation, resulting after sort in limited yield of antigen-reactive T cells ranging from 3,846 to 104,427 and 1,888 to 23,849 CMV- and allospecific-proliferating T cells, respectively, for TCR repertoire analysis. Moreover, our recent data show that immunodominant epitopes for one particular HLA-type, as detected and enriched by peptide/dextramer staining, do not reflect the whole response to a particular CMV protein. Therefore, we developed recently the method of T cell stimulation by whole protein-spanning overlapping peptide pools covering almost all epitopes in a HLA-independent matter (32). Applying this method here, we could detect all three categories of CMV-, donor alloantigen-, and cross-reactive T cells in all patients with sufficient yield after sorting derived from pre-transplant blood samples despite limited amounts of reactive T cells (and resulting reads in NGS). These results show the potency of recipients' memory/effector T cell pool to react in case of CMV reactivation post-transplantation with both a protective CMV-specific and a putatively harmful CMV/allo-cross reactive response. In other words, CMV reactivation because of breakthrough through or after weaning of antiviral prophylaxis that might be amplified by TNF-release following ATG application can trigger putatively harmful alloresponse by crossreactivity (33). In line with this, we could detect cross-reactive TCR-ß clonotypes in the kidney biopsies of 3 out of 6 patients with sufficient yield for analysis. Whether the absence of detectable shared cross-reactive TCR-ß sequences in the remaining three biopsy samples is due to sensitivity problems or missing triggering by CMV is not clear, but the high abundancy in the samples just of the two patients suffering from enhanced CMV viral load and concomitant acute rejection supports their pathogenic role in CMV-associated graft injury.

In summary, our data show that within the large peripheral population of CMV-specific memory T cells there is a pool of cross-reactive T cell clonotypes that can produce effector T cells capable of migrating into kidney allografts. Moreover, these T cell clonotypes (when in the presence of chronic antigenic stimuli, such as CMV) may be susceptible to enhanced proliferation and allograft rejection. This phenomenon seems to be universal and corresponds with previous hypotheses about the cross-reactive virus-alloimmune response (12, 34). Specific allo-HLA cross-reactivity has been reported for EBV, CMV, varicella-zoster virus (VZV), and influenza A virus-specific T cells at clonal level, while cross-reactivity has been shown to be mediated by the same TCRs (35, 36). However, our data demonstrate for the first time their occurrence in the unbiased bulk T cell pool from peripheral blood and intragraft.

The limitations of this study must also be acknowledged. The analysis was confined by the limited number of patients and TCR-β chains; furthermore, TCR-α rearrangements were not examined. The configuration of TCR-β chains (including D segments) building in particular the CDR3 region ensures much greater variability of rearranged sequences than TCR-α. Therefore, TCR-β is considered more informative than TCR-α and has been widely used in similar studies. Aside of T cells several other cells (e.g., NK cells) may produce IFNγ after stimulation. Therefore, we phenotypized IFNγ-producing cells stimulated by CMV antigens by flow cytometry. However, the majority of IFNγ-producing cells were T lymphocytes (55%), while NK cells accounted for 5% of IFNγ-producing cells only. The "cross-reactive cohort" subjected TCR- β NGS comprised only by CMV seropositive donor-recipient pairs. Among CMV seropositive-donors cells the CMV-infected cells might be present (37). To minimize the risk of potential activation by CMV infected donor cells, we evaluated those donors for the presence of CMV in their peripheral blood and found none CMV genome.

Our data show that CMV-specific cellular response pre-transplant predicts rejection and document that surprisingly large proportion of patients harbors CMV and donor cross-reactive clones. CMV and donor cross-reactive T cells might thus directly damage the donor cells, being expanded by CMV antigenic stimulation during CMV reactivation. This effect might be supported by CMV specific response that builds inflammatory environment in the kidney. We recommend the approaches aimed at preventing CMV reactivation to be employed more aggressively; not only to prevent CMV disease but also to limit cross-reactivity-induced graft rejection.

In conclusion, we report that in our patient cohort the presence of cytomegalovirus IE-1-specific memory/effector IFN-gamma secreting T cells predict kidney transplant rejection and poorer 1 year graft function. Since we established the presence of functional, cross-reactive T cells and their clonotypes in peripheral blood, tracking the clonotypes directly in the kidney tissue, it is therefore likely that CMV-donor cross-reactivity as well as CMV specific T cell elicited inflammation is involved in the processes that affect allograft outcomes. Future studies should be carried out to determine whether more aggressive prevention and treatment of CMV reactivation might possibly limit alloimmune injury boosted by cross-reactive T cells.

DATA AVAILABILITY STATEMENT

All datasets generated for this study are included in the article/**Supplementary Material**.

ETHICS STATEMENT

The study protocol was approved by the Ethics Commintee of the Institute for Clinical and Experimental Medicine and Thomayer Hospital under number: G14-08-38. All subjects gave written informed consent in accordance with the Declaration of Helsinki.

AUTHOR CONTRIBUTIONS

OV and TK share senior authorship designed and supervised the research and wrote the manuscript. LS, OP, MS, PHr, AS, and EF performed the research, participated in the data analysis, and manuscript writing. JF, JM, PHu, and KO helped with carrying out the research. PR and H-DV helped in establishment of the ELISPOT technology and significantly contributed to writing the manuscript.

FUNDING

This study was supported by the Ministry of Health of the Czech Republic (Grant No. 15-26865A) and in part by Bio-DrIM (EU FP7 program). EF and MS were supported by PRIMUS/17/MED11. TK and OP were supported by the Ministry of Education, Youth and Sports of the Czech Republic (NPU I project LO1604).

ACKNOWLEDGMENTS

We are grateful to Petr Kolar from the Information Technology Division at IKEM for his clinical database support, Maik Stein from BIH Centre for Regenerative Therapies for his help with establishing the ELISPOT method, Janka Slatinska and Vladimir Hanzal from the Department of Nephrology at IKEM for their help with patient management, Renata Zamecnikova and Tereza Neradova for their help with living donor management, Michaela Cerna, Bohumira Kronosova, and Romana Polackova for the sample collection and, finally, Michael Fitzgerald for English correction.

SUPPLEMENTARY MATERIAL

The Supplementary Material for this article can be found online at: https://www.frontiersin.org/articles/10.3389/fimmu.2019.02549/full#supplementary-material

REFERENCES

1. Reinke P, Prosch S, Kern F, Volk HD. Mechanisms of human cytomegalovirus (HCMV) (re)activation and its impact on organ transplant patients. *Transpl Infect Dis*. (1999) 1:157–64. doi: 10.1034/j.1399-3062.1999.010304.x
2. Rafailidis PI, Mourtzoukou EG, Varbobitis IC, Falagas ME. Severe cytomegalovirus infection in apparently immunocompetent patients: a systematic review. *Virol J*. (2008) 5:47. doi: 10.1186/1743-422X-5-47
3. Klenerman P, Oxenius A. T cell responses to cytomegalovirus. *Nat Rev Immunol*. (2016) 16:367–77. doi: 10.1038/nri.2016.38
4. Reinke P, Fietze E, Ode-Hakim S, Prosch S, Lippert J, Ewert R, et al. Late-acute renal allograft rejection and symptomless cytomegalovirus infection. *Lancet*. (1994) 344:1737–8. doi: 10.1016/S0140-6736(94)92887-8
5. Cainelli F, Vento S. Infections and solid organ transplant rejection: a cause-and-effect relationship? *Lancet Infect Dis*. (2002) 2:539–49. doi: 10.1016/S1473-3099(02)00370-5
6. Sharma S, Thomas PG. The two faces of heterologous immunity: protection or immunopathology. *J Leukoc Biol*. (2014) 95:405–16. doi: 10.1189/jlb.0713386
7. Gamadia LE, Remmerswaal EB, Surachno S, Lardy NM, Wertheim-van Dillen PM, van Lier RA, et al. Cross-reactivity of cytomegalovirus-specific CD8+ T cells to allo-major histocompatibility complex class I molecules. *Transplantation*. (2004) 77:1879–85. doi: 10.1097/01.TP.0000131158.81346.64
8. Heutinck KM, Yong SL, Tonneijck L, van den Heuvel H, van der Weerd NC, van der Pant KA, et al. Virus-specific CD8(+) T cells cross-reactive to donor-alloantigen are transiently present in the circulation of kidney transplant recipients infected with CMV and/or EBV. *Am J Transplant*. (2016) 16:1480–91. doi: 10.1111/ajt.13618
9. Kim SK, Brehm MA, Welsh RM, Selin LK. Dynamics of memory T cell proliferation under conditions of heterologous immunity and bystander stimulation. *J Immunol*. (2002) 169:90–8. doi: 10.4049/jimmunol.169.1.90
10. Yin Y, Mariuzza RA. The multiple mechanisms of T cell receptor cross-reactivity. *Immunity*. (2009) 31:849–51. doi: 10.1016/j.immuni.2009.12.002
11. van den Heuvel H, Heutinck KM, van der Meer-Prins EP, Yong SL, Claas FH, Ten Berge IJ. Detection of virus-specific CD8+ T cells with cross-reactivity against alloantigens: potency and flaws of present experimental methods. *Transplant Direct*. (2015) 1:e40. doi: 10.1097/TXD.0000000000000550
12. D'Orsogna L, van den Heuvel H, van Kooten C, Heidt S, Claas FHJ. Infectious pathogens may trigger specific allo-HLA reactivity via multiple mechanisms. *Immunogenetics*. (2017) 69:631–41. doi: 10.1007/s00251-017-0989-3
13. Viklicky O, Hribova P, Volk HD, Slatinska J, Petrasek J, Bandur S, et al. Molecular phenotypes of acute rejection predict kidney graft prognosis. *J Am Soc Nephrol*. (2010) 21:173–80. doi: 10.1681/ASN.2008121268
14. Nickel P, Bold G, Presber F, Biti D, Babel N, Kreutzer S, et al. High levels of CMV-IE-1-specific memory T cells are associated with less alloimmunity and improved renal allograft function. *Transpl Immunol*. (2009) 20:238–42. doi: 10.1016/j.trim.2008.11.002
15. Bestard O, Lucia M, Crespo E, Van Liempt B, Palacio D, Melilli E, et al. Pretransplant immediately early-1-specific T cell responses provide protection for CMV infection after kidney transplantation. *Am J Transplant*. (2013) 13:1793–805. doi: 10.1111/ajt.12256
16. Gebauer BS, Hricik DE, Atallah A, Bryan K, Riley J, Tary-Lehmann M, et al. Evolution of the enzyme-linked immunosorbent spot assay for post-transplant alloreactivity as a potentially useful immune monitoring tool. *Am J Transplant*. (2002) 2:857–66. doi: 10.1034/j.1600-6143.2002.20908.x
17. Tanaka N, Kimura H, Iida K, Saito Y, Tsuge I, Yoshimi A, et al. Quantitative analysis of cytomegalovirus load using a real-time PCR assay. *J Med Virol*. (2000) 60:455–62. doi: 10.1002/(SICI)1096-9071(200004)60:4<455::AID-JMV14>3.0.CO;2-Q
18. Hubacek P, Virgili A, Ward KN, Pohlreich D, Keslova P, Goldova B, et al. HHV-6 DNA throughout the tissues of two stem cell transplant patients with chromosomally integrated HHV-6 and fatal CMV pneumonitis. *Br J Haematol*. (2009) 145:394–8. doi: 10.1111/j.1365-2141.2009.07622.x
19. Kotrova M, Muzikova K, Mejstrikova E, Novakova M, Bakardjieva-Mihaylova V, Fiser K, et al. The predictive strength of next-generation sequencing MRD detection for relapse compared with current methods in childhood ALL. *Blood*. (2015) 126:1045–7. doi: 10.1182/blood-2015-07-655159
20. Theunissen P, Mejstrikova E, Sedek L, van der Sluijs-Gelling AJ, Gaipa G, Bartels M, et al. Standardized flow cytometry for highly sensitive MRD measurements in B-cell acute lymphoblastic leukemia. *Blood*. (2017) 129:347– 57. doi: 10.1182/blood-2016-07-726307
21. van Dongen JJ, Langerak AW, Bruggemann M, Evans PA, Hummel M, Lavender FL, et al. Design and standardization of PCR primers and protocols for detection of clonal immunoglobulin and T-cell receptor gene recombinations in suspect lymphoproliferations: report of the BIOMED-2 concerted action BMH4-CT98–3936. *Leukemia*. (2003) 17:2257–317. doi: 10.1038/sj.leu.2403202
22. Duez M, Giraud M, Herbert R, Rocher T, Salson M, Thonier F. Vidjil: A web platform for analysis of high-throughput repertoire sequencing. *PLoS ONE*. (2016) 11:e0166126. doi: 10.1371/journal.pone.0166126
23. Crespo E, Lucia M, Cruzado JM, Luque S, Melilli E, Manonelles A, et al. Pre-transplant donor-specific T-cell alloreactivity is strongly associated with early acute cellular rejection in kidney transplant recipients not receiving T-cell depleting induction therapy. *PLoS ONE*. (2015) 10:e0117618. doi: 10.1371/journal.pone.0117618

24. Hricik DE. Transplant immunology and immunosuppression: core curriculum 2015. *Am J Kidney Dis*. (2015) 65:956–66. doi: 10.1053/j.ajkd.2015.01.026
25. Slezak SL, Bettinotti M, Selleri S, Adams S, Marincola FM, Stroncek DF. CMV pp65 and IE-1 T cell epitopes recognized by healthy subjects. *J Transl Med*. (2007) 5:17. doi: 10.1186/1479-5876-5-17
26. Selvey LA, Lim WH, Boan P, Swaminathan R, Slimings C, Harrison AE, et al. Cytomegalovirus viraemia and mortality in renal transplant recipients in the era of antiviral prophylaxis. Lessons from the western Australian experience. *BMC Infect Dis*. (2017) 17:501. doi: 10.1186/s12879-017-2599-y
27. Fisher RA. Cytomegalovirus infection and disease in the new era of immunosuppression following solid organ transplantation. *Transpl Infect Dis*. (2009) 11:195–202. doi: 10.1111/j.1399-3062.2009.00372.x
28. Humar A, Lebranchu Y, Vincenti F, Blumberg EA, Punch JD, Limaye AP, et al. The efficacy and safety of 200 days valganciclovir cytomegalovirus prophylaxis in high-risk kidney transplant recipients. *Am J Transplant*. (2010) 10:1228–37. doi: 10.1111/j.1600-6143.2010.03074.x
29. Reischig T, Hribova P, Jindra P, Hes O, Bouda M, Treska V, et al. Long-term outcomes of pre-emptive valganciclovir compared with valacyclovir prophylaxis for prevention of cytomegalovirus in renal transplantation. *J Am Soc Nephrol*. (2012) 23:1588–97. doi: 10.1681/ASN.2012010100
30. Sylwester AW, Mitchell BL, Edgar JB, Taormina C, Pelte C, Ruchti F, et al. Broadly targeted human cytomegalovirus-specific CD4+ and CD8+ T cells dominate the memory compartments of exposed subjects. *J Exp Med*. (2005) 202:673–85. doi: 10.1084/jem.20050882
31. Ford ML. Virally-induced heterologous immunity in renal transplant recipients: important or inconsequential? *Am J Transplant*. (2016) 16:1348–9. doi: 10.1111/ajt.13657
32. Kern F, Faulhaber N, Frommel C, Khatamzas E, Prosch S, Schonemann C, et al. Analysis of CD8 T cell reactivity to cytomegalovirus using protein-spanning pools of overlapping pentadecapeptides. *Eur J Immunol*. (2000) 30:1676–82. doi: 10.1002/1521-4141(200006)30:6<1676::AID-IMMU1676>3. 0.CO;2-V
33. Prosch S, Staak K, Stein J, Liebenthal C, Stamminger T, Volk HD, et al. Stimulation of the human cytomegalovirus IE enhancer/promoter in HL-60 cells by TNFalpha is mediated via induction of NF-kappaB. *Virology*. (1995) 208:197–206. doi: 10.1006/viro.1995.1143
34. Zeng G, Huang Y, Huang Y, Lyu Z, Lesniak D, Randhawa P. Antigen-specificity of T cell infiltrates in biopsies with T cell-mediated rejection and BK polyomavirus viremia: analysis by next generation sequencing. *Am J Transplant*. (2016) 16:3131–8. doi: 10.1111/ajt.13911
35. Amir AL, D'Orsogna LJ, Roelen DL, van Loenen MM, Hagedoorn RS, de Boer R, et al. Allo-HLA reactivity of virus-specific memory T cells is common. *Blood*. (2010) 115:3146–57. doi: 10.1182/blood-2009-07-234906
36. D'Orsogna LJ, Roelen DL, van der Meer-Prins EM, van der Pol P, Franke-van Dijk ME, Eikmans M, et al. Tissue specificity of cross-reactive allogeneic responses by EBV EBNA3A-specific memory T cells. *Transplantation*. (2011) 91:494–500. doi: 10.1097/TP.0b013e318207944c
37. Jackson SE, Sedikides GX, Okecha G, Poole EL, Sinclair JH, Wills MR. Latent Cytomegalovirus (CMV) infection does not detrimentally alter T cell responses in the healthy old, but increased latent CMV carriage is related to expanded CMV-specific T cells. *Front Immunol*. (2017) 8:733. doi: 10.3389/fimmu.2017.00733

Conflict of Interest: The authors declare that the research was conducted in the absence of any commercial or financial relationships that could be construed as a potential conflict of interest.

Příloha 9.3

Cytometry PART A
Journal of the International Society for Advancement of Cytometry

MIFlowCyt

Lymphocyte Enrichment Using CD81-Targeted Immunoaffinity Matrix

Ondrej Pelak,[1] Daniela Kuzılkova,[1] Daniel Thurner,€[1] Marie-Luise Kiene,[2] Kristian Stanar,[2] Jan Stuchly,[1] Martina Vaskova,[1] Jan Stary,[1] Ondrej Hrusak,[1] Herbert Stadler,[2] Tomas Kalina[1]*

[1]CLIP - Childhood Leukemia Investigation Prague, Department of Pediatric Hematology and Oncology, 2nd Faculty of Medicine, Charles University Prague and University Hospital Motol, Prague, Czech Republic

[2]IBA GmbH, G€ottingen, Germany

Received 14 March 2016; Revised 9 May 2016; Accepted 5 July 2016

Grant sponsor: Czech Health Research Council, Czech Republic, Grant number: 15-26588A

Additional Supporting Information may be found in the online version of this article.

*Correspondence to: Tomas Kalina, Department of Pediatric Hematology and Oncology, 2nd Faculty of Medicine, Charles University, Prague, Postal address: V Uvalu 84, 150 06 Prague 5, Czech Republic. E-mail: tomas.kalina@ lfmotol.cuni.cz

Published online 4 August 2016 in Wiley Online Library (wileyonlinelibrary.com)

DOI: 10.1002/cyto.a.22918

Abstract

In mass cytometry, the isolation of pure lymphocytes is very important to obtain reproducible results and to shorten the time spent on data acquisition. To prepare high-ly purified cell suspensions of peripheral blood lymphocytes for further analysis on mass cytometer, we used the new CD811 immune affinity chromatography cell isola-tion approach. Using 21 metal conjugated antibodies in a single tube we were able to identify all basic cell subsets and compare their relative abundance in final products obtained by density gradient (Ficoll-Paque) and immune affinity chromatography (CD811 T-catch^{TM}) isolation approach. We show that T-catch isolation approach results in purer final product than Ficoll-Paque (P values 0.0156), with fewer platelets bound to target cells. As a result acquisition time of 10^5 nucleated cells was 3.5 shorter. We then applied unsupervised high dimensional analysis viSNE algorithm to compare the two isolation protocols, which allowed us to evaluate the contribution of unsuper-vised analysis over supervised manual gating. ViSNE algorithm effectively characterized almost all supervised cell subsets. Moreover, viSNE uncovered previously overseen cell subsets and showed inaccuracies in Maxpar^{TM} Human peripheral blood phenotyping panel kit recommended gating strategy. These findings emphasize the use of unsuper-vised analysis tools in parallel with conventional gating strategy to mine the complete information from a set of samples. They also stress the importance of the impurity
removal to sensitively detect rare cell populations in unsupervised analysis.
International Society for Advancement of Cytometry

Key terms

CD81; T-catch^{TM}; Ficoll-Paque; mass cytometry; CyTOF; human PBMC; viSNE; platelets

Introduction

Mass cytometry currently allows for measurement of up to 44 markers per single cell at the cost of lower acquisition speed (500 events/s), making rare cell analysis time consuming. In this study, we set out to develop and validate a method of lym-phocyte isolation that would enable us to perform immunophenotyping and func-tional testing of target cells. Current standard approaches of cell isolation for mass cytometry rely either on whole blood preparation (with erythrocyte lysis) or on lympho-mononuclear fraction separation using Ficoll-Paque density gradient centri-fugation. These are well-established methods in many laboratories but final products are usually contaminated by high amounts of platelets and platelets-to-cells aggre-gates (1). Whole blood staining does not offer any preenrichment and cell concentra-tion that are important for the feasibility of processing large lymphocyte numbers for rare cell analysis. Ficoll-Paque density gradient separation is time consuming, error prone and difficult to standardize and automate. While commercial solutions that simplify the density gradient separation exist (2), we were also concerned that a

mild negative impact on lymphocytes' condition (higher non-specific antibody binding) after Ficoll-Paque density gradient has been reported (3).

Our aim was to prepare a sample of highly enriched lym-phocytes from whole peripheral blood, with limited cell losses, negligible contaminations by unwanted cells (platelets, red blood cells, and granulocytes) and platelet to cell adhesion, which would help us to speed up the sample acquisition on mass cytometer.

We sought an enrichment method that would be fast, reproducible and would allow for automation (parallelization and hands-on time reduction). We chose Fab Streptamer (releasable low affinity FAB antibody fragments) (4) affinity immunoselection for a positive selection of lymphocytes. The capture method was modified using the affinity chromatogra-phy principle, where cells of interest were reversibly captured to agarose beads coated with Fab Streptamers.

As a selection target, we chose CD81 since the expression of this tetraspanin is high on all major subsets of lymphocytes (5).

A secondary aim was to create a controlled experiment that would serve as a good training material for unsupervised analysis of highly multiparametric data.

Methods

Cell Isolation

EDTA anticoagulated blood samples were obtained from seven adult healthy donors. Peripheral blood mononuclear cells (PBMC) or CD81 positive cells were isolated in parallel using density gradient separation (Ficoll-Paque™ Plus, GE Healthcare, Uppsala, Sweden) or CD81 positive Fab Strep-tamer (4) selection adapted to column-based cell affinity chromatography (T-catch™, IBA GmbH, Gottingen,€ Germa-ny), respectively. T-catch was performed on automated Fabian™ device (IBA GmbH). The University Hospital Motol Review Board approved this study and all individuals provid-ed written informed consent.

T-Catch Principle

T-catch works on the basis of an immune affinity chro-matography. Agarose beads coated with Strep-Tactin were loaded into columns with 30 mm mesh. Before the separation procedure, the columns were loaded with 3 mg of Strep-tag recombinant low affinity anti CD81 FAB fragments for each 1 ml of agarose beads. Low affinity anti-CD81 FAB fragments allow isolation of only those cells that have high CD81 expres-sion and also allow the subsequent dissociation of FAB mole-cules from the target epitope. CD81 Strep-tag recombinant low affinity FAB fragment was constructed upon our request by IBA GmbH.

T-Catch Cell Isolation Procedure

12 ml peripheral blood from each donor was diluted to a final volume of 18 ml with Buffer IS (IBA GmbH, Gottingen,€ Germany, cat. no. 6-5602-050) supplemented with 2 mM EDTA and split into three 30 ml tubes with flat bottom (Sar-stedt, Nurmbrecht,€ Germany). The whole isolation procedure was done on FABian™ (IBA GmbH, Gottingen,€ Germany, cat. no. 6-6100-00), a fully automated isolation device, according to manufacturer's instructions. For the isolation of lympho-cytes, the catch column prefilled with 1.5 ml agarose beads (IBA GmbH, Gottingen,€ Germany, cat. no. 6-1510-000) was loaded with 4.5 mg of low affinity CD81 Fab Strep Human (IBA GmbH, Gottingen,€ Germany, cat. no. 6-8015-100). Tar-get cells were released from agarose beads by addition of D-biotin (Stadler et al., manuscript in preparation). Positive fractions were subsequently combined and washed once in phosphate buffer saline (PBS) (1000 g, 5 min).

Ficoll-Paque Cell Isolation Procedure

24 ml of Ficoll-Paque was added to a 50 ml conical tube and overlaid with a mixture of 12 ml PBS and 12 ml peripher-al blood. After 20 min of low speed centrifugation (500 g) PBMC were carefully harvested from the buffy coat layer and washed once with 20 ml PBS (1000 g, 5 min).

Flow Cytometry

We determined the yield values for both separation pro-cedures by measuring the absolute CD81 positive cell counts in the 12 ml of original blood samples and after the cell sepa-ration using conventional flow cytometry. Flow cytometry allows determination of absolute cell counts when lyse no-wash protocol is used (6). Cells were stained with Syto16 (Life Technologies, Carlsbad, CA, cat. no. S-7578), CD45 PerCP (Exbio, Prague, Czech Republic, cat. no. PC-222-T100), CD81 APC, CD14 APC-H7 (BD Biosciences, San Jose, CA, cat. no. 551112 and 641394, respectively), CD3 ECD, CD19 PC7, CD66c PE (Beckman Coulter, Brea, CA, cat. no. A07748, IM3628 and IM2357, respectively) and DAPI (Molecular Probes, Eugene, OR, cat. no. D3571) for 15 min in RT. Red blood leftovers were then lysed using lyse no-wash protocol in 1 ml of EasyLyse™ (Dako, Glostrup, Denmark, cat. no. S2364). Absolute counts of cells were obtained by adding 50 ml of AccuCount Fluorescent Particles (Spherotech, Lake For-est, IL, cat. no. ACFP-70-10). All stained samples were mea-sured on BD LSRII flow cytometer (BD Biosciences).

Purity and Contamination Determination

Purity was calculated as a number of CD451 CD811 cells divided by CD451 events recorded by conventional flow cytometer or by mass cytometer.

Contamination was determined as percentage of CD81 negative events of all events recorded on CyTOF detector.

Sample Preparation for Mass Cytometry

For analysis on mass cytometer, up to 3 3 10^6 fresh mononuclear cells of the final product obtained by Ficoll-Paque or T-catch approach were used. Cells were washed once in 2 ml Maxpar™ cell staining buffer (Fluidigm, Sunnyvale, CA, cat. no. 201068), resuspended in 50 ml Maxpar cell stain-ing buffer and stained with 50 ml antibody cocktail containing all 21 metal conjugated antibodies (Supplementary Table 1) (100 ml total staining volume). For the identification of main peripheral blood cell subsets we used 17 antibodies from Maxpar Human Peripheral Blood Phenotyping Panel Kit (Fluidigm, Sunnyvale, CA, cat. no. 201304) and four other

Table 1. Overview of samples, acquired events and time of acquisition

DONORS	GENDER	AGE	ISOLATION METHOD	TOTAL UNGATED EVENTS	FICOLL-PAQUE/ T-CATCH™ UNGATED	TOTAL IR1911 SINGLET EVENTS	FICOLL-PAQUE/ T-CATCH™ IR1911 EVENTS	TIME OF ACQ (MIN)	FICOLL-PAQUE/ T-CATCH™ (TOTAL TIME)	10^5 IR1911 SINGLETS/ MIN	FICOLL-PAQUE/ T-CATCH™ (TIME TO ACQUIRE 10^5 IR1911 EVENTS)
Donor 1	M	44	T-catch™	1,604,220		311,322		40		12.85	
Donor 1	M	44	Ficoll-Paque	3,843,299	2.40	142,767	0.46	100	2.50	70.04	5.45
Donor 2	M	50	T-catch™	1,338,459		449,498		70		15.57	
Donor 2	M	50	Ficoll-Paque	2,616,338	1.95	462,165	1.03	120	1.71	25.96	1.67
Donor 3	M	40	T-catch™	828,930		352,884		60		17.00	
Donor 3	M	40	Ficoll-Paque	1,787,482	2.16	124,462	0.35	70	1.17	56.24	3.31
Donor 4	M	27	T-catch™	868,616		414,452		60		14.48	
Donor 4	M	27	Ficoll-Paque	5,909,630	6.80	182,945	0.44	220	3.67	120.25	8.31
Donor 5	F	22	T-catch™	1,301,318		216,257		40		18.50	
Donor 5	F	22	Ficoll-Paque	3,733,315	2.87	178,795	0.83	100	2.50	55.93	3.02
Donor 6	M	28	T-catch™	547,057		282,666		40		14.15	
Donor 6	M	28	Ficoll-Paque	1,430,787	2.62	361,733	1.28	80	2.00	22.12	1.56
Donor 7	F	36	T-catch™	454,253		170,572		40		23.45	
Donor 7	F	36	Ficoll-Paque	2,463,393	5.42	355,209	2.08	120	3.00	33.78	1.44
Ficoll-Paque median (range)				868,616 (454,253–1,604,220)		311,322 (170,572-–449,498)		40 (40–70)		15.6 (12.8–23.5)	
T-catch™ median (range)				2,616,338 (1,430,787–5,909,630)		182,945 (124,462–462,165)		100 (70–220)		55.9 (22.1–120.3)	
Ficoll-Paque/T-catch™ ratio					3.46		0.92		2.36		3.54

antibodies, which were either already metal conjugated (CD71 and CD56 from Fluidigm) or in-house metal conjugated using purified antibodies from BD biosciences and metal-labeling kits from Fluidigm (CD81 and CD99). After 30 min of incu-bation at RT cells were washed twice with 2 ml of Maxpar cell staining buffer and stained with 1 ml of 125 nM Iridium inter-calator (Fluidigm, Sunnyvale, CA, cat. no. 201192A) in 1 ml Maxpar Fix and Perm Buffer (Fluidigm, Sunnyvale, CA, cat. no. 201067) over night at 48C. Next morning cells were washed twice in Maxpar cell staining buffer (800 g, 5 min), washed once in Maxpar Water (800 g, 5 min) (Fluidigm, Sun-nyvale, CA, cat. no. 201069) and then diluted in 20% EQ^{TM} Four Element Calibration Beads (Fluidgm, Sunnyvale, CA, cat. no. 201078) (final concentration 10^6 events/ml). Cells were passed through a 35 mm nylon mesh cell-strainer cap (BD Biosciences, cat. no. 352235) immediately before injec-tion into the mass cytometer. Samples were acquired at a con-stant concentration of 500,000 events per 0.5 ml of sample using CyTOF2 (Fluidigm) with CyTOF software version 6.0.626. The noise reduction (cell length 10–150, lower convo-lution threshold 200) was applied during acquisition. Signal was normalized through a Fluidigm algorithm which is based on the "Bead Passport" concept.

Data Processing

All 14 (7 for each separation procedure) mass cytometry FCS files were transformed to have the same channel numbers and names using the CyTOFCore script (https://github.com/nolanlab/cytofCore) in R-package version 3.2.3, http://CRAN. R-project.org and uploaded for viSNE analysis to Cytobank software. Files were also further analyzed in FlowJo version 10.0.8 (FlowJo, LLC, Ashland, OR). For viSNE analysis, equal number of DNA containing singlets (25,000) were sampled from each of the 14 FCS files and combined together to create a viSNE map. ViSNE map was created from singlet gated events (event length vs DNA content) based on 19 parameters, 17 of which were included in the recommended gating strate-gy by Maxpar Human Peripheral Blood Phenotyping Panel Kit, and two additional markers (CD81 and CD56) (Supple-mentary Table 1).

Data Analysis

R software (R-package version 3.2.3, http://CRAN.R-pro-ject.org) was used to determine P-values of Wilcox-paired test between all cell populations acquired either by Ficoll-Paque or T-catch isolation method. SPICE algorithm in R software (R-package version 3.2.3, http://CRAN.R-project.org) by Roe-derer et al. (7) was used to verify no interpopulation changes among B cells, CD41 and CD81 T cells between samples obtained by either T-catch or Ficoll-Paque method.

Projection of viSNE Clusters into the Supervised Gating Strategy

To identify the main peripheral blood cell subsets seen in the supervised gating analysis also in the viSNE projection, we made several steps: 1) we assumed that the main populations should create unique clusters in the viSNE projection as well. 2) After creating the viSNE map as described above, we downloaded the viSNE FCS files corresponding to each of the measured samples and concatenated them together in FlowJo.

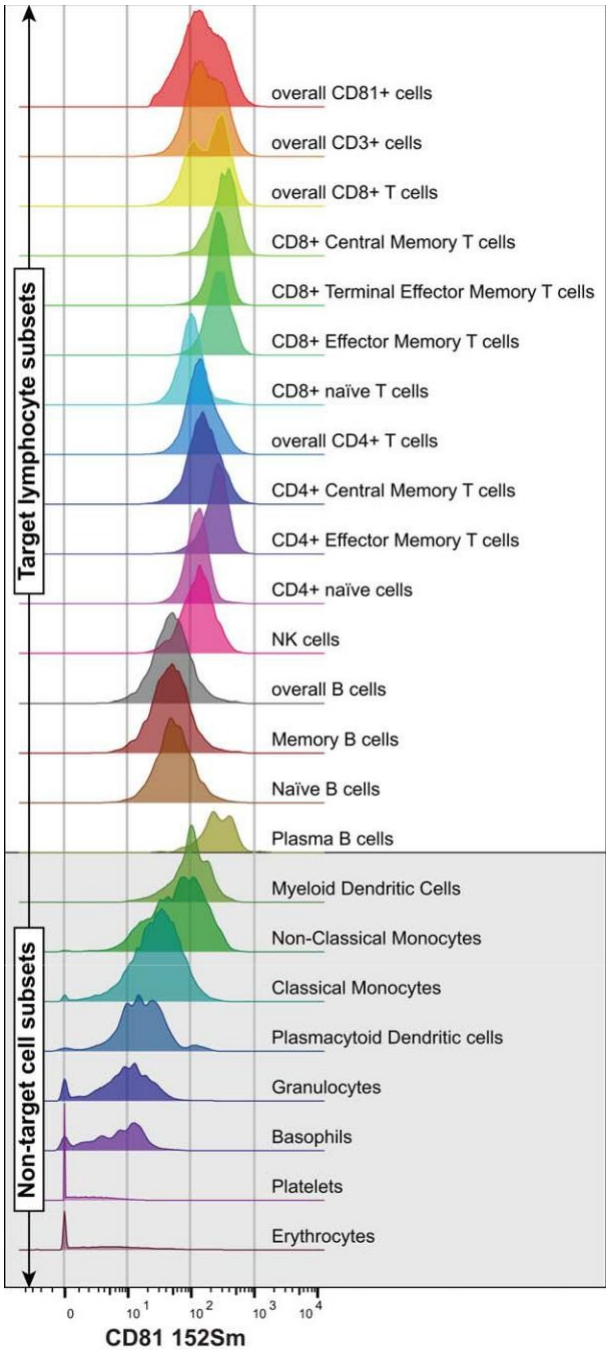

Figure 1. Levels of CD81 expression. Histograms show the amount of CD81 expressed on various cell subsets in whole peripheral blood, as measured on mass cytometer for one repre-sentative donor. [Color figure can be viewed in the online issue, which is available at wileyonlinelibrary.com.]

(xvii) In FlowJo, we then drew gates around each cluster in the concatenated viSNE projection. This way we were able to define the borders of all clusters in the viSNE projection.

(xviii) We exported the gated clusters as single FCS files to have

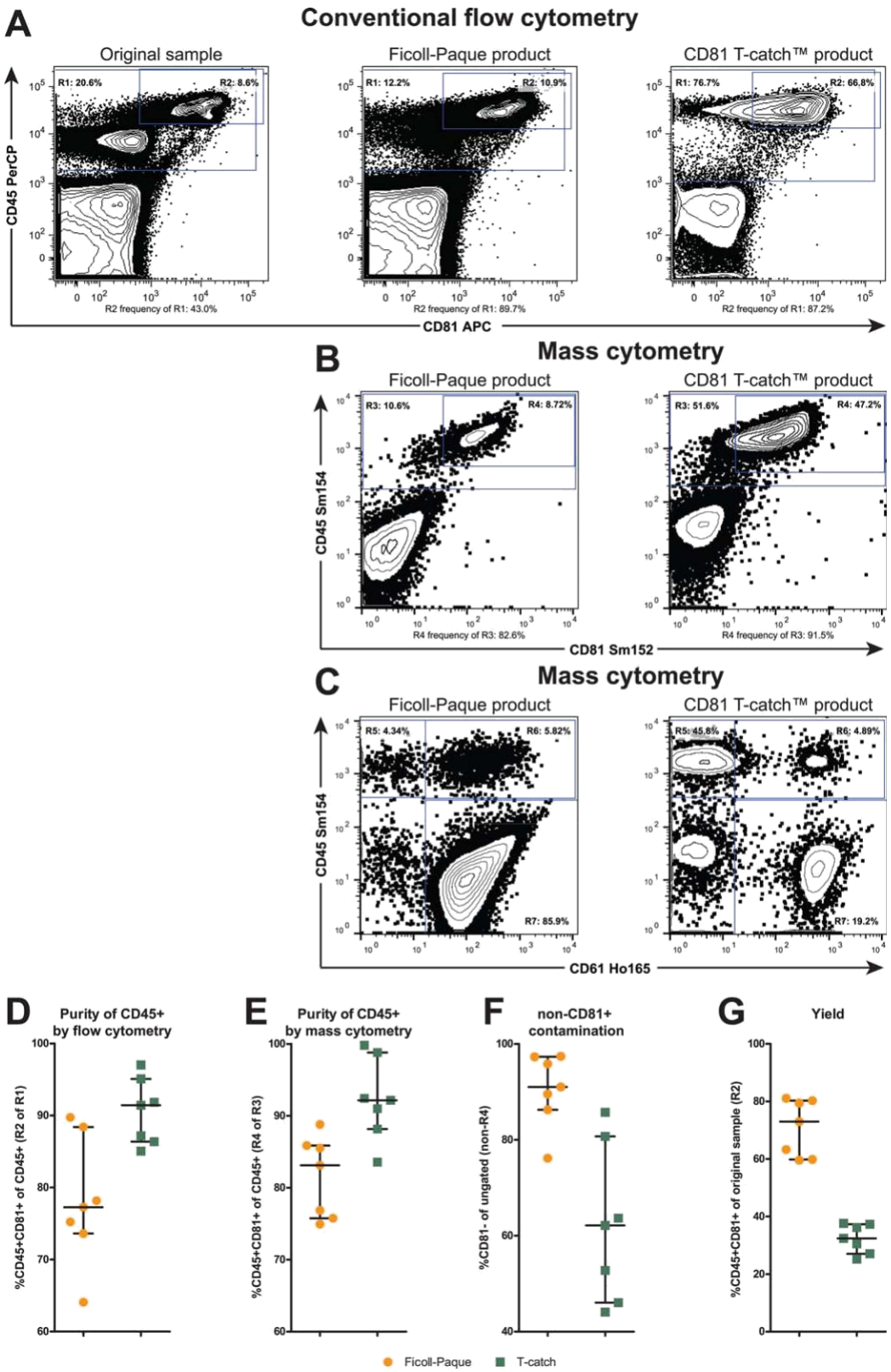

Figure 2. Characterization of final products obtained by Ficoll-Paque and T-catch^{TM}. (A) The graphs show the frequency of CD451 cells (R1) or CD451CD811 cells (R2) of total events in the samples measured for CD81 yield determination on conventional flow cytometer (summarized in D and G). (B) Mass cytometry contour plot showing the enriched products of the Ficoll-Paque or T-catch procedures and frequencies of CD451 cells (R3) or target CD451CD811 cells (R4), contamination with nontarget CD812 (non-R4) events are present (sum-marized in E and F). (C) Mass cytometry contour plot showing the contaminating CD452 events are platelets (R7), in the same time CD451 (R5 and R6) cells contain large proportion of CD611 (R6) platelet bound cells. (D) Summary of the CD451CD811 population purity of CD451 cells measured on conventional flow cytometer (E) Summary of the CD451CD811 population purity of all events as recorded on mass cytometer. (F) The isolated CD811 cell yield is shown as a percentage of total CD811 cells that were put into each isolation proce-dure at the beginning. [Color figure can be viewed in the online issue, which is available at wileyonlinelibrary.com.]

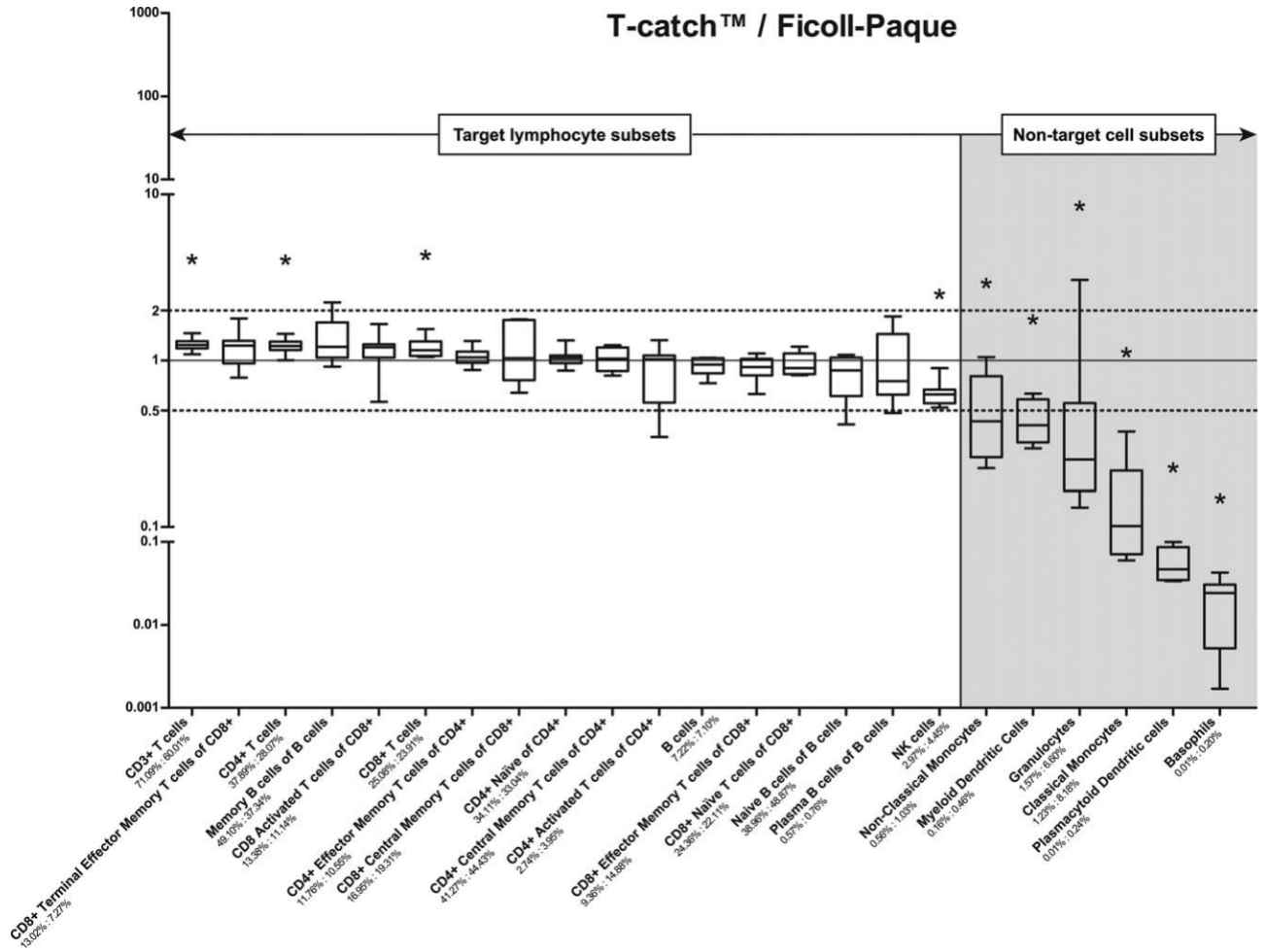

Figure 3. The comparison of enrichment or depletion of cell subsets obtained through Ficoll-Paque and T-catch™ procedures. The fold enrichment of defined cell populations in the T-catch product over the Ficoll-Paque product as measured on mass cytometer is shown. For each pair of samples, the percentages of supervised gated cell populations of singlet events in the T-catch final product were divided by the percentages obtained in the Ficoll-Paque product and the results are shown as boxplots (Median of the seven pairs of samples with interquartile range is shown). Asterisks indicate significantly enriched or depleted cell populations by Wilcox-paired test. Numbers under the population names represent the medians of each cell population proportion in T-catch product and the Ficoll-Paque, respectively. Rel-ative abundance of cell subsets refers to singlet gated events if not stated different.

each cluster as a new sample. 5) In the final step we applied the gating strategy from the supervised analysis to each FCS cluster file and checked whether the cluster falls in any of the defined population.

To compare the two separation procedures we took the number of events which fall within the defined cluster bound-ary and compared them between the samples.

Results

CD81 Expression

To use CD81 molecule as a target for lymphocyte isola-tion, we first checked its expression on various leukocyte sub-sets in a sample of peripheral blood (Fig. 1). In accordance with previous studies we confirmed high expression of CD81 on T, B, and NK lymphocytes (5) and myeloid dendritic cells (mDCs) (8). CD81 was expressed with lower intensity and greater variability on granulocytes, classical monocytes, nonclassical monocytes, basophils, and plasmacytoid dendrit-ic cells (PDCs), while no expression was detected on erythro-cytes and platelets. Thus, we utilized the CD81 expression pattern to isolate purified lymphocytes for further analysis on a mass cytometer.

Cell Isolation Results

The most frequently used method for isolation of PBMC is Ficoll-Paque PLUS gradient centrifugation. To evaluate the T-catch method, we compared the purity and the yield of the final product obtained through T-catch and Ficoll-Paque (Fig. 2A). Products of both methods reached comparable enrich-ment of CD45 and CD81 double positive cells of CD45 posi-tive events (Figs. 2D and 2E), but T-catch method resulted in a cleaner product with less nonnuclear events (median 62.14% of all acquired events were CD81 negative cells as compared to median of 91.01% in Ficoll-Paque product (Fig.

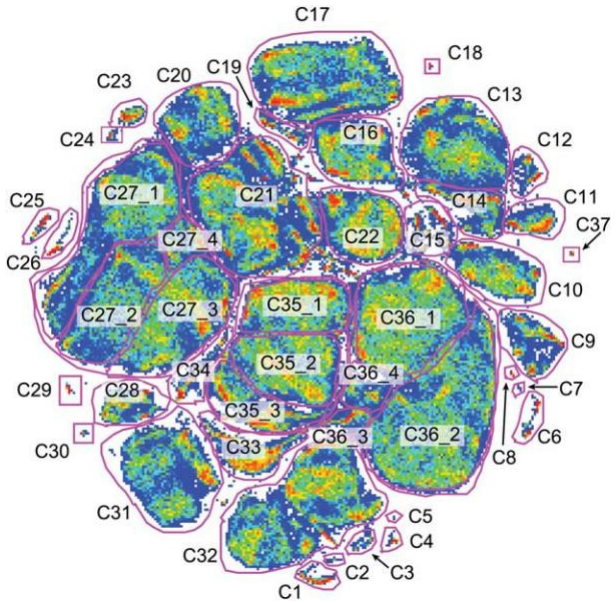

Figure 4. The merged viSNE projection of Ir1911 singlet gated events of all 14 samples.ViSNE graphs were calculated in cyto-bank using 19 markers (see the "Methods" section for more infor-mation) for all 14 samples and subsequently merged into one shown file. The positions and the names of manually created gates around the distinct clusters of events are shown. [Color fig-ure can be viewed in the online issue, which is available at wileyonlinelibrary.com.]

2F). At the same time, Ficoll-Paque procedure yielded median 72.97% of CD81 positive cells compared to median 32.40% by T-catch procedure (Fig. 2G).

Impact on Mass Cytometer Acquisition Time

Using identical event rate for acquisition, we spent on aver-age 2.4 times more time on processing Ficoll separated cell sus-pension, however while we acquired 3.5 times more events total we acquired slightly less Ir1911 events as compared to T-catch separated cells. When we divided total time by total number of Ir1911 cells we calculated time needed to process 10^5 Ir1911 cells prepared by T-catch method as 15.6 min (12.9–23.5) medi-an (range) as compared to 55.9 min (22.1–120.3), Table 1.

Differential Cell Subset Specific Depletion

First, we tested changes in frequencies of known leukocyte populations. We applied the gating hierarchy recommended in Maxpar Human Peripheral Blood Phenotyping Kit to all sam-ples with two modifications: 1) plasma B cells were identified just as CD191 and not as CD191 CD201 and 2) CD38 was replaced by CD56 for more precise identification of NK cells in the final gating branch (CD81 was not involved in the gating hierarchy). The whole gating strategy for one representative sample isolated by Ficoll-Paque or by T-catch method is shown in Supplementary Figures 1A and 1B, respectively. For all lym-phocytes (T, B, NK cells, and their subsets) we have seen similar proportions in Ficoll-Paque separated and T-catch separated samples (within twofold enrichment or depletion on average) (Fig. 3), yet CD31 T cells as well as CD41 and CD81 T cells evaluated separately were modestly but significantly enriched by T-catch, while NK cells were depleted. In addition, we tested distribution of subsets among CD41 and CD81 T-cells that was not different by SPICE analysis (7). On the other hand, innate leukocytes: nonclassical and classical monocytes, granu-locytes, basophils, myeloid, and plasmacytoid dendritic cells (mDC and pDCs) were mildly or profoundly depleted in the T-catch product. These results were in concordance with the amount of CD81 expressed on the cell surface. Surprisingly, the major difference between the products was the amount of CD45 negative events (Fig. 2C), which turned out to be free platelets comprising 93.09% (median of all events) in the Ficoll-Paque as compared to 22.30% in the T-catch product. This led us to investigate possible enrichment or depletion of any unanticipated cell population (not involved in the gating strategy based on expected cell subsets).

Unsupervised Analysis

We used viSNE algorithm for unsupervised high-dimensional data analysis. ViSNE enables projection of the cells from the high-dimensional space into two dimensions such that pairwise distances between the cells are best conserved between the high- and low-dimensional spaces (9). Using viSNE visualization we were able to identify 37 unique clusters (Fig. 4), while we gated only 19 cells subsets in the supervised strategy above. We then projected these clusters one by one into the gating strategy used above to find an overlap with the previ-ously gated cell subsets. The match between the cluster from the viSNE projection and the known population is shown as a blue bar in the Figure 5. For all supervised cell subsets, but erythrocytes, we were able to identify at least one cluster con-taining the target population. Oftentimes, a known subset was found in two distinct clusters. This was mainly caused by the platelets to cells aggregates where viSNE identified these cells as two distinct populations. Overall, we found bound platelets on median 57.19% of CD451 cells in Ficoll-Paque product in con-trast to median 12.27% cells in T-catch product. In fact, 12 of 37 clusters were formed thanks to a significant CD61 signal on the cell subset (see bound platelet column in Fig. 5 and the rep-resentative example shown in Fig. 6A). To a much lesser degree we found also bound erythrocytes (median 1.68% and 0.72%, in Ficoll-Paque and T-catch product, respectively) but they did not contribute to cluster formation. In addition, monocytes, granulocytes, and NK cells formed subclusters not identified initially (see the interpretation of cluster content in Fig. 5). ViSNE projection heatmaps of all markers involved in sample staining for one representative sample isolated by Ficoll-Paque or T-catch are shown in Supplementary Figure 2.

There were eight clusters where majority of cells (>60% cells) was unidentified by conventional gating (empty rows). Clusters C6 and C8 contained doublets or triplets (CD3 and CD20 positive cells or CD3, CD20, and CD66 positive cells) that were missed in the initial aggregate removal by DNA sig-nal. Clusters C20 and C34 contained CD31 CD4 1CD81 double positive or CD31 CD42 CD82 double negative T cells (known populations but omitted from the gating struc-ture). Additional unknown clusters (C2, C7, C9, and C15) of

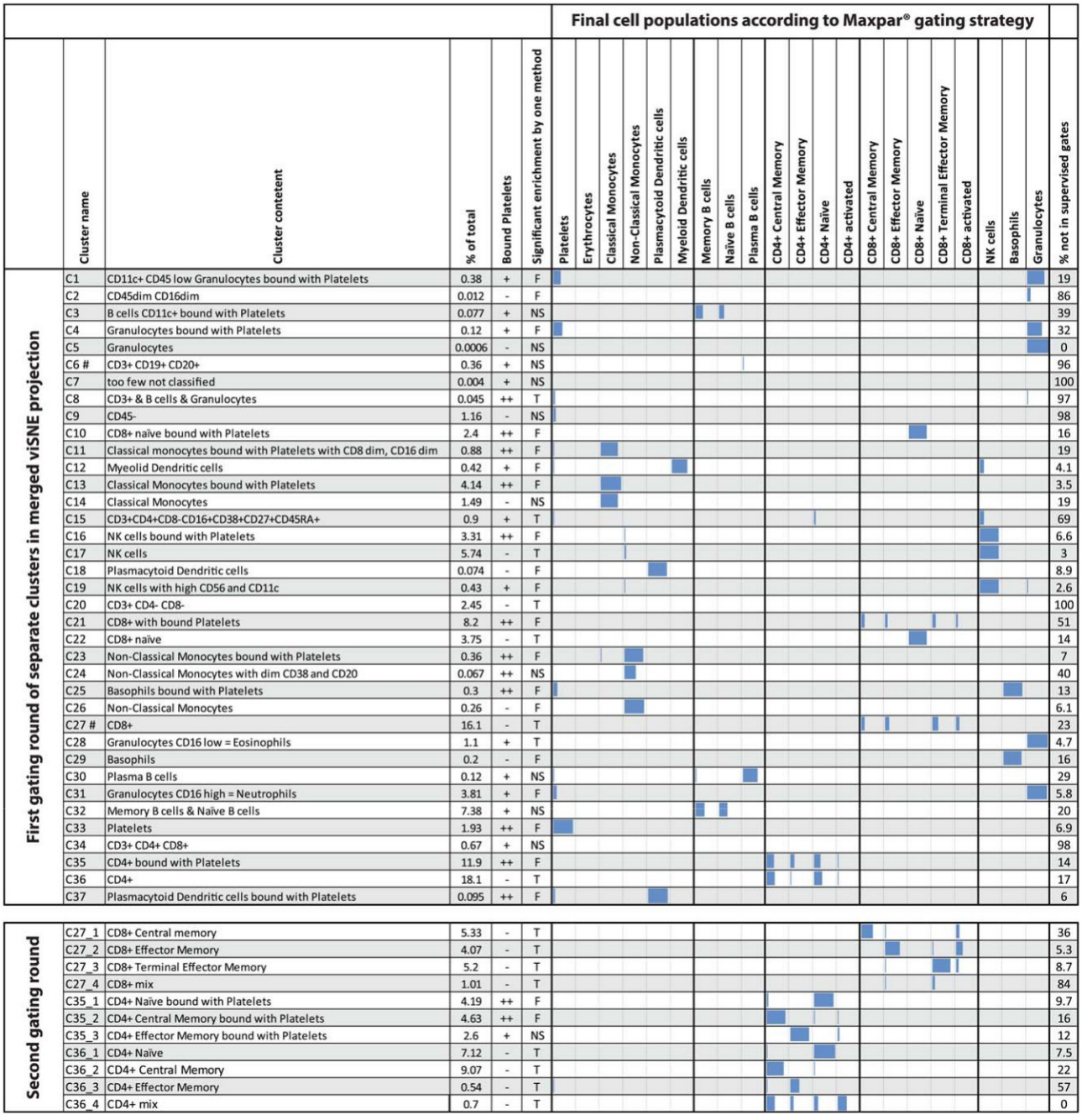

Figure 5. The overlap of supervised cell populations with viSNE clusters.Clusters' names and content according to the supervised gating strategy and its relative abundance is shown. The blue bars show the match between the cluster from viSNE projection and the super-vised gated population. Clusters gated in the first gating round and clusters gated in the second, more precise, round are shown. Hash signs indicate clusters for which the whole gating strategy can be found in the Supplementary Figures 3 and 4. Bound Platelets column abbreviations: -, less than 20%; 1, 20–50%; 11, more than 50% of platelets contaminations. F, T, or NS stands for significant enrichment according to the Wilcox-paired test for Ficoll-Paque, T-catch™ or not significant, respectively. [Color figure can be viewed in the online issue, which is available at wileyonlinelibrary.com.]

low abundant cells (0.01–1%) did not show a particular phenotype signature with the panel used here and thus remained unclassified (Supplementary Fig. 3).

Lastly, some clusters contained several supervised subpopulations, which was the case of CD41, CD81 and B cells subpopulations (C27, C32, C35, and C36) (Supplementary Fig. 4). We have identified the subsets by conventional gating and then we mapped them on the viSNE projection. This showed that the clusters C27, C35, and C36 can be further subdivided into subclusters (Figures 4 and 5).

Finally, we compared enrichment or depletion of the viSNE clusters by Ficoll-Paque or T-catch (Fig. 6B). Out of

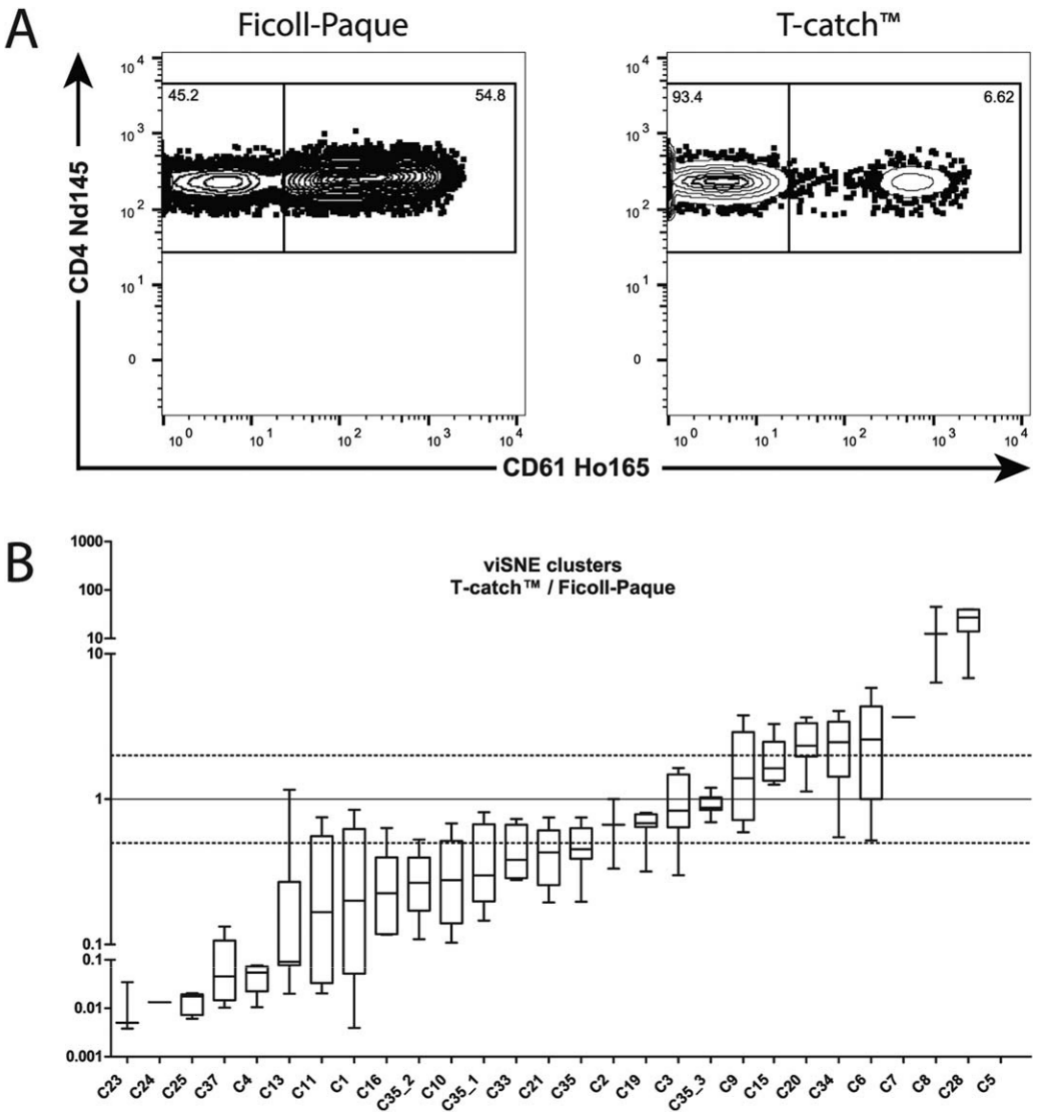

Figure 6. The comparison of the effect of the two isolation methods on the cell subsets newly identified by viSNE. (A) Shows the repre-sentative case of platelets contaminating the CD4 positive cells in the Ficoll-Paque or T-catch^{TM} product, respectively. (B) Shows the fold enrichment of the newly identified cell subsets in the viSNE projection obtained in the T-catch product over the Ficoll-Paque product (the same graph as is shown in Fig. 3 for the expected cell populations).

the 19 clusters enriched in Ficoll-Paque separated products, 15 were sister clusters of conventional subsets but with plate-lets bound on them. Three additional clusters contained pDC (C18), nonclassical monocytes (C26) and basophils (C29). The remaining Ficoll-Paque enriched cluster was a small sub-set (0.02%) of unknown CD45dim CD16dim cells (C2). Enriched in T-catch were eight clusters, which contained CD8 (C22 and C27), CD4 (C36) and double negative (C20) T cells, eosinophils (C28) and NK cells (C17), and two small clusters: C8 (aggregates) and C15 (unknown).

Discussion

We have shown a new lymphocyte enrichment method that is superior in purity to the Ficoll-Paque gradient separation. In contrast to Ficoll-Paque, which separates both lymphocytes and monocytes, T-catch isolates all lymphocytes, while only part of monocytic subsets is preserved. In the reported beta-testing experiments, we optimized the automat-ed washing steps on Fabian device to reach high purity of the product, while yield was a secondary parameter that will be further optimized. It should be noted that the most experi-enced person performed Ficoll-Paque separation. We observe a very mild but significant enrichment of T cell subsets in the T-catch product, which is in concordance with the observa-tions of Appay et al. (10), who reported a selective loss of effector CD81 T cells in Ficoll-Paque separation products. Furthermore, external quality control study reported underes-timation of T cell subsets in density gradient separated mono-nuclear cells (11). In fact, several studies argue that whole

blood and not Ficoll-Paque separated lymphocytes should be used for accurate lymphocyte distribution assessment (12,13). However, an in depth analysis of rare cell subsets is lacking. Our study has been designed to measure large cell numbers in order to analyze rare lymphocyte subsets present in the sam-ple, where whole blood processing is not feasible (as an exam-ple, we could acquire no >3 plasma cells from 100 ml of whole blood in three donors (data not shown). Thus, sample pre-enrichment and concentration method is warranted. Alterna-tive methods for pre-enrichment of target cells used so far are Rosette-Sep™ (antibody mediated crosslinking of nontarget cells to erythrocyte rosettes followed by gradient centrifuga-tion) and various manual or automated magnetic-particles based positive or negative separations. Disadvantage of the former is that it would suffer from the same issues as Ficoll-Paque procedure in general (platelet contamination and plate-let to cell aggregation), in the case of the later, positive selec-tion would block the epitope and leave the ferromagnetic particles bound onto the target cells. Formation of cell to cell or platelet to cell aggregates is largely neglected in most stud-ies, even though it was conclusively shown that a formation of so called "escapees" (14,15) presents a significant problem in samples from particular donors (IIa-R131 polymorphism of FccRIIa) when using particular sample preparation methods and reagents. High frequency of platelet to cell aggregates was a surprising finding in our study and it did introduce artificial subsets on unsupervised analysis. T-catch separation was able to prevent it, likely because it separates the target cells on the affinity matrix while the platelets are washed off before the cell suspension is subject to a centrifugation that mechanisti-cally pushes the cells together. Furthermore, T-catch can be automated and scaled-up for parallel processing of many sam-ples. Other selection reagents can be easily used instead of CD81 (anti-CD19, anti-CD45, unpublished data of HS and TK) when dictated by experimental needs. We are testing this procedure also for lymphocyte separation for functional tests (in vitro response to CMV antigen).

In contrast to fluorescence based conventional cytometry, mass cytometry is relatively slow in acquisition (500 events/s), it lacks light scatter signals for signal collection triggering and essentially all events reach and hit the TOF detector. Thus, samples containing large numbers of unwanted events pro-long the measurement considerably. Indeed, even when the sample concentration was adjusted to 1,000,000 particles/ml, the Ficoll-Paque isolated cell suspension acquisition of Ir191̃1 events is 3.5 times slower than the acquisition of T-catch isolated suspension.

We have successfully employed two complementary methods of highly multiparameter dataset analysis: the con-ventional gating of known subsets and the analysis of differ-ences aided by viSNE projection and visual clustering of subsets with similar immunophenotype. We show here that both analysis methods are indeed complementary. One of the biggest issues of cell analysis using only viSNE projection is the possible omission of rare cell populations which could be displayed as few clustered dots. This is illustrated in the exam-ple of basophils which were present in median of 0.200% and 0.006% of singlets in Ficoll-Paque and T-catch products, respectively. The cluster was omitted during the initial gating of clusters but later, after the search for missing supervised populations, we were able to map this cluster. The difficulty to find rare cell subsets presents additional rationale for sam-ple enrichment, e.g., with anti-CD81 T-catch. ViSNE projec-tion was not able to delineate memory stages of CD4 and CD8 T-cells as separate clusters. This was caused by indiscrete (gradual) changes of expression of CD45RA and CD27. Here, manual gating was more appropriate. On the other hand, pro-jection in viSNE has revealed some subsets of cells as distinct clusters (neutrophils vs eosinophils within granulocytes or CD56 bright cells within NK cells). Furthermore, it showed the heterogeneous composition of monocytes (classical and nonclassical). ViSNE projection also revealed the inaccuracy in the recommended gating strategy. This issue is well illus-trated on the example of NK cells where viSNE projection showed a tight population of cells in cluster C17, but after the projection of this cluster into the supervised population anal-ysis there were only 43% of matching cells. After a more thor-oughgoing analysis of this cluster we found out that the rest of the cells in this cluster were highly expressing CD11c. CD11c on NK cells was previously reported as a marker of activation (16,17). In this case, viSNE algorithm enabled us to refine the supervised gating strategy to include previously overlooked activated subpopulation of NK cells. Thus, through the combination of conventional gating and viSNE we were able to achieve full interpretation of cell subsets con-tained in the samples and to assess their enrichment/depletion in the T-catch procedure.

In conclusion, CD81 Fab T-catch is reliable, fast and effective method of lymphocyte preparation. CD81 Fab can also reduce platelet contamination and results in shorter acquisition on mass cytometer, reduces detector wear and tear and ultimately it has a positive impact on data quality and ease of analysis (by removing platelets and platelets to cell aggregates).

Acknowledgments

This work is main output of Ministry of Health of the Czech Republic project no. 15-26588A. Tomas Kalina was sup-ported as an ISAC Scholar 2011-2015. CyTOF2 instrument was financed through Operational Program Prague Competi-tiveness (CZ.2.16/3.1.00/21540). Infrastructure is supported by Ministry of Education, Youth and Sports NPU I no. LO1604 and a project 00064203 University Hospital Motol, Prague, Czech Republic. M.L.K. and K.S. are employees of IBA GmbH and were involved in the development of the pro-tocol tested here. H.S. is a board member of IBA GmbH. IBA GmbH kindly supplied the reagents free of charge for the study. We thank to Nada Brdickova for proofreading and valu-able discussions.

Literature Cited

× Lad PM. A method for the preparation of mononuclear cells devoid of platelet con-tamination and its application to the evaluation of putative c-receptors in normal and asthmatic subjects. J Immunol Methods 1988;110:193–202.

β Ruitenberg JJ, Mulder CB, Maino VC, Landay AL, Ghanekar SA. VACUTAINER CPT and Ficoll density gradient separation perform equivalently in maintaining the quali-ty and function of PBMC from HIV seropositive blood samples. BMC Immunol 2006;7:11. doi: 10.1186/1471-2172-7-11

β Tamul KR, Schmitz JL, Kane K, Folds JD. Comparison of the effects of Ficoll-Hypaque separation and whole blood lysis on results of immunophenotypic analysis of blood and bone marrow samples from patients with hematologic malignancies. Clin Diagn Lab Immunol 1995;2:337–342.

β Stemberger C, Dreher S, Tschulik C, Piossek C, Bet J, Yamamoto TN, Schiemann M, Neuenhahn M, Martin K, Schlapschy M, et al. Novel serial positive enrichment tech-nology enables clinical multiparameter cell sorting. PLoS One 2012;7:e35798. doi: 10.1371/journal.pone.0035798

β Kalina T, Flores-Montero J, Lecrevisse Q, Pedreira CE, van der Velden VHJ, Novakova M, Mejstrikova E, Hrusak O, Bottcher€ S, Karsch D, et al. Quality assess-ment program for EuroFlow protocols: Summary results of four-year (2010-2013) quality assurance rounds. Cytometry Part A 2015;87A:145–156.

β Mandy F, Brando B. Enumeration of absolute cell counts using immunophenotypic techniques. Curr Protoc Cytom 2001; Chapter 6: Unit 6.8. doi: 10.1002/0471142956.cy0608s13

β Roederer M, Nozzi JL, Nason MC. SPICE: Exploration and analysis of post-cytometric complex multivariate datasets. Cytometry Part A 2011;79A:167–174.

β Levy S, Todd SC, Maecker HT. CD81 (TAPA-1): A molecule involved in signal trans-duction and cell adhesion in the immune system. Annu Rev Immunol 1998;16:89– 109.

α Amir ED, Davis KL, Tadmor MD, Simonds EF, Jacob H. viSNE enables visualization of high dimensional data and phenotypic heterogeneity of leukemia. Nat Biotechnol 2014;31:545–552.

α Appay V, Reynard S, Voelter V, Romero P, Speiser DE, Leyvraz S. Immuno-monitor-ing of CD81 T cells in whole blood versus PBMC samples. J Immunol Methods 2006;309:192–199.

α Levering WHBM, van Wieringen WN, Kraan J, van Beers WAM, Sintnicolaas K, van Rhenen DJ, Gratama JW. Flow cytometric lymphocyte subset enumeration: 10 years of external quality assessment in the Benelux countries. Cytometry B Clin Cytom 2008;74B:79–90.

α Assumpcio Romeu M, Mestre M, Gonzalez L, Valls A, Verdaguer J, Corominas M, Corominas M, Bas J, Massip E, Buendia E, et al. Lymphocyte immunophenotyping by flow cytometry in normal adults. J Immunol Methods 1992;154:7–10.

α Renzi P, Ginns LC. Analysis of T cell subsets in normal adults. J Immunol Methods 1987; 98:53–56.

α Prince HE, York J, Kuttner DK. Reduction of escapee formation in flow cytometric analysis of lymphocyte subsets. J Immunol Methods 1994;177:165–173.

α Gratama JW, van der Linden R, van der Holt B, Bolhuis RL, van de Winkel JG. Anal-ysis of factors contributing to the formation of mononuclear cell aggregates (“escapees”) in flow cytometric immunophenotyping. Cytometry 1997;29:250–260.

α Werfel T, Witter W, Gotze€ O. CD11b and CD11c antigens are rapidly increased on human natural killer cells upon activation. J Immunol Am Assoc Immnol 1991;147: 2423–2427.

α Aranami T, Miyake S, Yamamura T. Differential expression of CD11c by peripheral blood NK cells reflects temporal activity of multiple sclerosis. J Immunol 2006;177:5659–5667.

Příloha 9.4

proteins
STRUCTURE FUNCTION BIOINFORMATICS

Human interleukin-23 receptor antagonists derived from an albumin-binding domain scaffold inhibit IL-23-dependent ex vivo expansion of IL-17-producing T-cells

Milan Kuchar,[1] Lucie Vankova,[1] Hana Petrokova,[1] Jirı Cerny,[2] Radim Osicka,[3]* Ondrej Pelak,[4] Hana Sıpova,[5] Bohdan Schneider,[2] Jirı Homola,[5] Peter Sebo,[1,3] Tomas Kalina,[4] and Petr Maly[1]*

‡ Laboratory of Ligand Engineering, Institute of Biotechnology AS CR, v. v. i., Vıdenska 1083, 142 20 Prague, Czech Republic

‡ Laboratory of Molecular Recognition, Institute of Biotechnology AS CR, v. v. i., Vıdenska 1083, 142 20 Prague, Czech Republic

‡ Institute of Microbiology AS CR, v. v. i., Vıdenska 1083, 142 20 Prague, Czech Republic

‡ Department of Pediatric Hematology and Oncology, 2nd Faculty of Medicine, Charles University and University Hospital Motol, Prague, Czech Republic

‡ Institute of Photonics and Electronics AS CR, v. v. i., Chaberska 57, 182 51, Prague, Czech Republic

ABSTRACT

Engineered combinatorial libraries derived from small protein scaffolds represent a powerful tool for generating novel binders with high affinity, required specificity and designed inhibitory function. This work was aimed to generate a collection of recombinant binders of human interleukin-23 receptor (IL-23R), which is a key element of proinflammatory IL-23-mediated sig-naling. A library of variants derived from the three-helix bundle scaffold of the albumin-binding domain (ABD) of streptococcal protein G and ribosome display were used to select for high-affinity binders of recombinant extracellular IL-23R. A collection of 34 IL-23R-binding proteins (called REX binders), corresponding to 18 different sequence variants, was used to identify a group of ligands that inhibited binding of the recombinant p19 subunit of IL-23, or the biologically active human IL-23 cytokine, to the recombinant IL-23R or soluble IL-23R-IgG chimera. The strongest competitors for IL-23R binding in ELISA were confirmed to recognize human IL-23R-IgG in surface plasmon resonance experiments, estimating the binding affinity in the sub- to nano-molar range. We further demonstrated that several REX variants bind to human leukemic cell lines K-562, THP-1 and Jurkat, and this binding correlated with IL-23R cell-surface expression. The REX125, REX009 and REX128 variants competed with the p19 protein for binding to THP-1 cells. Moreover, the presence of REX125, REX009 and REX115 variants significantly inhibited the IL-23-driven expansion of IL-17-producing primary human CD4[1] T-cells. Thus, we conclude that unique IL-23R antagonists derived from the ABD scaffold were generated that might be useful in designing novel anti-inflammatory biologicals.

Proteins 2014; 82:975–989.

Key words: cytokine; psoriasis; engineered binding protein; protein scaffold; combinatorial library; ribosome display.

INTRODUCTION

Autoimmune diseases such as psoriasis, Crohn0s disease, rheumatoid arthritis, or multiple sclerosis have recently been found to be associated with IL-23-mediated signaling promoted by IL-23 receptor-expressing TH-17 and other lymphocyte subsets.[1–7] In these cell types, dendritic cell-released IL-23 cytokine, consisting of a unique p19 subu-nit and a common p40 subunit shared with IL-12,[8,9] acti-vates signaling via interaction of the p19 subunit with its cognate cell surface receptor, IL-23R, while the p40 subu-nit of IL-23 binds to IL-12 receptor b1[10,11] (Fig. 1). Syn-ergistic tethering of the IL-23 heterodimer to both receptor units leads to receptor heterodimerization fol-

Grant sponsor: Czech Science Foundation; Grant numbers: P303/10/1849 (to P.M.) and P302/11/0580 (to R.O.); Grant sponsor: Institutional Research Concept; Grant numbers: AV0Z50520701, RVO 86652036, and RVO 61388971; Grant sponsor: Motol Hospital Project (to T.K. and O.P.); Grant numbers: 00064203 and UNCE 204012. This study was supported by BIOCEV CZ.1.05/1.1.00/02.0109 from the ERDF.

*Correspondence to: Petr Maly, Institute of Biotechnology AS CR, v.v.i., Vıdenska 1083, 142 20 Prague 4, Czech Republic. E-mail: petr.maly@img.cas.cz Received 1 June 2013; Revised 30 October 2013; Accepted 4 November 2013 Published online 12 November 2013 in Wiley Online Library (wileyonlinelibrary. com).

DOI: 10.1002/prot.24472

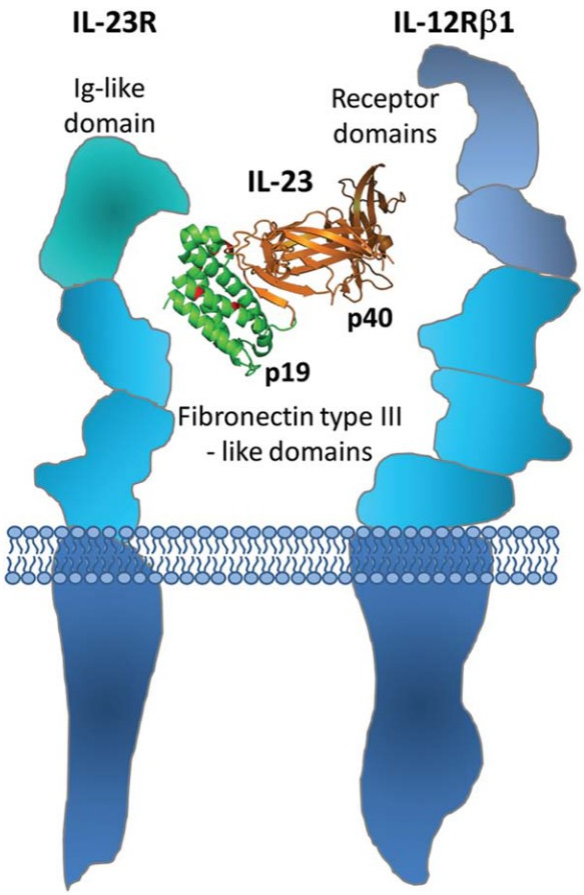

Figure 1

Scheme demonstrating the interaction of IL-23 cytokine with IL-23 receptor complex. The alpha subunit of IL-23, the p19 protein, interacts with IL-23 receptor domains, while the beta subunit, the p40 protein, binds to a putative cytokine homology region of IL-12b1 receptor domains, thus promoting intracellular signaling.

lowed by quaternary complex formation and triggering of the Jak/Stat signaling cascade, involving Jak2, Tyk2, Stat1, Stat3, Stat4, and Stat5.[10] Transduction of signal activates the transcription machinery and results in secretion of a cocktail of inflammatory modulators such as IL-17A, IL-17F, IL-22, and of certain chemokines that stimulate kera-tinocytes and other cell types, thereby playing a pivotal role in pro-inflammatory processes (reviewed in Ref. 12).

Efficient therapeutic intervention, preventing hyperproliferation of keratinocytes in clinical manifestations of psoriasis, depends on the blockade of interaction between p19/p40 subunits of IL-23 and their cognate cell membrane receptors.[13–15] Recently it has been demonstrated that monoclonal antibody-based drug Stelara (ustekinumab, Janssen Biotech), blocking the p40 subunit of IL-23 and preventing it from the interaction with IL-12 receptor b1, reached an excellent efficacy in the treatment of medium to severe form of psoriasis.[16–18] However, this drug inhibits the binding of the common p40 subunit, shared both by IL-12 and IL-23, and thus interferes with two different signaling pathways. This often leads to complications, including cardiovascular side effects or higher risk of cancer development. Novel therapeutic strategies, therefore, require development of novel IL-23R antagonists that will separate IL-23-mediated signaling from the IL-12 cascade, thus preserving T_H-1 cell differentiation and immunity. Recently, anti-p19 specific antibodies MK-3222 (Merck), CNTO 1959 (Janssen Biotech) and AMG 139 (Amgen/MedImmune)[19] have been developed.

As an alternative to conventional monoclonal antibody-based drugs, artificial ligands derived from small protein scaffolds attract attention as robust diagnostic probes and next generation protein therapeutics.[20–22] Among different structure-instructed approaches, three-helix bundle scaf-folds have recently demonstrated sufficient thermal stability, solubility and mutability for being used as a proof-of-concept domain suitable for generation of highly complex combinatorial libraries.[23–26] The well-established Affibody molecules originally selected from Protein A domain-Z-based libraries by phage display selection approaches are currently being used as practical binders for in vitro detec-tion, in vivo diagnostics or high-affinity bioanalytical proce-dures.[27–29] Preservation of folding function together with easy scaffold modifications and low molecular weight, allowing excellent tissue penetration, move the Affibody-derived binders close to the therapeutic use.

The albumin-binding domain of streptococcal protein G[30–33] is another example of three-helix bundle scaffold being successfully used for the construction of combinatorial libraries. Recently we have demonstrated that randomization of 11 residues of a flat helical surface, formed by two helices with an inter-link loop (Fig. 2), was sufficient to yield a combinatorial library of a theoretical complexity of 10^{16} codon variants that was then successfully used for the selection of high-affinity binders of human IFN-g.[34] In this type of library, natural HSA-binding affinity of the ABD domain was compromised in favor of newly engineered affinity for the chosen target. Alternatively, another group randomized 11 residues of a different ABD scaffold surface to generate a combinatorial library that yielded new affinity yet preserved the original HSA binding. This type of "dual-affinity library" was used to select binders of human TNF-a[35] and ErbB3.[36]

IL-23 receptor belongs to the class-I cytokine receptor family and shares typical features with tandem fibronectin-type III (FnIII) domains containing a hallmark pattern of disulfide bonds and WQPWS sequence tag sim-ilar to a conserved WSXWS cytokine receptor consensus located in the transmembrane-proximal FnIII domain.[10] Both domains form a cytokine-binding homology region (CHR) which, in concert with a terminal Ig-like domain, is believed to play a substantial role in IL-23 binding.

The molecular structure of the IL-23/IL-23R complex is not available yet, therefore, designing efficient inhibi-tors of IL-23 function with a promising therapeutic

potential remains cumbersome. Here we describe generation of a set of novel recombinant antagonists of the human IL-23 receptor. Their inhibitory potency on IL-23 function is demonstrated on several arrangements of in vitro binding assays, cell-surface competition experiments and ex vivo functional assays. Our data further document that the three-helix bundle scaffold of ABD is suitable for development of anti-inflammatory IL-23 receptor-based next generation therapeutics.

MATERIALS AND METHODS

Antibodies and detection agents

Monoclonal antibodies (mAbs) anti-human IL-23R-allophycocyanin (APC) (mouse IgG2b) specific for the human IL-23 receptor and IgG2b isotype control-APC (mouse IgG2b) were obtained from R&D Systems, Minneapolis, MN. Mouse anti-p19 mAb was purchased from Biolegend, San Diego, CA. Cy5-conjugated goat anti-mouse IgG ($F(ab^0)_2$ fragment) was obtained from Jackson ImmunoResearch Laboratories, West Grove, PA. Streptavidin-phycoerythrin was purchased from eBioscience, San Diego, CA.

Cell lines and growth conditions

The cell lines used in the experiments were a human acute monocytic leukemia cell line, THP-1 (ATCC number: TIB-202), a human leukemic cell line, K2562 (ATCC number: CCL-243) and a human T-cell lym-phoma cell line, Jurkat (ATCC number: TIB-152). The cells were grown in RPMI-1640 medium (Sigma-Aldrich, St. Louis, MO) supplemented with 10% fetal calf serum (FCS) (GIBCO, Grand Island, N.Y.) and antibiotic anti-mycotic solution (ATB) (Sigma-Aldrich, St. Louis, MO).

Production of recombinant IL-23R

cDNA coding for the extracellular part (fragment Gly24-Asn350) of the human IL-23 receptor (IL-23R, GenBank: AF461422.1) was amplified by PCR using for-ward primer IL23Rex-F-Nco-his (ATTACCATGGGCAG CAGCCACCATCATCATCATCACAGCAGCGGAATTACA AATATAAACTGCTCTGG), containing the start codon and the His_6-tag sequence, and a reverse primer IL23Rex-R-Xho(GGGCACCTTACTTCTGACAACTGAC TCGAGATAT) bearing the TGA stop codon. The resulting PCR product was inserted into the pET-28b vector (Novagen, Germany) using NcoI and XhoI clon-ing sites and introduced in Escherichia coli TOP10 cells. The obtained plasmid was used for exIL-23R protein production in E. coli SHuffle strain (SHuffleV_R T7 Express Competent E. coli, New England Biolabs, Ipswich, MA). Bacteria were grown in liquid LB media with kanamycin (60 mg/L) at 30 C, induced with 1 mM isopropyl-b-D-thiogalactopyranoside (IPTG). The

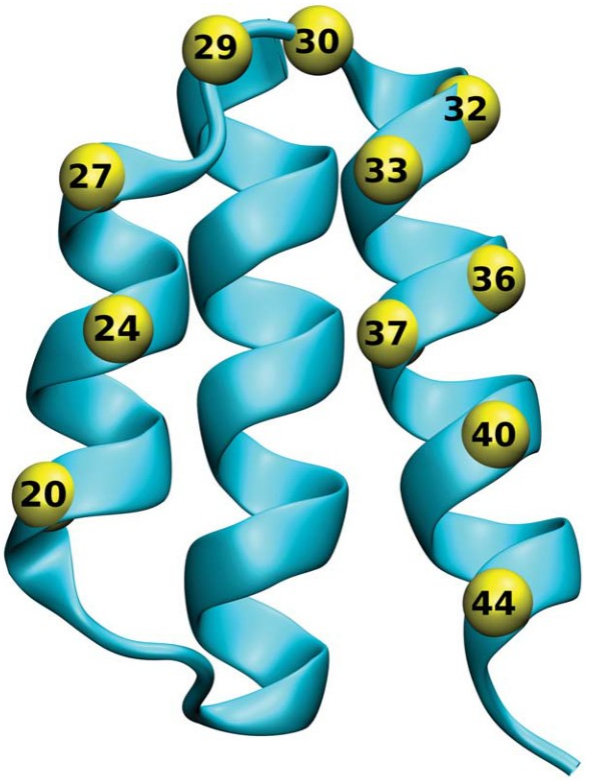

Figure 2

Location of randomized positions in the ABD scaffold. The protein structure of the ABD domain of streptococcal protein G (PDBID 1GJT) is shown in ribbon representation, with the Ca positions of the 11 residues selected for randomization shown as yellow spheres.

exIL-23R protein was extracted from isolated inclu-sion bodies with 8M urea in TN buffer (50 mM Tris, 1 mM NaCl, pH 5 8.0) and purified by Ni-NTA affinity chromatography.

For protein production targeted into bacterial periplasm, the exIL-23R cDNA was inserted downstream of the pelB leader sequence into the pET-26b vector (Novagen, Germany) using the same restriction sites as above and introduced into the E. coli BL21 (kDE3) strain. The LB broth culture with kanamycin (60 mg/L) was grown at 30 C to reach cell density OD_{600} 5 1.0, protein production was induced by 1 mM IPTG, and protein was harvested after 4 h. The resulting expression led to the production of an insoluble protein that was extracted after the sonication by 8M urea in the TN buffer and purified on a Ni-NTA column.

Production of recombinant p19 subunit of IL-23

The DH-p19 recombinant form of the p19 subunit of IL-23 (calculated M_W 23.3 kDa) was produced in fusion to an N-terminal double-His_6-TEV purification tag con-taining the TEV protease consensus cleavage site.

Synthetic, codon-optimized p19 cDNA (GENEART, Germany) was inserted into the pET-28b vector as a NcoI-XhoI fragment and the DH-p19 protein was produced in E. coli BL21 (kDE3) host cells. The DH-p19 protein was extracted from inclusion bodies and purified in Ni-NTA agarose.

Alternatively, soluble p19 protein was produced in the form of a protein fusion to maltose-binding protein (MBP) carrying a double-His_6-tag at the N-terminus (DH-MBP-p19, calculated M_W 69 kDa). Primers p19-F-NheI (GGGCTAGC TAGCAGAGCTGTGCCTGGGGGC) and p19-R-XhoI (GCGCCTCGAGGGGACTCAGGGTTGC TGCTC) were used to amplify DNA encoding p19 for insertion into a pET28b-derived vector into which sequences coding for double-His_6–MBP-TEV-MCS-TEV-His_6 were introduced. The double-His_6–MBP-TEV-p19-TEV-His_6 fusion protein was produced in the cytoplasmic fraction of E. coli BL21 (kDE3) cells and purified on a 5 mL His-Trap column using AKTA purifier (GE Healthcare, UK) and stepwise gradient of 250, 500, and 1000 mM imidazole.

Test of the binding activity of exIL-23R and p19 by ELISA

The recombinant extracellular portion of the IL-23 receptor (exIL-23R) or the p19 protein were immobilized directly on the NUNC Polysorp 96-well plate surface in coating buffer (100 mM bicarbonate/carbonate solution, pH 5 9.6) at a concentration of 5 to 10 mg/mL at 7 C overnight. The plate was washed with PBS buffer containing 0.05% Tween (PBST) and blocked by 1% BSA in the same buffer (PBSTB). Serial dilutions of purified DH-MBP-p19 or DH-p19 recombinant proteins were prepared in PBSTB buffer and p19 binding was detected using mouse anti-human IL-23 (anti-p19) polyclonal antibody followed by goat anti-mouse IgG horseradish peroxidase (HRP) conjugate (BioLegend, San Diego, CA), both diluted in PBSTB 1:1000. exIL-23R binding to immobilized DH-MBP-p19 was detected using goat anti-IL-23R polyclonal antibody (1:250) followed by secondary rabbit anti-goat HRP conjugate (1:1000) (R&D Systems, Minneapolis, MN). OPD substrate (Sigma-Aldrich, St. Luis, MO) was used as HRP substrate in citrate buffer (3.31% sodium citrate tribasic dihydrate, phosphoric acid, pH 5 5.0), reactions were stopped with 2M sulfuric acid and absorbance was read at 492 nm.

ABD library construction and ribosome display selection of REX binders

Combinatorial DNA library was generated as described previously.[34] HPLC-purified synthetic oligonucleotides were used. The forward primer ABDLIB-setB1c (5^0-TTA GCTGAAGCTAAAGTCTTAGCTAACAGAGAACTTGACA AATATGGAGTAAGTGAC-3^0) and the reverse primer setB-rev (5^0-ACCGCGGATCCAGGTAA-3^0) were used for PCR. The latter had distinct codons randomized at defined positions (5^0-ACCGCGGATCCAGGTAAMNNAG CTAAAATMNNATCTATMNNMNNTTTTACMNNMNN AACMNNMNNGGCMNNGTTGATMNNGTTCTTGTA MNNGTCACTTACTCCATATTTGTC-3^0), in which M represents C/A, and N any nucleotides out of A, G, C, or T. To serve as a protein spacer for ribosome display, the tolA gene (GENE ID: 946625 tolA) was amplified from E. coli K12 strain genomic DNA, using the primer pairs ABDLIB-tolA-link (5^0-TTACCTGGATCCGCGGTCGGTTC GAGCTCCAAGCTTGGATCTGGT GGCCAGAAGCAA-3^0) and tolArev (5^0-TTTCCGCTCGAGCTACGGTTT GAAGT CCAATGGCGC-3^0). The obtained products were linked to the randomized ABD sequences using amplification with primer pairs EWT5-ABDfor1 (5^0-TTCCTCCATGGGTATG AGAGGATCGCATCACCATCACCATCACTTAGCTGAAGC TAAAGTCTTA-3^0) and tolArev. To add the T7 promoter and ribosome binding site sequences, the obtained DNA fragment was subjected to further PCR amplifications with the set of primers T7B (5^0-ATACGAAATTAATACGACT CACTATAGGGAGACCACAACGG-3^0), SD-EW (5^0-GGGA GACCACAACGGTTTCCCTCTAGAAATAATTTTGTTTAA CTTTAAGAAGGAGATATACCATGGGTATGAGAGGATC G-3^0) and tolAk (5^0-CCGCACACCAGTAAGGTGTG CGGTTTCAGTTGCCGCTTTCTTTCT-3^0), generating a DNA library of ABD variants lacking the downstream stop codon. The assembled library was in vitro tran-scribed/translated in a single step reaction using E. coli extract (EasyXpress Protein Synthesis Mini Kit, QIA-GEN, Germany) and used for the selection of translated binders in ribosome display screening.

For the selection of binders, wells of Maxisorp plates (NUNC, Denmark) were coated with decreasing concentrations of recombinant H-exIL-23R protein (round 1 and 2: 25 mg/mL, round 3: 10 mg/mL, round 4: 4 mg/mL, round 5: 1 mg/mL) and blocked with 3% BSA. Preselection was performed in wells coated with BSA only. The plate wells were washed three times with TBS (50 mM Tris-HCl pH 7.4, 150 mM NaCl), followed by 10 times washing with cold WBT (50 mM Tris-acetate, pH 7.0, 150 mM NaCl, 50 mM MgAc with increasing concentra-tions of Tween-20 (round 1 and 2: 0.05%, round 3: 0.25%, round 4: 0.5%, round 5: 1%). To release mRNA from the bound ribosome complex, elution with elution buffer (50 mM Tris-acetate, pH 7.5, 150 mM NaCl, 50 mM EDTA) containing 50 mg/mL of Saccharomyces cere-visiae RNA as a carrier was performed. Purified RNA was transcribed into cDNA using specific reverse transcrip-tion with the setB-rev reverse primer, and annealing to the 3^0end of the ABD cDNA. Double-strand DNA was next obtained by PCR using EWT5-ABDfor1 and setB-rev primers. The final amplified DNA encoding selected ABD variants contained T7 promoter and RBS sequences and a truncated tolA fragment.

Two groups of ABD binder cDNA libraries, obtained by reverse transcription after the third or the fifth round

of a ribosome display selection campaign, were obtained and cloned as NcoI and XhoI fragments[34] in the pET-28b vector containing an in-frame inserted full length tolA DNA sequence. Later, the AviTag in vivo biotinyla-tion sequence (GLNDIFEAQKIEWHE) was added to the C-terminus of the TolA spacer to allow biotinylated pro-tein detection by streptavidin. The AviTag sequence was introduced using PCR with forward primer EWT5-ABDfor1 and reverse primer tolA-AVIrev1 (TTTCCGCT CGAGCTATTCGTGCCATTCGATTTTCTGAGCCTCGAA GATGTCGTTCAGGCCCGGTTTGAAGTCCAATGGCGC).

The final His_6-REX-TolA-AVI fusion proteins were pro-duced as biotinylated proteins in the E. coli BL21 (kDE3) BirA strain expressing biotin ligase (BirA) in the presence of 50 mM d-biotin in the LB medium and following induction with 2 mM IPTG. The soluble proteins were purified from cell extracts on Ni-NTA agarose columns.

For all binding assays, a control TolA fusion protein with the original albumin binding domain (ABDwt) was used as a negative control. To construct ABDwt with TolA and AviTag sequences (His_6-ABDwt-TolA-AVI), PCR amplification with ABDwt-tolA plasmid DNA as a template and forward primer EWT5-ABDfor1 (as mentioned above) and reverse primer ABDrev (TTACTAG-GATCCAGGTAATGCAGCTAAAATTTC) was used. The amplified PCR product was digested by NcoI and BamHI enzymes and ligated into the pET-28b vector carrying the tolA-AVI sequence downstream of the BamHI site. The resulting expressed His_6-ABDwt-TolA-AVI protein was produced and purified in the same way as REX var-iants described above.

Screening of IL-23R-binding REX variants by ELISA

For binding assays, selected clones were picked, the inserted sequence was verified by DNA sequencing and proteins were produced in the E. coli BL21 (kDE3) BirA strain as previously described,[34] where appropriate REX proteins purified on Ni-NTA columns were used. Two different sandwich layouts were used for the binding assays. In the first case, NUNC Polysorp plates were coated directly with exIL-23R protein (5 mg/mL, recombinant variant produced in E. coli SHuffle strain) in coating buffer at low temperature (7 C) overnight and the washed plates were blocked by PBSTB. The seri-ally diluted cell lysates or purified REX proteins were applied in PBSTB and the amount of bound biotinylated REX proteins was detected using streptavidin Poly-HRP conjugate (1:5000). In the second setup, the plates were coated with streptavidin (1 mg/mL) in coating buffer, and biotinylated REX proteins (5 mg/mL) were immobilized through binding to streptavidin. Serially diluted exIL-23R in PBSTB was added into the wells and receptor binding to immobilized REX variants was detected by goat anti-IL-23Rex polyclonal antibody (1:250) sandwich with secondary rabbit anti-goat HRP conjugate (1:1000, R&D Systems, Minneapolis, MN).

Sequence analysis and clustering of selected REX variants

DNA constructs of selected clones expressing full-length REX variants were sequenced. Amino acid multiple sequence alignment of all selected clones and construction of the similarity tree were performed using the ClustalW program. The tree is presented as a phenogram rendered by the Phylodendron online service (http://iubio.bio.indiana.edu/treeapp).

Competition ELISA assay

Maxisorp or Polysorp plates (NUNC, Denmark) were coated with recombinant H-exIL-23R or pelB-exIL-23R and binding of DH-MBP-p19 or DH-p19 as analytes was detected using antibodies as above. Alternatively, plates were coated with DH-MBP-p19 or DH-p19 and binding of IL-23R variants was detected using the corresponding antibod-ies; 20 nM DH-MBP-p19, 50 nM DH-p19, and 60 nM exIL-23R or pelB-exIL-23R in PBSTB were used as constant concentrations of analytes in the experiments where the concentration of the competitor REX binders varied.

Three of the best inhibitory variants, REX125, REX115, and REX009, were examined for binding to immobilized recombinant human IL-23R-IgG chimera (R&D Systems, Minneapolis, MN), produced as soluble and glycosylated protein secreted by a mouse myeloma cell line. A Polysorp plate was coated with 1 to 2 mg/mL IL-23R-IgG chimera diluted in coating buffer, and 20 nM DH-MBP-p19 protein or 23 nM human IL-23 (R&D Systems, Minneapolis, MN) were used to compete with REX ligands.

Fluorescence-based thermal-shift assay

Protein samples (0.1 mg/mL) in HEPES, and 53 Sypro Orange dye (Sigma-Aldrich, St. Luis, MO) were added into 25 mL total volume. Using the real-time PCR Detection System CFX96 Touch (Bio-Rad Laboratories), the proteins were incubated in a thermal gradient from 20 C to 80 C at increments of 0.5 C and with 30 s-hold intervals. The degree of protein unfolding was monitored by the FRET (fluorescence resonance energy transfer) channel that captured the spectral properties of Sypro Orange unfolded protein complexes (excitation wavelength 470 nm and emission wavelength 570 nm). The data were analyzed by CFX Manager software and the melting temperatures were determined using the first derivative spectra.

Surface plasmon resonance measurement

Surface plasmon resonance measurements were carried out using custom SPR biosensors (Institute of Photonics

and Electronics, Prague, Czech Republic) with four independent sensing spots.[37] The REX proteins were immobilized to the SPR chip using the protocol described in Ref. 38. Briefly, the SPR sensor chip was coated with self-assembled monolayer of $HSC_{11}(EG)_2$-OH and $HSC_{11}(EG)_3OCH_2COOH$ alkenthiols. The functionalized SPR chip was mounted to the SPR sensor and all the subse-quent molecular interactions were monitored in real-time at temperature 25 C and flow rate 30 lL/min. The REX009, REX125 and ABDwt proteins were diluted in SA buffer (10 mM sodium acetate, pH 5.0 at 25 C) at 5 mg/mL concentration. Each protein was immobilized to a separate sensing spot via amide-bond-forming chemistry. The noncovalently bound proteins were then washed away with a buffer of high ionic strength (PBS_{Na}; 1.4 mM KH_2PO_4, 8 mM Na_2HPO_4, 2.7 mM KCl, 0.75M NaCl, pH 7.4 at 25 C). The remaining carboxylic groups were deactivated with 5-min injection of 1M ethanolamine-hydrochloride (pH 8.5). After a baseline was established in the SA buffer, the solution of IL23-R was pumped in the sensor for 10 min. The measurement was repeated on three different chips. The interaction kinetics was compensated for reference sensor response (measured in channel with ABD_{WT}) and analyzed with BiaEvaluation software (GE Healthcare, Uppsala, Sweden).

Detection of cell surface IL-23R and binding of REX variants, p19 or IL-23 to the surface of cultured human cells

All binding assays were performed in HBSS buffer (10 mM HEPES, pH 7.4, 140 mM NaCl, 5 mM KCl) comple-mented with 2 mM $CaCl_2$, 2 mM $MgCl_2$ and 1% (v/v) FCS (cHBSS) in 96-well culture plates (Nunc, Roskilde, Denmark).

For staining of the IL-23R molecules on the cell sur-face, 5×10^5 cells were incubated for 30 min at 4 C in 50 mL of cHBSS buffer containing anti-human IL-23R-APC (1:5 dilution) or isotype control-APC (1:5 dilution) mAbs. For REX binding assay, 5×10^5 cells were incu-bated in 100 mL of cHBSS with biotinylated REX binders or ABDwt controls (10 mg/mL) for 30 min at 4 C, washed with cHBSS, and the cell-bound biotinylated REX-TolA-AVI or ABDwt-TolA-AVI was stained with streptavidin-phycoerythrin (dilution 1:400) for 30 min at 4 C. For DH-p19 binding assay, 5×10^5 cells were incu-bated in 100 mL of cHBSS with or without DH-p19 (10 mg/mL) for 30 min at 4 C. The cells were washed with cHBSS and the cell-bound DH-p19 was stained with mouse anti-p19 mAb (1:50 dilution) for 30 min at 4 C and after washing with goat anti-mouse IgG antibody labeled with Cy5 (1:50 dilution) for 30 min at 4 C.

Cells were washed, resuspended in 100 mL of HBSS and analyzed by flow cytometry in a FACS LSR II instru-ment (BD Biosciences, San Jose, CA) in the presence of 5 mg/mL of propidium iodide. Appropriate gatings were used to exclude cell aggregates and dead cells and bind-ing data were deduced from the mean fluorescence inten-sities (MFI).

Competition between DH-p19 and REX ligands for binding to THP-1 cells

For blocking of REX binding to the IL-23 receptor molecule by DH-p19, THP-1 cells (2×10^5) were prein-cubated for 15 min at 4 C in the presence of serially-diluted DH-p19 in 50 mL of cHBSS buffer. Biotinylated REX-TolA-AVI clones (or ABDwt-TolA-AVI negative con-trol) were added to the cells in the continuous presence of DH-p19 in 50 mL of cHBSS buffer to a final concen-tration of 13 nM and incubated at 4 C for 30 min. The cells were washed with cHBSS and the bound biotinyl-ated REX ligands or ABDwt were detected by streptavidin-phycoerythrin conjugate (dilution 1:400) for 30 min at 4 C. Cells were washed, resuspended in 100 mL of HBSS and analyzed by flow cytometry as described above.

IL-23-dependent ex vivo expansion of human IL-17-producing T-cells in PBMC suspensions

Peripheral blood drawn into EDTA-containing tubes was used to obtain purified mononuclear cells (PBMCs) on Ficoll-Paque gradients (Pharmacia, Uppsala, Sweden). PBMCs were washed once with PBS and resuspended in complete RPMI 1640 media (RPMI 1640 supplemented with 10% heat-inactivated FCS, 100 U/mL penicillin, 100 lg/mL streptomycin sulfate and 1.7 mM sodium gluta-mate). PBMCs were adjusted to 2×10^6 cells/mL and activated on a 96-well plate pre-coated with anti-CD3 (MEM-57, 10 lg/mL, Exbio Praha a.s., Praha, Czech Republic) in the presence of co-stimulatory antibodies against CD28 and CD49d (1 lg/mL, BD Biosciences, San Jose, CA), in the presence of IL-23 (10 ng/mL) and IL-2 (100 U/mL). REX009, REX115, REX125, REX128 binders (7 lg/mL) or control ABDwt were added and cells were incubated for three days at 37 C. After overnight rest at 37 C, cells were re-stimulated again (as above) for 6 h at 37 C (last 4 h exocytosis was blocked with Brefeldin A (10 lg/mL, Sigma-Aldrich). Next, cells were stained with antibodies to CD8 Horizon V-500 (BDB) for 15 min in the dark, washed with PBS containing 0.1% sodium azide and 2% gelatin from cold fish (Sigma-Aldrich) and fixed using FACS lysing solution/FACS Perm 2 (BDB) according to the manufacturer0s instructions. Upon fur-ther washing, cells were next stained for CD3 (PerCP-Cy5.5, eBioscience, San Diego, CA), for CD4 (ECD, Immunotech, Marseille, France) and with antibodies for IFN-g (PE Cy7), IL-2 (APC), IL-17 (PB) (eBioscience) and CD154 (PE, Immunotech). Cells were washed again and measured in flow cytometr BD FACS Aria III (BDB). Absolute cell counts were obtained using BD Truecount

(BDB). Viable, nucleated cells were counterstained with Syto-16 and DAPI (Invitrogen).

RESULTS

Production of recombinant human IL-23R and p19 proteins

The human IL-23 receptor gene consists of 10 exons that code for a 629 amino acid-long transmembrane receptor molecule. For the purpose of being used as a target in ribosome display selection of ABD scaffold-derived ligands, we produced a recombinant form of the extracellular domain of IL-23R (exIL-23R) comprising the residues 24 to 350. This part of IL-23R contains five cysteine pairs encoded within sequences forming both fibronectin type III and terminal Ig-like domains. Therefore, the E. coli SHuffle strain supporting formation of disulphide bridges in bacterial cytoplasm was used to express the N-terminally His_6-tagged IL-23R (H-exIL-23R). The protein was extracted with 8 M urea from inclusion bodies formed in bacterial cells. Alternatively, we cloned the same receptor cDNA fragment into the pET-26b vector containing a periplasm-targeting pelB leader sequence (pelB-exIL-23R) and expressed the recep-tor in E. coli BL21 (kDE3) strain. However, the protein was also produced as insoluble fraction and was, there-fore, refolded from urea-containing extracts. Both pro-teins were affinity-purified by Ni-NTA chromatography and refolded by dilution from urea-solutions prior to use in ELISA binding assays and ribosome display selection. The identity of the proteins was confirmed by Western blots using anti-His and anti-IL-23R antibodies (data not shown).

For studies of the interactions between IL-23R and IL-23 cytokine, we also produced a recombinant form of the 170 amino acid residue-long p19 subunit of human IL-23. A 23 kDa fusion p19 protein, consisting of a mature portion of p19 with an N-terminal double-poly-histidinyl tag (DH-p19), was produced into inclusion bodies in E. coli cells, extracted with 8M urea, and DH-p19 was affinity purified by Ni-NTA chromatography. Its identity was confirmed by detection with anti-IL-23 anti-body on Western blots (data not shown).

In search for solubility-mediating modifications of the p19 protein using several different solubility-supporting fusion tags, the maltose-binding protein (MBP) in combination with a C-terminal modification were found to support the solubility of the produced p19-MBP fusion protein as the only found variant. In this case, the 69 kDa N-terminally double-His_6-MBP-p19 fusion protein contained a C-terminal prolongation, installing an additional 40 aa solubility-supporting sequence (LEKKTCTSR ASSTTTTTTEIRLLTKPERKLSWLLPPLSNN). Yet this modification was found unintentionally, all other tested C-terminal modifications, including removal of this sequence by a stop codon termination and replacement by a single-his tag, Streptag or FLAG tag sequence consensus, converted the DH-MBP-p19 protein into the insoluble form. Therefore, this soluble version of p19 was used for further studies as an affinity purified product.

To verify that the recombinant refolded exIL-23R protein still bound the recombinant form of the p19 subu-nit, ELISA experiments with immobilized exIL-23R were performed. As shown in Figure 3, both the refolded DH-p19 protein and the soluble purified DH-MBP-p19 specifically bound to immobilized H-exIL-23R in a saturable manner. This was further confirmed in a reversed setup where the coated DH-MBP-p19 or refolded DH-p19 protein bound the refolded soluble H-exIL-23R protein (data not shown). These data suggested that the refolded recombinant exIL-23R protein maintained the capacity to specifically bind the p19 subunit of IL-23. Therefore, this protein could be used as a target in ribosome display for selection of IL-23R-specific binders derived from the ABD scaffold.

Ribosome display selection of human IL-23R binders

Recently we have demonstrated that randomization of 11 residues in the ABD domain scaffold was sufficient for identification of binders of human interferon-g with nanomolar range of affinity.[34] We therefore used the same approach for the generation of a combinatorial ABD library of a theoretical complexity of 10^{14} protein variants (Fig. 2). In combination with ribosome display screening, we identified a collection of binders raised against recombinant H-exIL23R. To be able to produce in vivo biotinylated ABD variants required for verifica-tion of their binding affinity to H-exIL-23R by ELISA, ABD variants found after three- or five-round selection campaigns (called REX binders) were modified by instal-ling the AviTag sequence downstream of TolA C-terminus. ELISA-positive cell lysates of REX-TolA-AVI clones were selected for further analysis using Western blot. DNA sequences of 34 REX binders were sequentially analyzed and their amino acid sequence similarity com-pared. As shown in Figure 4, we identified 18 different REX variants, but displaying significant sequence redun-dancy. All 18 biotinylated REX-TolA-AVI proteins were purified in Ni-NTA agarose and the binding affinity to both immobilized H-exIL-23R and pelB-H-exIL-23R receptor proteins was analyzed using ELISA (data not shown). Analysis of several ELISA-negative REX-TolA-AVI variants by restriction digestion and DNA sequenc-ing revealed that these clones lack the ABD cDNA sequence, thus forming the spliced REX version His_6-TolA-AVI. One of such clones, called DABD, was purified and used for further experiments as another important negative control over the original His_6-ABDwt-TolA-AVI.

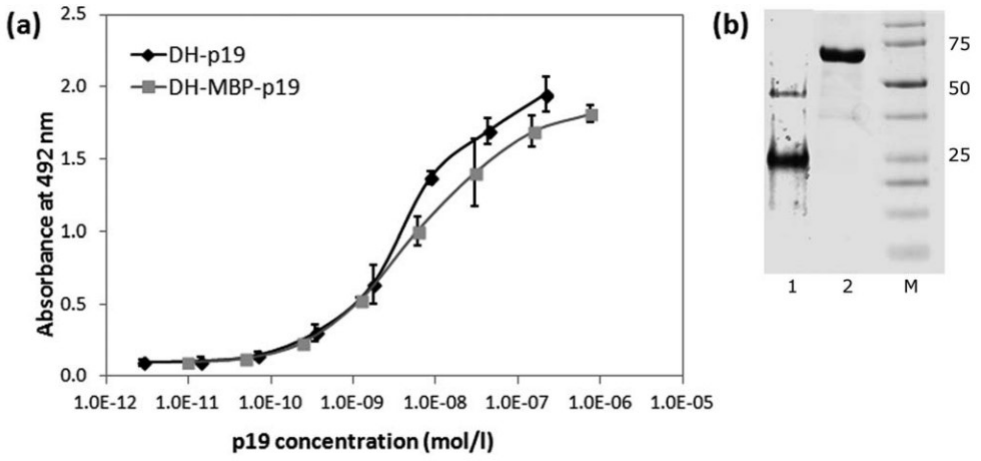

Figure 3

Recombinant extracellular IL-23 receptor binds the recombinant p19 subunit of IL-23. (a) The extracellular portion (residues 24 to 350) of human IL-23 receptor was expressed in E. coli SHuffle cells, purified and refolded from 8M urea extracts of inclusion bodies and coated on ELISA plates. Binding of soluble DH-MBP-p19 fusion protein or of refolded DH-p19 protein to immobilized receptor was detected by anti-human IL-23 (p19) polyclonal antibody sandwich with secondary anti-IgG-HRP. Error bars represent standard deviations. (b) SDS-PAGE of DH-p19 (lane 1) and DH-MBP-p19 (lane 2). The DH-p19 and DH-MBP-p19 proteins were purified from E. coli cell lysates on Ni-NTA and separated on 12,5% polyacrylamide gel stained by Coomassie blue. M indicates the protein marker.

Identification of inhibitory REX variants

Based on the results of binding assays performed for all 18 different REX-TolA-AVI variants, 15 clones of the complete REX collection were investigated for their ability to inhibit p19/IL-23 binding. To this goal, we used competition ELISA with the immobilized H-exIL-23R and a constant amount of DH-MBP-p19 as an analyte, spiked with an increasing level of the REX-TolA-AVI var-iants. We found that 11 of the 15 tested REX variants inhibited p19 binding in the micromolar to nanomolar concentration range. The results of the competition ELISA for the four best REX variants are presented in Figure 5. For these inhibitory variants, the sequence sim-ilarity comparison is documented in Table I. Sequence analysis of all tested variants indicated that two of the inhibitory variants, REX001 and REX009, contain one cysteine residue in the 11 randomized positions.

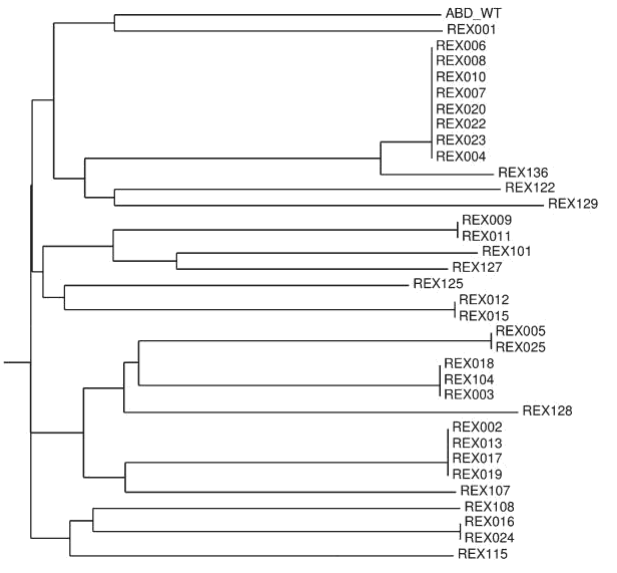

Figure 4

Similarity tree of polypeptide sequences of the obtained REX variants binding exIL-23R. Sequence analysis of 34 cloned REX binders of exIL-23R obtained by ribosome display selection revealed 18 unique sequence variants. For similarity analysis, only the sequences between residues 20 and 46 were compared, as the N-terminal amino acid posi-tions 1 to 19 were nonrandomized.

To further confirm the inhibitory potency of the REX binders, we performed competition ELISA with a different receptor-cytokine protein pair. REX inhibitors found in the previous setup of the competition ELISA also inhibited binding of the DH-p19 protein to the coated pelB-H-exIL-23R (not shown). In correlation with the result shown in Figure 5, all tested REX binders were found to suppress the p19 binding. To verify that the found competition potency of the tested REX clones can be attributed to the specific binding of the REX proteins to the refolded receptor molecule rather than to non-specific or misfolded protein binding, we performed additional competition assays with the same protein pairs but in the opposite ELISA layouts in which DH-MBP-p19 or DH-p19 were immobilized on the plastic plate. These results did confirm previous data (not shown).

To investigate whether inhibitory REX binders recognize the soluble and glycosylated form of IL-23R, we performed ELISA experiments with a commercial product of recombinant human IL-23R-IgG chimera (R&D Systems), secreted by an NS0-derived murine myeloma cell

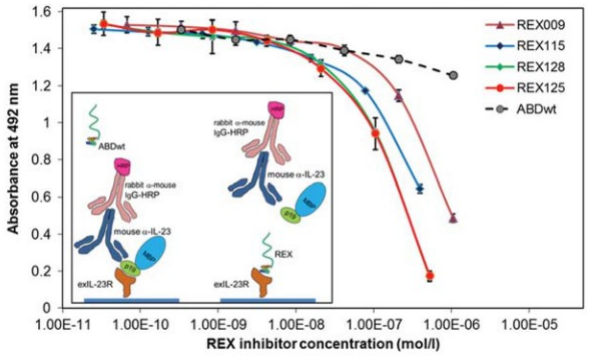

Figure 5

REX binders compete with the soluble recombinant p19 subunit of IL-23 for binding to immobilized exIL-23R. REX-TolA-AVI variants were serially diluted in PBST solution containing 20 nM DH-MBP-p19 as ligand of immobilized exIL-23R. Bound p19 was detected with anti-IL-23 (p19) polyclonal antibody sandwich with secondary anti-IgG-HRP. ABDwt-TolA-AVI, recognizing human serum albumin, served as a negative control. Error bars are shown as standard deviations.

line. As shown in Figure 6, increasing concentration of REX125, REX115, and REX009 binders decreased the binding of DH-MBP-p19 to the immobilized IL-23R-IgG. A similar inhibitory effect of the REX binders was also found for the recombinant Sf 21 (baculovirus)-derived human single-chain IL-23 (R&D Systems) (not shown). Thus, we conclude that we identified REX var-iants with the ability to suppress p19/IL-23 binding to IL-23R, as demonstrated in several layouts of direct ELISA.

Biophysical characterization of REX inhibitors

SPR biosensor binding analysis was used to further characterize the binding interactions between IL-23R and the REX ligands. The chip of a 4-channel SPR biosensor was functionalized with self-assembled monolayer of alkanethiols, to which His_6-REX-TolA-AVI and His_6-ABDwt-TolA-AVI proteins were attached. The response to IL-23R-IgG chimera interaction of such SPR biosensor is shown in Figure 7 for sensor surfaces functionalized with REX125, REX009 and control ABDwt proteins, respectively. It can be seen that the sensor response to IL-23R-IgG was much higher in the channels coated with the REX proteins than in the reference channel function-alized with ABDwt. Interestingly, the interaction of IL-23R-IgG with the REX variants was very sensitive to pH and salt composition of the running buffer. The complex was stable at pH 5.0 of the sodium acetate (SA) buffer, while it was very rapidly dissociated at pH 7.4 in PBS buffer. Similar results were obtained when IL-23R-IgG was immobilized to the sensor surface and REX proteins were flowed over the sensor (data not shown). The reference-compensated sensor responses to binding of IL-23R-IgG chimera to immobilized REX009, or REX125, respectively, at pH 5 were analyzed using an 1:1 interac-tion model in the kinetic BiaEvaluation software. Global fit of four concentrations in the range of 20–200nM indi-cated a dissociation constant K_d 5 1.3 6 0.7 3 10^{29}M for REX009. The binding affinity for REX125 could not be precisely determined due to a more complex interac-

tion mode, but it was estimated to be in the order of 10^{29}M.

To investigate the thermal stability of the strongest inhibitory binders, we performed the fluorescence-based thermal shift assay (data not shown). Melting tempera-tures (T_m) for REX125 and REX128 were found to be 56 and 56.5 C, respectively, and for REX009 between 50 and 53 C, while the Tm value for WT control was found to be 58 C. This suggested that the randomization of mutable residues of the ABD domain did not signifi-cantly affect the basic stability of the scaffold structure.

REX ligands competitively inhibit p19 subunit binding to the native IL-23 receptor on human cells

To explore whether the REX ligands bind to the native IL-23 receptor molecules on the cell surface, we first investigated cultured human K-562 and Jurkat leukemic cells for the expression of IL-23R. We found that both K-562 and Jurkat cells express IL-23R [Fig. 8(a,b)] and this expression is further increased upon T-cell activa-tion, as documented 24 h after the induction [Fig. 8(c)]. We also found that THP-1 cells express more IL-23R

Table I
Sequence Similarity Comparison of REX Binders

	20	21	22	23	24	25	26	27	28	29	30	31	32	33	34	35	36	37	38	39	40	41	42	43	44	45	46
ABDwt	Y	Y	K	N	L	I	N	N	A	K	T	V	E	G	V	K	A	L	I	D	E	I	L	A	A	L	P
REX009	Y	Y	K	N	R	I	N	P	A	C	H	V	L	S	V	K	S	N	I	D	W	I	L	A	S	L	P
REX115	V	Y	K	N	T	I	N	I	A	I	P	V	R	V	V	K	R	V	I	D	W	I	L	A	V	L	P
REX125	H	Y	K	N	W	I	N	P	A	R	R	V	R	P	V	K	W	L	I	D	A	I	L	A	A	L	P
REX128	R	Y	K	N	S	I	N	R	A	L	P	V	A	A	V	K	W	A	L	D	L	I	L	A	W	L	P

Parental nonmutated ABD (ABDwt) of streptococcal protein G (G148_GA3) was aligned with the randomized portions of sequenced REX clones that were selected in ribosome display for IL-23R binding and belong to the best binders. Grey boxes indicate the 11 positions at which the residues of ABD (aa 20 to 46) were randomized. The dark box marks an unintended mutation I38L found in REX128. In the nonrandomized N-terminal part of ABD (residues 1–19), the LAEAKVLANRELDKYGVSD amino acid sequence was present. Multiple alignment was performed in ClustalW.

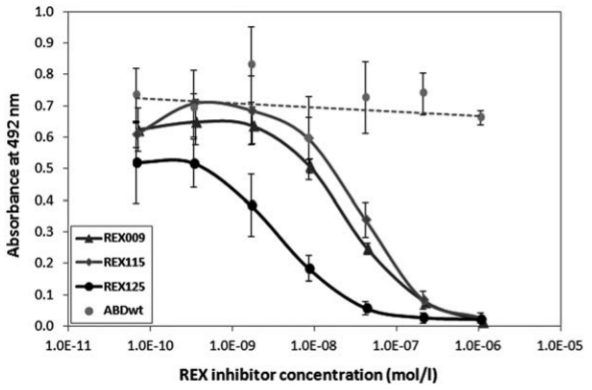

Figure 6

REX binders compete with p19 subunit-mediated binding of IL-23 to the IL-23R-IgG receptor chimera. The IL-23R-IgG receptor chimera was immobilized on an ELISA plate and serially diluted inhibitory REX-TolA-AVI ligands were used to compete for binding with 20 nM of DH-MBP-p19. Bound p19 was detected with anti-IL-23 (p19) polyclo-nal antibody sandwich with secondary anti-IgG-HRP. ABDwt-TolA-AVI served as a negative control. Error bars represent standard deviations.

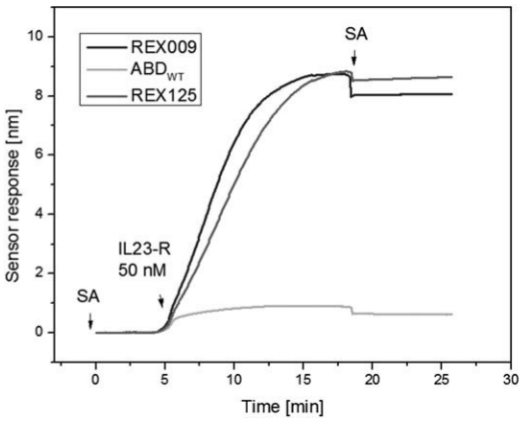

Figure 7

Immobilized REX ligands bind the soluble IL-23R-IgG receptor chi-mera. The REX-TolA-AVI variants REX009 and REX125, or ABDwt-TolA-AVI (ABD_{WT}), were attached to the surface of SPR sensor over which the IL-23R-IgG receptor chimera was passed at 50 nM concentra-tion. SA indicates sodium acetate buffer.

than K-562, as documented in Figure 9(a) by IL-23R-specific polyclonal antibody and, therefore, both these cell lines were further used as targets for REX ligand-binding assay. As shown in Figure 9(b), all of the tested REX variants bound to K-562 as well as THP-1 cells, and the extent of REX ligand binding correlated well with the observed level of IL-23R expression on the surface of both cell types [Fig. 9(a)]. To further demonstrate that binding of REX ligands correlates with IL-23R expres-sion, we performed a cell-surface binding test with Jurkat cells that express lower amounts of IL-23 receptor per cell than the K-562 cells [Fig. 9(c)]. As shown in Figure 9(d), all tested REX binders exhibited reduced binding to Jurkat cells in comparison with the K562 cells, in agree-ment with the reduced IL-23R expression on Jurkat cells. These results strongly suggested that the generated REX ligands can bind to native IL-23R molecules exposed on the human cell surface.

To corroborate this observation, we performed assays in which the p19 protein was allowed to compete with REX ligands for the binding to IL-23R on the cell sur-face. For this purpose, we used THP-1 cells expressing higher levels of IL-23R [Fig. 9(a)], to which also higher amounts of DH-p19 protein were bound than to K-562 cells [Fig. 10(a)]. As shown in Figure 10(b), at increasing concentrations of the DH-p19 protein, the binding of all

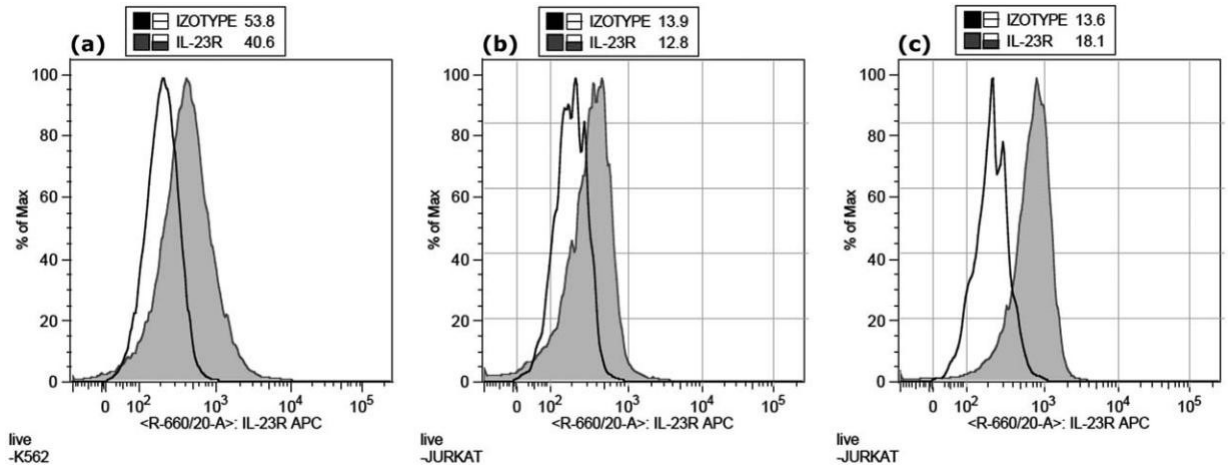

Figure 8

Expression of IL-23R on K562 cells (a), before stimulation on Jurkat cells (b) and 24 h after the induction of Jurkat cells with anti-CD3 (c). The cells were stained with anti-human IL-23R-APC or isotype-APC control mAbs and analyzed by flow cytometry.

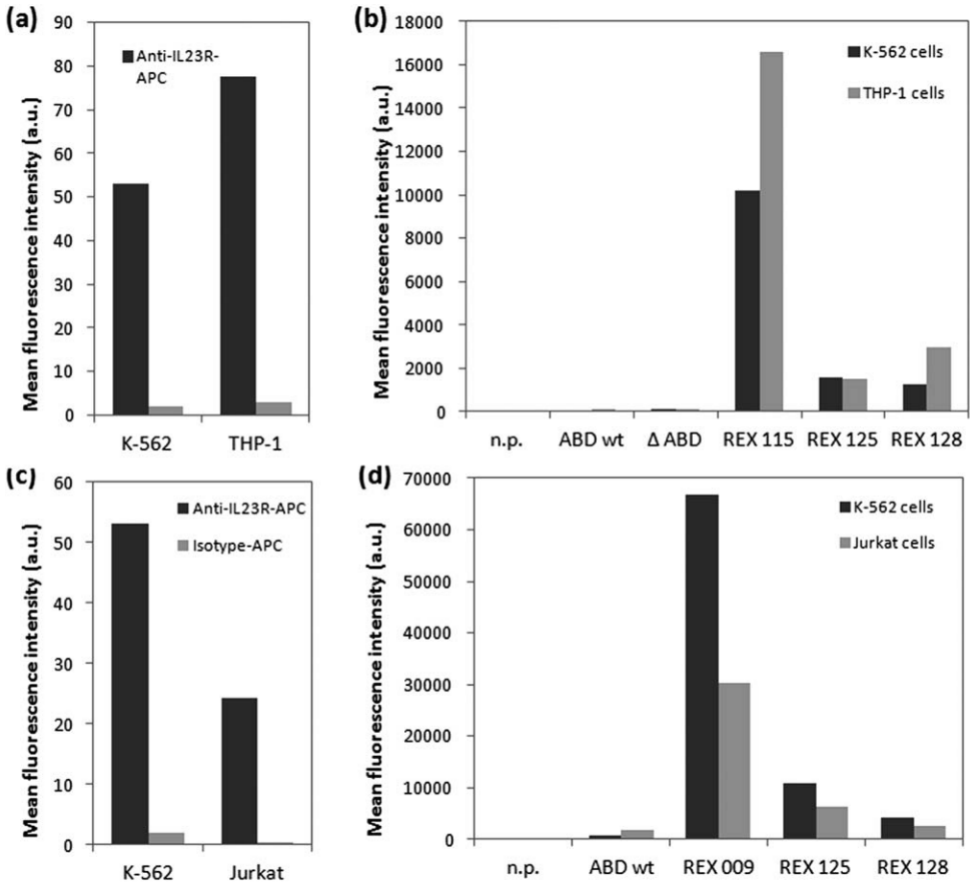

Figure 9

Binding of REX variants to human cell lines correlates with IL-23R expression levels. (a) Expression of IL-23 receptor molecules on the surface of cultured human K-562 and THP-1 cells was detected by flow cytometry using anti-human IL-23R-APC or isotype control-APC mAbs. (b) Binding of REX-TolA-AVI variants to K-562 and THP-1 cells. The cells were incubated with in vivo biotinylated REX-TolA-AVI proteins or negative ABD-TolA-AVI controls (ABDwt, DABD) and the cell-bound proteins were stained with streptavidin-phycoerythrin and analyzed by flow cytometry. In the n.p. control, the REX binders and ABD controls were omitted. (c) Comparison of IL-23 receptor expression on K-562 and Jurkat cell surface. The cells were stained with anti-human IL-23R-APC or isotype-APC control mAbs and analyzed by flow cytometry. (d) Comparison of REX ligand binding to K-562 and Jurkat cells. The cells were incubated with biotinylated REX variants or ABDwt control and cell-bound proteins were detected with streptavidin-phycoerythrin by flow cytometry.

three tested REX ligands to THP-1 cells was significantly inhibited.

REX binders inhibit IL-23-dependent ex vivo expansion of IL-17-positive CD41 T-cells

The sum of the above-outlined results indicated that at least several of the generated REX ligands could bind to native IL-23R molecules on human cells and block the p19-subunit-mediated binding of the IL-23 cytokine to its receptor. Therefore, we assessed ex vivo whether the REX ligands could inhibit the IL-23 signaling function on primary human T-cells. We determined whether blocking of IL-23R by excess of REX ligands would inhibit IL-23-mediated expansion of primary human Th-17 lymphocytes. Mononuclear cells were isolated from the blood of healthy donors and stimulated with anti-CD3 monoclonal antibody and co-stimulated by activating antibodies binding CD28 and CD49d in the contin-ued presence of the Th-17 conditioning cytokines IL-23 and IL-2. As shown in Figure 11, over the 3 days of ex vivo cultivation of PBMC suspensions, a marked decrease of Th-17 cell expansion (decrease of counts of IL-17-secreting, IFN-g non-secreting T-cells) was observed when excess of the REX ligands was present, as compared with mock treatment or presence of the ABD-WT con-trol. In PBMC suspensions, the enhancement of Th171 cells after IL-23-mediated induction is documented as a difference between non-induced cells (sample NO IL-23, 0.52 6 0.11, n 5 6, P 5 0.0001) and normalized counts of IL-23 stimulation (IL-23 only, 51), shown as a boxplot in Figure 11(b). The addition of ABD-WT as a control into the PBMC suspensions had little effect on Th-171 cell expansion (0.88 6 0.26, n 5 7, P 5 0.2892). In

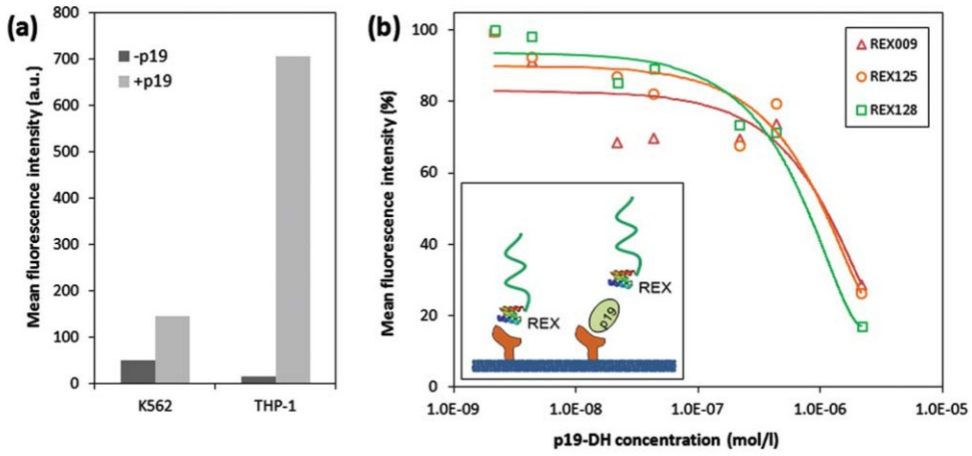

Figure 10

REX inhibitory variants compete with the p19 subunit of IL-23 for binding to THP-1 cells. (a) Comparison of DH-p19 protein binding to THP-1 and K-562 cells. Cell-bound DH-p19 molecules were detected by flow cytometry using a mouse anti-IL-23 mAb goat anti-mouse IgG antibody sandwich labeled with Cy5. (b) Micromolar concentrations of DH-p19 block binding of REX variants to THP-1 cells. The cells (2 3 10^5) were pre-incubated with indicated concentrations of DH-p19 before biotinylated REX-TolA-AVI or ABDwt-TolA-AVI control were added to a final concen-tration of 13 nM and incubation was continued for 30 min at 4 C. After washing of cells, the bound ligands were detected by flow cytometry using streptavidin-phycoerythrin. The results are representative of two independent but confirming experiments. Measured values for each of REX variants were supplemented by the particular polynomial trendline.

contrast, all tested REX variants significantly inhibited Th-171 cell expansion: REX009 (0.62 6 0.32, n 5 7, P 5 0.0559), REX115 (0.55 6 0.20, n 5 5, P 5 0.0074) and REX125 (0.42 6 0.17, n 5 5, P 5 0.0004), as documented in Figure 11(b).

To verify whether the observed inhibitory effect of REX binders in PBMC suspensions can be attributed to the T-cell-dependent cell expansion, we repeated the same experiment in samples with separated T cells isolated from the same PBMC donors. As shown in Figure 11(c), the IL-23-dependent Th-171 cell count enrichment was also detected (NO IL-23, 0.77 6 0.08, n 5 4, P 5 0.0116). T-cell suspensions with added ABD-WT control exhibited no inhibitory effect on T-cell expansion (0.99 6 0.26, n 5 4, P 5 0.9901). In striking contrast to this observation, REX variants demonstrated an immunosuppressive effect on T-cell expansion as follows: REX115 (0.69 6 0.17, n 5 3, P 5 0.0883), REX125 (0.65 6 0.16, n 5 3, P 5 0.0671) and REX009 (0.80 6 0.01, n 5 2, P 5 0.0139).

In summary, the collected data indicate that the tested REX variants inhibited IL-23-dependent Th-171 cell expansion to the level of no-IL-23-induced samples (REX009) or even below this level (REX115 and REX125) and this finding is valid for both PBMC and separated T-cell samples. While IL-23 was shown to promote development of Th-171 T-cells in man,[39] the mode of its action might be fixing the Th-17 commit-ment rather than "de novo" Th-17 development, survival or proliferation enhancement.[40] As shown here, REX ligands might block the IL-23 signaling function on human T-cells through selective binding and occupation of the IL-23 receptor.

DISCUSSION

In this work, we aimed to generate novel immunomodulatory binders suppressing the function of human IL-23 receptor, a crucial molecule of the IL-23-mediated signaling pathway. As a valuable alternative to conventionally developed neutralizing antibodies, we thought to use the three-helix bundle scaffold-derived combinatorial library of albumin-binding domain variants as a primary source for selection of IL-23 receptor binders. To this goal, we used our recently constructed high complex library that has been successfully used for selection of high-affinity binders of human IFN-g.[34] Using cam-paigns of ribosome display selection, we generated 18 sequence variants of high-affinity IL-23R binders, much less in comparison to the selection of IFN-g binders described before,[34] suggesting that a limited number of high-affinity epitopes were available as targets. This is further supported by a high redundancy of the found REX variants demonstrating that the selected high-stringency conditions used for high-affinity binder screening in ribosome display were properly adjusted. Among the 18 found sequence variants, 11 were observed to inhibit binding of p19 to the bacterial product of human IL-23R, suggesting that several surface-exposed epitopes are critical for the ligand-receptor interaction. Among seven best inhibiting clones, two (REX001 and REX009) contain a randomized cysteine residue located in the inter-loop between helices 2 and 3 (residues 29, 30). Another of the best inhibitory clones, REX125, includes an interesting randomized sequence pattern 24W-27P-29R-30R-32R-33P-36W with an intrinsic

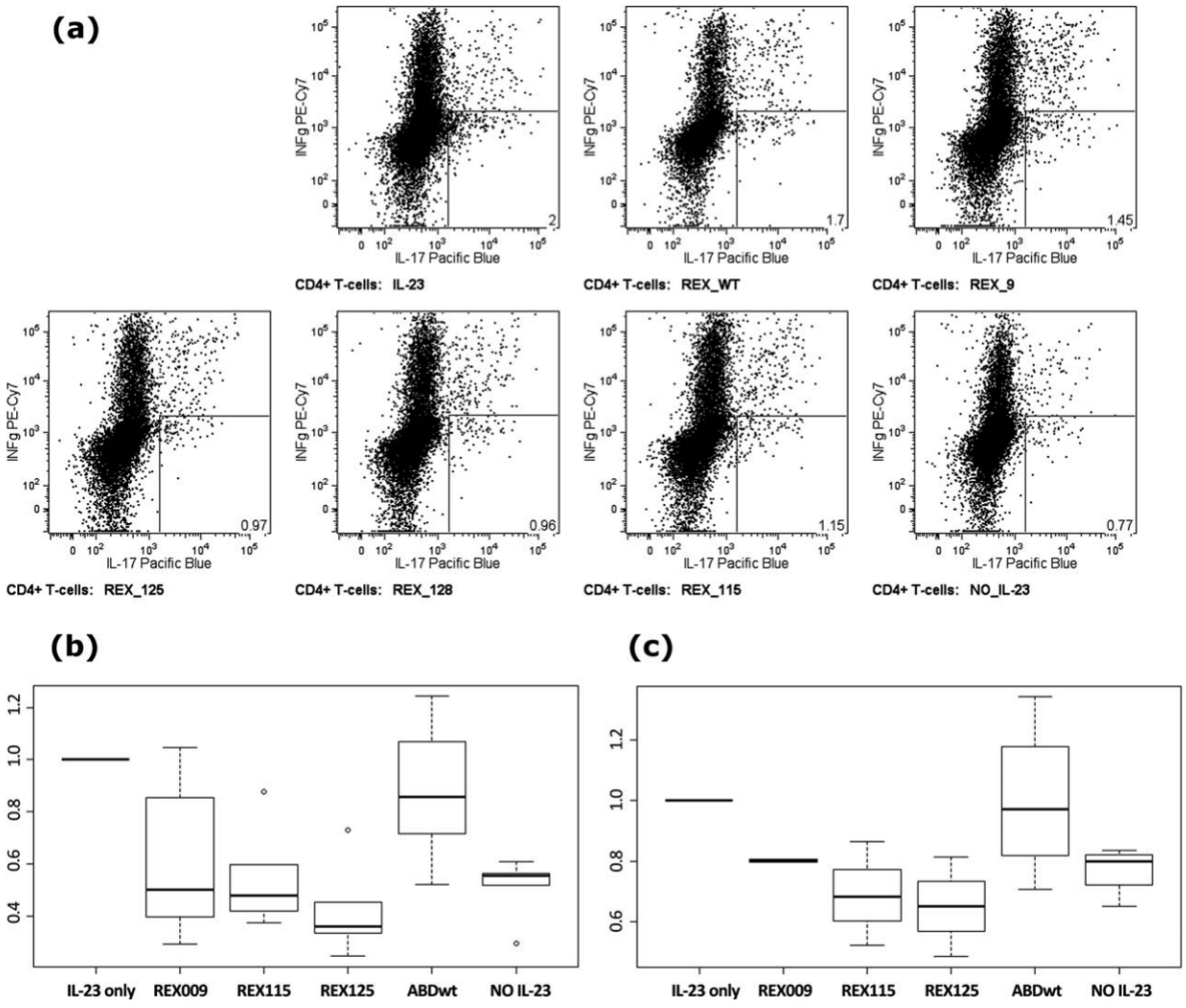

Figure 11

REX binders inhibit IL-23-dependent ex vivo expansion of IL-17-producing CD41 T-cells. PBMCs from seven healthy volunteers were activated using anti-CD3 and co-stimulation in the presence of IL-23 and IL-2 and in the presence or absence of indicated REX ligands for 3 days. (a) Detec-tion of IL-17-producing cells that were gated using FSC, SSC, CD3[1], and CD4[1]. The number in the right-hand bottom corner indicates the per-centage of the gated cell population producing solely IL-17 (IFN-g secretion marks T_H21 type response). (b, c) The amount of IL-17-producing cells recovered from PBMC (b) or separated T-cell (c) samples of healthy donors after 3 days of activation in the presence or absence of the REX ligands. Total cell numbers were normalized to cell counts in IL-23/IL-2-treated samples. Boxes range from 25th to 75th percentiles with a line at the median. Whiskers reach 10th and 90th percentiles. Outlying values are indicated as individual circles.

symmetry 24W-27P-30R-33P-36W between helices 2 and 3 that could be beneficial for the ligand binding. In addition, proline residues are known to break a-helical structures, so this may lead to a changed ABD scaffold geometry, affecting C- and N-terminal ends of the helices 2 and 3, respectively, and thereby to an increased flexibility of the inter-loop, supporting the binder[0]s affinity. Yet the detailed molecular structure of REX-IL-23R complexes needs to be further investigated, and installation of proline residues in amino acid positions 27–29-30–32-33 in the case of all the best inhibitory binders (REX009, REX115, REX125, REX128) attracts attention as cysteine and proline residues are being typically designed to be eliminated from the randomization during the combinatorial library construction.

Interestingly, the REX005 binder was found to inhibit the binding of the p19 protein to the used bacterial receptor products. This inhibitory effect was then confirmed in competition ELISA using a 46 amino acid synthetic form of ABD (not shown), excluding the possibility that the TolA spacer protein affects the bind-ing or inhibition. However, this clone does not bind to cell-surface IL-23R expressed in THP-1 and K-562 cells. It is possible that glycosylation of the Ig-like domain in the N-glycosylation consensus (residues 29, 47, and 81) or in the distal FnIII domain (residues 141 and 181)

prevents the binding to the cell-surface receptor. However, we cannot exclude that REX005 recognizes an unnatural epitope found in the bacterial receptor protein, yet this binder interacts with the cytoplasm-produced E. coli Shuffle strain as well as periplasm-targeted BL21 (kDE3) cell products.

To demonstrate that REX binders recognize cell-surface IL-23R, we thought to prepare cell transfectants expressing human IL-23R on the cell surface. To this goal we tested several different cell lines and found that all of them, including K-562, Jurkat, THP-1, HEK 293, COS-7, or CHO cells, to some extent bind anti-IL23R antibodies. In addition, several other human cell lines such as HeLa, A431 and NKT, or mouse NIH 3T3 cells, have been described to express IL-23R. Therefore, we decided to demonstrate specific binding of the generated REX variants using the correlation of cell-surface REX binding with IL-23R expression, in combination with a p19-specific competition binding assay. We clearly demonstrated that REX009, REX125 and REX128 compete with the p19 protein for binding to IL-23R-expressing and p19-protein-binding THP-1 cells. This level of evi-dence in combination with the ex vivo immunosuppress-ing effect on the PBMC-derived Th-171 cell expansion brought us to the conclusion that we generated a collection of novel antagonists of the IL-23 receptor. This is documented by a marked decrease of REX125-affected (decrease 52%, P 5 0.0029) and REX115-affected (38%, P 5 0.0317) Th-171 cell counts compared with the value of the control ABD-WT in PBMC cell suspensions, reaching the values below the counts of IL-23-non-stimulated samples. As ex vivo experiments were done with bacterial LPS-free REX proteins, we attribute the inhibitory effect solely to the function of the tested REX variants. The expansion of the Th-171 population in the presence of IL-23 is manifested by a comparison between IL-23-positive and IL-23-negative control samples, further suggesting that a significant amount of IL-231 cells have already been present in the no-IL-23 PBMC as well as separated T-cell samples. This is in correlation with the known fact[41] that also other cells, including gd T-cells, or certain natural-killer cell populations, express the IL-23 receptor. It is important to mention that REX binders tend to decrease the Th-171 cell counts even under the level of IL-23-negative control in the case of separated T-cell samples [Fig. 11(c)]. However, we also observed a slight decrease (12%) in the Th-171 cell counts when we used the ABD-WT control in compari-son to the untreated samples of PBMC [see sample IL-23 only, Fig. 11(b)], yet this decrease was absent in the sam-ples of separated T-cells (0.01% decrease, P 5 0.9901) [Fig. 11(c)]. We do not know the principal reason for this phenomenon found in the PBMC samples, but it could be caused by non-specific binding of ABD-WT to IL-23R or other cell receptors, especially under the con-ditions of more than 100-fold molar excess of the used ABD/REX molecules. This would correspond to the observed nonspecific binding of the ABD-WT control in ELISA experiments under the conditions of high concentrations. Another possibility is that the TolA spacer protein still maintains some effect on cell stimulation, although we show in Figure 9(b) that neither ABD-WT-TolA-AVI nor DABD-TolA-AVI control proteins substantially bind to the cell surface of human cells. This possibility was, however, excluded in further experiments in which we compared the inhibitory effect of a long ver-sion of REX009-TolA-AVI with a constructed short REX009-AVI variant (lacking the helical TolA spacer pro-tein), demonstrating that the same ex vivo inhibitory effect on T-cell expansion was reached with non-TolA-containing REX009 protein (data not shown).

Collectively, we demonstrated that the three-helix bundle scaffold of the ABD domain can be modified to generate high-affinity binders with immunomodulatory function. To our knowledge, this is the first example of described ABD-derived receptor antagonists with ex vivo immunosuppressive function. The unique REX inhibitory binders might be a useful clue for designing novel anti-IL-23R-based therapeutics, especially when the precise structural mode-of-function of the IL-23/IL-23R complex is not available. In addition, the small 5 kD size of the ABD domain brings new alternatives for skin-penetration-based drug delivery systems that might be essential for psoriasis treatment.

ACKNOWLEDGMENTS

The authors thank Petra Kadlc˘akova for excellent technical assistance.

REFERENCES

(xix) Oppmann B, Lesley R, Blom B, Timans JC, Xu Y, Hunte B, Vega F, Yu N, Wang J, Singh K, Zonin F, Vaisberg E, Churakova T, Liu M, Gorman D, Wagner J, Zurawski S, Liu Y, Abrams JS, Moore KW, Rennick D, de Waal-Malefyt R, Hannum C, Bazan JF, Kastelein RA. Novel p19 protein engages IL-12p40 to form a cytokine, IL-23, with biological activities similar as well as distinct from IL-12. Immunity 2000;13:715–725.

(xx) Cua DJ, Sherlock J, Chen Y, Murphy CA, Joyce B, Seymour B, Lucian L, To W, Kwan S, Churakova T, Zurawski S, Wiekowski M, Lira SA, Gorman D, Kastelein RA, Sedgwick JD. Interleukin-23 rather than interleukin-12 is the critical cytokine for autoimmune inflammation of the brain. Nature 2003;421:744–748.

(xxi) Langrish CL, Chen Y, Blumenschein WM, Mattson J, Basham B, Sedgwick JD, McClanahan T, Kastelein RA, Cua DJ. IL-23 drives a pathogenic T cell population that induces autoimmune inflammation. J Exp Med 2005;201:233–240.

(xxii) Chan JR, Blumenschein W, Murphy E, Diveu C, Wiekowski M, Abbondanzo S, Lucian L, Geissler R, Brodie S, Kimball AB, Gorman DM, Smith K, de Waal Malefyt R, Kastelein RA, McClanahan TK, Bowman EP. IL-23 stimulates epidermal hyperplasia via TNF and IL-20R2-dependent mechanisms with implications for psoriasis pathogenesis. J Exp Med 2006;203:2577–2587.

(xxiii) Capon F, Di Meglio P, Szaub J, Prescott NJ, Dunster C, Baumber L, Timms K, Gutin A, Abkevic V, Burden AD, Lanchbury J, Barker JN,

Trembath RC, Nestle FO. Sequence variants in the genes for the interleukin-23 receptor (IL23R) and its ligand (IL12B) confer protection against psoriasis. Hum Genet 2007;122:201–206.

× Vaknin-Dembinsky A, Balashov K, Weiner HL. IL-23 is increased in dendritic cells in multiple sclerosis and down-regulation of IL-23 by antisense oligos increases dendritic cell IL-10 production. J Immu-nol 2006;176:7768–7774.

× Duerr RH, Taylor KD, Brant SR, Rioux JD, Silverberg MS, Daly MJ, Steinhart AH, Abraham C, Regueiro M, Griffiths A, Dassopoulos T, Bitton A, Yang H, Targan S, Datta LW, Kistner EO, Schumm LP, Lee AT, Gregersen PK, Barmada MM, Rotter JI, Nicolae DL, Cho JH. A genome-wide association study identifies IL23R as an inflammatory bowel disease gene. Science 2006;314:1461–1463.

× Beyer BM, Ingram R, Ramanathan L, Reichert P, Le HV, Madison V, Orth P. Crystal structures of the pro-inflammatory cytokine interleukin-23 and its complex with a high-affinity neutralizing antibody. J Mol Biol 2008;382:942–955.

× Lupardus PJ, Garcia KC. The structure of interleukin-23 reveals the molecular basis of p40 subunit sharing with interleukin-12. J Mol Biol 2008;382:931–941.

× Parham C, Chirica M, Timans J, Vaisberg E, Travis M, Cheung J, Pflanz S, Zhang R, Singh KP, Vega F, To W, Wagner J, O^{0}Farrell AM, McClanahan T, Zurawski S, Hannum C, Gorman D, Rennick DM, Kastelein RA, de Waal Malefyt R, Moore KW. A receptor for the heterodimeric cytokine IL-23 is composed of IL-12Rbeta1 and a novel cytokine receptor subunit, IL-23R. J Immunol 2002;168:5699–5708.

× Kastelein RA, Hunter CA, Cua DJ. Discovery and biology of IL-23 and IL-27: related but functionally distinct regulators of inflammation. Annu Rev Immunol 2007;25:221–242.

× Boniface K, Blom B, Liu YJ, de Waal Malefyt R. From interleukin-23 to T-helper 17 cells: human T-helper cell differentiation revisited. Immunol Rev 2008;226:132–146.

× Toichi E, Torres G, McCormick TS, Chang T, Mascelli MA, Kauffman CL, Aria N, Gottlieb AB, Everitt DE, Frederick B, Pendley CE, Cooper KD. An anti-IL-12p40 antibody down-regulates type 1 cytokines, chemokines, and IL-12/IL-23 in psoriasis. J Immunol 2006;177:4917–4926.

× Krueger GG, Langley RG, Leonardi C, Yeilding N, Guzzo C, Wang Y, Dooley LT, Lebwohl M. A human interleukin-12/23 monoclonal antibody for the treatment of psoriasis. New Engl J Med 2007;356:580–592.

× Gottlieb AB, Cooper KD, McCormick TS, Toichi E, Everitt DE, Frederick B, Zhu Y, Pendley CE, Graham MA, Mascelli MA. A phase 1, double-blind, placebo-controlled study evaluating single subcuta-neous administrations of a human interleukin-12/23 monoclonal antibody in subjects with plaque psoriasis. Curr Med Res Opin 2007;23:1081–1092.

× Leonardi CL, Kimball AB, Papp KA, Yeilding N, Guzzo C, Wang Y, Li S, Dooley LT, Gordon KB. Efficacy and safety of ustekinumab, a human interleukin-12/23 monoclonal antibody, in patients with psoriasis: 76-week results from a randomised, double-blind, pla-cebo-controlled trial (PHOENIX 1). Lancet 2008;371:1665–1674.

× Papp KA, Langley RG, Lebwohl M, Krueger GG, Szapary P, Yeilding N, Guzzo C, Hsu MC, Wang Y, Li S, Dooley LT, Reich K. Efficacy and safety of ustekinumab, a human interleukin-12/23 monoclonal antibody, in patients with psoriasis: 52-week results from a rando-mised, double-blind, placebo-controlled trial (PHOENIX 2). Lancet 2008;371:1675–1684.

× Schmidt C. Ustekinumab poised to enter the psoriasis market. Nat Biotechnol 2008;26:1317–1318.

× Garber K. Anti-IL-17 mAbs herald new options in psoriasis. Nat Biotechnol 2012;30:475–477.

× Binz HK, Pluckthun A. Engineered proteins as specific binding reagents. Curr Opin Biotechnol 2005;16:459–469.

× Nygren PA, Skerra A. Binding proteins from alternative scaffolds. J Immunol Methods 2004;290:3–28.

β Gronwall C, Stahl S. Engineered affinity proteins–generation and applications. J Biotechnol 2009;140:254–269.

β Nord K, Nilsson J, Nilsson B, Uhlen M, Nygren PA. A combinatorial library of an alpha-helical bacterial receptor domain. Protein Eng 1995;8:601–608.

β Nord K, Gunneriusson E, Ringdahl J, Stahl S, Uhlen M, Nygren PA. Binding proteins selected from combinatorial libraries of an alpha-helical bacterial receptor domain. Nat Biotechnol 1997;15:772–777.

β Nygren PA, Uhlen M. Scaffolds for engineering novel binding sites in proteins. Curr Opin Struct Biol 1997;7:463–469.

β Nord K, Nord O, Uhlen M, Kelley B, Ljungqvist C, Nygren PA. Recombinant human factor VIII-specific affinity ligands selected from phage-displayed combinatorial libraries of protein A. Eur J Biochem 2001;268:4269–4277.

β Nilsson FY, Tolmachev V. Affibody molecules: new protein domains for molecular imaging and targeted tumor therapy. Curr Opin Drug Discov Dev 2007;10:167–175.

β Gronwall C, Sjoberg A, Ramstrom M, Hoiden-Guthenberg I, Hober S, Jonasson P, Stahl S. Affibody-mediated transferrin depletion for proteomics applications. Biotechnol J 2007;2:1389–1398.

β Lofblom J, Feldwisch J, Tolmachev V, Carlsson J, Stahl S, Frejd FY. Affibody molecules: engineered proteins for therapeutic, diagnostic and biotechnological applications. FEBS Lett 2010;584:2670–2680.

β Johansson MU, Frick IM, Nilsson H, Kraulis PJ, Hober S, Jonasson P, Linhult M, Nygren PA, Uhlen M, Bjorck L, Drakenberg T, Forsen S, Wikstrom M. Structure, specificity, and mode of interaction for bac-terial albumin-binding modules. J Biol Chem 2002;277:8114–8120.

β Kraulis PJ, Jonasson P, Nygren PA, Uhlen M, Jendeberg L, Nilsson B, Kordel J. The serum albumin-binding domain of streptococcal protein G is a three-helical bundle: A heteronuclear NMR study. FEBS Lett 1996;378:190–194.

β Linhult M, Binz HK, Uhlen M, Hober S. Mutational analysis of the interaction between albumin-binding domain from streptococcal protein G and human serum albumin. Protein Sci 2002;11:206–213.

β Lejon S, Frick IM, Bjorck L, Wikstrom M, Svensson S. Crystal structure and biological implications of a bacterial albumin binding module in complex with human serum albumin. J Biol Chem 2004; 279:42924–42928.

β Ahmad JN, Li J, Biedermannova L, Kuchar M, Sipova H, Semeradtova A, Cerny J, Petrokova H, Mikulecky P, Polinek J, Stanek O, Vondrasek J, Homola J, Maly J, Osicka R, Sebo P, Maly P. Novel high-affinity binders of human interferon gamma derived from albumin-binding domain of protein G. Proteins: Struct Funct Bioinform 2012;80:774–789.

β Nilvebrant J, Alm T, Hober S, Lofblom J. Engineering bispecificity into a single albumin-binding domain. PLoS One 2011;6:e25791.

β Nilvebrant J, Astrand M, Lofblom J, Hober S. Development and characterization of small bispecific albumin-binding domains with high affinity for ErbB3. Cell Mol Life Sci 2013;70:3973–3985.

β Vaisocherova H, Zitova A, Lachmanova M, Stepanek J, Kralikova S, Liboska R, Rejman D, Rosenberg I, Homola J. Investigating oligonucleotide hybridization at subnanomolar level by surface plasmon resonance biosensor method. Biopolymers 2006;82:394–398.

β Sipova H, Sevcu V, Kuchar M, Ahmad JN, Mikulecky P, Osicka R, Maly P, Homola J. Surface plasmon resonance biosensor based on engineered proteins for direct detection of interferon-gamma in diluted blood plasma. Sens Actuators B Chem 2012;174:306–311.

β Acosta-Rodriguez EV, Napolitani G, Lanzavecchia A, Sallusto F. Interleukins 1beta and 6 but not transforming growth factor-beta are essential for the differentiation of interleukin 17-producing human T helper cells. Nat Immunol 2007;8:942–949.

β Stritesky GL, Yeh N, Kaplan MH. IL-23 promotes maintenance but not commitment to the Th17 lineage. J Immunol 2008;181:5948–5955.

β Iwakura Y, Ishigame H, Saijo S, Nakae S. Functional Specialization of Interleukin-17 Family Members. Immunity 2011;34:149–162.

Příloha 9.5

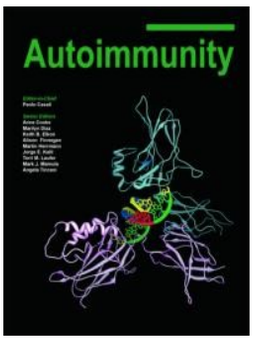

Autoimmunity

ISSN: 0891-6934 (Print) 1607-842X (Online) Journal homepage: http://www.tandfonline.com/loi/iaut20

p19-targeted ABD-derived protein variants inhibit IL-23 binding and exert suppressive control over IL-23-stimulated expansion of primary human IL-17+ T-cells

Lucie Křížová, Milan Kuchař, Hana Petroková, Radim Osička, Marie Hlavničková, Ondřej Pelák, Jiří Černý, Tomáš Kalina & Petr Malý

To cite this article: Lucie Křížová, Milan Kuchař, Hana Petroková, Radim Osička, Marie Hlavničková, Ondřej Pelák, Jiří Černý, Tomáš Kalina & Petr Malý (2017): p19-targeted ABD-derived protein variants inhibit IL-23 binding and exert suppressive control over IL-23-stimulated expansion of primary human IL-17+ T-cells, Autoimmunity, DOI: 10.1080/08916934.2016.1272598

To link to this article: http://dx.doi.org/10.1080/08916934.2016.1272598

Published online: 19 Jan 2017.

Autoimmunity

http://informahealthcare.com/aut
ISSN: 0891-6934 (print), 1607-842X (electronic)

Autoimmunity, Early Online: 1–12
© 2017 Informa UK Limited, trading as Taylor & Francis Group. DOI: 10.1080/08916934.2016.1272598

Taylor & Francis
Taylor & Francis Group

ORIGINAL ARTICLE

p19-targeted ABD-derived protein variants inhibit IL-23 binding and exert suppressive control over IL-23-stimulated expansion of primary human IL-17+ T-cells

Lucie Krızova[1], Milan Kuchar[1], Hana Petrokova´[1], Radim Osicka[2], Marie Hlavnickova[1], Ondrej Pelak[3], Jirı´ Cerny´[4], Toma´s Kalina[3], and Petr Maly´[1]

[1]Laboratory of Ligand Engineering, Institute of Biotechnology, Czech Academy of Sciences, v. v. i, BIOCEV Research Center, Vestec, Czech Republic, [2]Laboratory of Molecular Biology of the Bacterial Pathogens, Institute of Microbiology, Czech Academy of Sciences, Prague, Czech Republic, [3]CLIP, Department of Pediatric Hematology and Oncology, 2nd Faculty of Medicine, Charles University and University Hospital Motol, Prague, Czech Republic, and [4]Laboratory of Biomolecular Recognition, Institute of Biotechnology, Czech Academy of Sciences, v. v. i, BIOCEV Research Center, Vestec, Czech Republic

Abstract

Interleukin-23 (IL-23), a heterodimeric cytokine of covalently bound p19 and p40 proteins, has recently been closely associated with development of several chronic autoimmune diseases such as psoriasis, psoriatic arthritis or inflammatory bowel disease. Released by activated dendritic cells, IL-23 interacts with IL-23 receptor (IL-23R) on Th17 cells, thus promoting intracellular signaling, a pivotal step in Th17-driven pro-inflammatory axis. Here, we aimed to block the binding of IL-23 cytokine to its cell-surface receptor by novel inhibitory protein binders targeted to the p19 subunit of human IL-23. To this goal, we used a combinatorial library derived from a scaffold of albumin-binding domain (ABD) of streptococcal protein G, and ribosome display selection, to yield a collection of ABD-derived p19-targeted variants, called ILP binders. From 214 clones analyzed by ELISA, Western blot and DNA sequencing, 53 provided 35 different sequence variants that were further characterized. Using in silico docking in combination with cell-surface competition binding assay, we identified a group of inhibitory candidates that substantially diminished binding of recombinant p19 to the IL-23R on human monocytic THP-1 cells. Of these best p19-blockers, ILP030, ILP317 and ILP323 inhibited IL-23-driven expansion of IL-17-producing primary human $CD4^+$ T-cells. Thus, these novel binders represent unique IL-23-targeted probes useful for IL-23/IL-23R epitope mapping studies and could be used for designing novel p19/IL-23-targeted anti-inflammatory biologics.

Keywords

Psoriasis, autoimmune disease, Th17 cell, IL-23, protein binder

History

Received 29 August 2016
Accepted 5 December 2016
Published online 4 January 2017

Introduction

Psoriasis, a chronic inflammatory disease affecting population of more than 100 million people worldwide, is closely associated with interleukin-23 (IL-23) signaling in Th17 cells, a specific subset of CD4+ T helper cells [1–4]. Although the precise molecular mechanisms of other chronic inflammatory diseases have not been yet fully understood, IL-23 has been also described to play a crucial role in psoriatic arthritis, rheumatoid and Lyme arthritis, multiple sclerosis and inflammatory bowel disease [5].

IL-23 is a heterodimer of a 19 kDa subunit (p19) that is covalently linked to a 40 kDa subunit (p40) through a disulfide bridge ([6], Figure 1a, pdb id 3duh). The p19 subunit has a characteristic four-a-helix bundle (Figure 1a, a red structure) and the p40 subunit forms b-barrel structure (Figure 1a, an orange structure) with four internal disulfide bonds. While no post-translational modifications of p19 have been described, three potential N-glycosylation sites have been identified in p40. The p40 subunit exhibits a sequence similarity to an Ig-like C-type 2 domain at the N-terminus and to a fibronectin type III domain at the C-terminus.

IL-23 is predominantly secreted by activated dendritic and phagocytic cells, and binds to two surface receptors, IL-23R and IL-12Rb1 [7,8]. IL-23R is mainly expressed by T cells and natural killer cells, but weaker expression was found in dendritic cells and monocytes [8,9]. Signaling molecules activated by IL-23 in Th17 cells include Janus kinase (JAK) signal transducer and STAT proteins [10]. Through the signaling cascade, IL-23 stimulates the secretion of a cocktail of cell modulators and of certain chemokines that stimulate keratinocytes and cause their hyper-proliferation, a clinical manifestation of psoriasis [11–13]. A great deal of data indicates that the Th17 signaling pathway is a key mediator in the development and maintenance of psoriasis [14]. The number of Th17 cells and downstream effector molecules

Correspondence: Petr Maly´, Institute of Biotechnology CAS, v.v.i., BIOCEV Research Center, Pru˚myslova´ 595, Vestec, 252 50 Vestec, Czech Republic. Tel: +420325873763. E-mail: petr.maly@ibt.cas.cz. URL: www.ibt.cas.cz

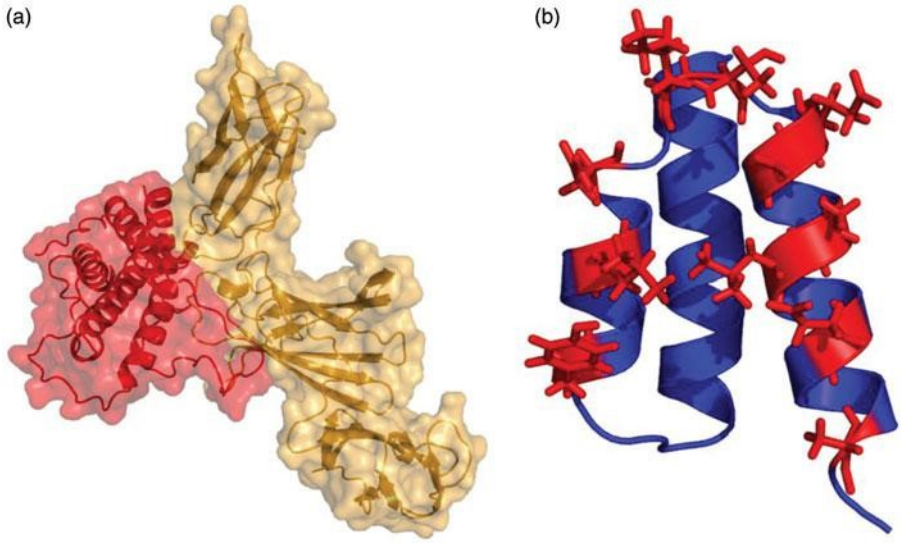

Figure 1. Structures of human IL-23 and albumin-binding domain scaffold. (a) Crystal structure of human IL-23 (pdb id 3duh) cytokine shown as a helical p19 protein (a-subunit, in red) covalently bound to a p40 protein (b-subunit, in orange). (b) Structure (pdb id 1gjt) of an ABD scaffold shown with 11 residues selected for the randomization (red sticks).

such as IL-17A, IL-17F, TNF-a and IL-22 are increased in psoriatic skin lesions [15]. In mouse model, intradermal injection of recombinant murine IL-23 induced expression of Th17 cytokines IL-17A, IL-17F and IL-22 and resulted in psoriasis-like inflammatory changes such as parakeratosis, acanthosis, neutrophilic microabscess formation and inflammatory infiltrates [16–18]. However, recently published data ascribed a role for IL-23 also in tumor initiation and growth promotion [19], suggesting that suppression of IL-23-mediating functions could be of a high therapeutic value not only for the autoimmune disorders but also in cancer treatment.

As the p40 subunit is also present in IL-12, therapeutic interventions require blocking of the p19 subunit to preserve Th-1 immunity [20–22], thus avoiding undesired cardiovascular side effects recently seen in psoriatic patients treated with the anti-p40 antibody-based drug ustekinumab [23,24]. Therefore, several companies put a great deal of effort for the development of more specific anti-p19 monoclonal antibody-based therapeutics [25,26].

In accordance with this therapeutic strategy, we have recently demonstrated that recombinant ligands derived from a protein scaffold of an albumin-binding domain (ABD) of streptococcal protein G (Figure 1b) can be used as a non-immunoglobulin protein alternative for efficient blocking of IL-23-mediated pro-inflammatory function, as demonstrated by several inhibitory REX binders, novel unique IL-23 receptor (IL-23R) antagonists [27]. These binders were shown to substantially suppress IL-23-driven ex vivo expan-sion of primary human IL-17-producing CD4+/CD8+ cells, shown in counts of IL-17-positive/IFNg-negative peripheral blood mononuclear cells (PBMCs) or separated T-cells. Thus, we presented that the ABD-scaffold-derived combinatorial library can be used for selection of immunomodulatory ligands that can also be useful as unique probes for structural and epitope-mapping studies, especially when the molecular structure of the IL-23/IL-23R complex remains unavailable. Recently, a non-canonical IL-23R complex assembly has been proposed [28], but crucial p19/IL-23R interacting residues and the precise mode of function remain to be identified.

In the present study, we describe the generation of a unique collection of p19-targeted binding proteins, called ILP binders, that were derived from the ABD scaffold using our recently described high-complex combinatorial library [29] and further selected by the ribosome display approach. We demonstrate that the ILP variants bind the recombinant human p19 protein as well as the biologically active human IL-23 cytokine. Several ILP variants exhibit an inhibitory potential demonstrated by a cell-surface competition binding assay using IL-23R-expressing THP-1 cells and suppress IL-23-driven expansion of IL-17-producing primary human $CD4^+$ T-cells.

Materials and methods

Antibodies and detection agents

Mouse anti-IL-23(p19) polyclonal antibody as well as horseradish peroxidase (HRP)-conjugated goat anti-mouse IgG, was purchased from Biolegend, San Diego, CA. Cy5-conjugated goat anti-mouse IgG ($F(ab^0)2$ fragment) was obtained from Jackson ImmunoResearch Laboratories, West Grove, PA. Streptavidin–phycoerythrin was purchased from eBioscience, San Diego, CA. Streptavidin–HRP conjugate was obtained from Thermo Scientific, Rockford, IL. The monoclonal anti-poly-histidine-HRP antibody produced in mouse was obtained from Sigma-Aldrich, St. Louis, MO.

Cell line and growth conditions

Cell line used in the study was a human acute monocytic leukemia cell line, THP-1 (ATCC number: TIB-202). The cells were grown in DMEM medium (Sigma-Aldrich, St. Louis, MO) supplemented with 10% fetal calf serum (FCS) (GIBCO, Grand Island, NY) and antibiotic antimycotic solution (ATB) (Sigma-Aldrich, St. Louis, MO).

Production of recombinant p19 proteins

The recombinant p19 protein (calculated Mw 23.3 kDa) fused with an N-terminal double His_6-TEV protease cleavage site (DH-p19) was produced using a synthetic, codon optimized p19 cDNA (GENEART, Regensburg, Germany) inserted into

the pET-28b vector by NcoI + XhoI cloning in E. coli Top10 cells. The protein was produced in E. coli BL21(DE3) host cells. Overnight (o/n) culture of 50 ml LB medium containing 60 mg/ml kanamycin was used to inoculate 1 l of LB medium and let to grow at 37 C to reach OD600 ¼ 1.0. The culture was induced with 1 mM IPTG for 4 h at 37 C. Cells were harvested by centrifugation (6000 g, 20 min), washed with TN buffer (50 mM Tris–HCl and 150 mM NaCl, pH ¼ 8) and centrifuged again (5000 g, 10 min). Cell pellets were resus-pended in 10 ml TN buffer and disrupted by MISONIX 3000 sonicator. The lysates were centrifuged at 40 000 g for 20 min and the insoluble DH-p19 was extracted from inclusion bodies with 2 ml of 8 M urea in TN buffer. The urea extract was left shaking for 1 h at room temperature (RT) and centrifuged at 40 000 g for 20 min. The supernatant was applied on 1 ml Ni-NTA agarose column equilibrated with 5 ml of TN buffer. The washing was performed with 10 ml of TN buffer with 8 M urea and, subsequently, with TN buffer containing 8 M urea and 20 mM imidazole. The DH-p19 was eluted with TN buffer containing 8 M urea and 250 mM imidazole in 0.5 ml fractions. Alternatively, soluble p19 was produced from an engineered plasmid construct in the form of a fusion protein with maltose binding protein (MBP) and a double His_6-tag at the N-terminus (calculated Mw 69 kDa). Briefly, the DNA sequence encoding p19 was inserted into an assembled pET28b-derived vector, carrying sequence coding for double His_6–MBP-TEV-MCS-TEV-His_6, using primers p19-F-NheI (GGGCTAGCTAGCAGAGCTGTGCCTGGG GGC) and p19-R-XhoI (GCGCCTCGAGGGGACTCAG GGTTGCTGCTC). E. coli TOP10 (Life Technologies, Carlsbad, CA) host cells were transformed with the p19-cloned vector and plated on LB-agar supplemented with 60 mg/ml kanamycin. The protein was produced in E. coli BL21(DE3). A single colony was used to inoculate 50 ml LB medium containing 60 mg/ml kanamycin. Twenty milliliters o/ n culture was used to inoculate 1 l of culture medium and grown at 37 C to OD ¼ 0.6. Culture was induced with IPTG at 20 C and let to grow for 4 h. Cells were harvested by centrifugation at 6000 g for 20 min, washed with TN buffer (pH ¼ 8) and centrifuged at 5000 g for 10 min.

Cell pellets were re-suspended in 10 ml of TN buffer and disrupted by ultrasound pulses on MISONIX 3000 sonicator. The lysates were centrifuged for 20 min at 40 000 g. The cytoplasmic fraction containing soluble DH-MBP-p19 was loaded on column 5 ml His-Trap packed with Ni-NTA agarose on AKTA purifier (GE Healthcare, Buckinghamshire, UK). Elution was done in three steps with buffer containing 250, 500 and 1000 mM imidazole. 1.5 ml fractions from the elution with 500 mM imidazole were analyzed on SDS-PAGE and those with DH-MBP-p19 were collected and used further.

Test of binding of the p19 proteins by ELISA

Binding of both recombinant forms of the p19 protein to the IL-23R was tested as described previously [27]. Shortly, the recombinant extracellular portion of the IL-23R was immobilized directly on the NUNC Polysorp 96-well plate in coating buffer (100 mM bicarbonate/carbonate solution, pH 9.6). Serial dilutions of the purified DH-MBP-p19 and DH-p19 recombinant proteins were prepared in PBS buffer containing 0.05% Tween and 1% BSA (PBSTB) and p19 binding was detected using mouse anti-human IL-23(p19) polyclonal antibody followed by goat anti-mouse IgG-HRP conjugate. OPD substrate (Sigma-Aldrich, St. Luis, MO) was used as HRP substrate in citrate buffer (3.31% sodium citrate tribasic dihydrate, phosphoric acid, pH ¼ 5.0), reactions were stopped with 2 M sulfuric acid and absorbance was read at 492 nm.

ABD-library construction and ribosome display selection of ILP binders

Combinatorial DNA library was generated as described previously [29]. The assembled library was in vitro transcribed/translated in a single step reaction using E. coli extract (EasyXpress Protein Synthesis Mini Kit, QIAGEN, Hilden, Germany) and used for the selection of translated binders in ribosome display screening. For the selection of binders, wells of Maxisorp plates (NUNC, Roskilde, Denmark) were coated with recombinant DH-MBP-p19 protein and blocked with 3% BSA. Pre-selection was performed in wells coated with DH-MBP and blocked with BSA. Two groups of ABD binder cDNA libraries, obtained by reverse transcription after the third or the fifth round of a ribosome display selection campaign, were obtained and cloned as NcoI and XhoI fragments in a pET-28b vector containing an in-frame inserted full-length tolA DNA sequence. Later, the AviTag in vivo biotinylation sequence (GLNDIFEAQKIEWHE) was added to the C-terminus of the TolA spacer to allow biotinylated protein detection by streptavidin as described previously [27]. The final ILP-TolA-AVI fusion proteins were produced as biotinylated proteins in the E. coli BL21(DE3) BirA strain expressing biotin ligase (BirA) in the presence of 50 mM d-biotin in LB medium and following induction with 1.5 mM IPTG. The soluble proteins were purified from cell extracts on Ni-NTA agarose columns. For all binding assays, a control TolA fusion protein with the original non-mutated parental albumin binding domain (ABDwt-TolA-AVI) was used.

Screening of ILP variants for binding to the p19 protein by ELISA

For binding assays, selected clones were picked, the inserted sequence was verified by DNA sequencing and proteins were produced in the E. coli BL21(DE3) BirA strain. The ILP-TolA-AVI proteins were purified on Ni-NTA columns and two different sandwich ELISA layouts were used for binding assays. In the first case, NUNC Polysorp plates were coated directly with DH-MBP-p19 or DH-p19 (5 mg/ml) in coating buffer at low temperature (7 C) overnight and the washed plates were blocked by PBSTB. The serially diluted purified ILP-TolA-AVI proteins were applied in PBSTB and the amount of bound biotinylated proteins was detected using streptavidin–HRP conjugate (1:1000). In the second setup, the plates were coated with streptavidin (1 mg/ml) in coating buffer and biotinylated ILP-TolA-AVI proteins (5 mg/ml) were immobilized through binding to streptavidin produced in Arctic Express E. coli and purified on iminobiotin agarose. Serially diluted DH-MBP-p19 or DH-p19 in PBSTB were

added into the wells and p19 binding to the immobilized ILP variants was detected by mouse-anti-IL-23(p19) polyclonal antibody (1:1000) followed by goat anti-mouse polyclonal antibody (1:1000).

Sequence analysis and clustering of selected ILP variants

DNA constructs of selected clones expressing ILP-TolA-AVI variants were sequenced. Amino acid multiple sequence alignment of all selected variants and construction of the similarity tree were performed using Molecular Evolutionary Genetics Analysis version 5 (MEGA5) integrated tool (http://www.megasoftware.net).

Fluorescence-based thermal-shift assay

Protein samples (0.1 mg/ml) in PBS and 5 Sypro Orange dye (Sigma-Aldrich, St. Louis, MO) were mixed in total volume of 25 ml. Using the real-time PCR Detection System CFX96 Touch (Bio-Rad Laboratories, Hercules, CA), the proteins were incubated in a thermal gradient from 20 C to 80 C with increments of 0.5 C and with 30 s-hold intervals. The degree of protein unfolding was monitored by the FRET (fluorescence resonance energy transfer) channel that captured the spectral properties of Sypro Orange unfolded protein complexes (excitation wavelength

470 nm and emission wavelength 570 nm). The data were analyzed by CFX Manager software and the melting temperatures were determined using the first derivative spectra.

Analysis of binding of p19 and ILP variants to human THP-1 cells by flow cytometry

All binding assays were performed in HEPES buffered salt solution (HBSS buffer; 10 mM HEPES, pH 7.4, 140 mM NaCl, 5 mM KCl) complemented with 2 mM $CaCl_2$, 2 mM $MgCl_2$, 1% (w/v) glucose and 1% (v/v) FCS (cHBSS) in 96-well culture plates (TPP Techno Plastic Products AG, Trasadingen, Switzerland). For DH-p19 binding assay, 2.5 10^5 cells were incubated in 50 ml of cHBSS with or without DH-p19 (10 mg/ml) for 30 min at 4 C. The cells were washed with cHBSS and the cell-bound DH-p19 was stained with mouse anti-IL-23(p19) polyclonal antibody (1:50 dilution) for 30 min at 4 C and after washing with Cy5-conjugated goat anti-mouse IgG, F(ab^0)2 fragment (1:200 dilution) for 30 min at 4 C. For ILP binding assay, 2.5 10^5 cells were incubated in 50 ml of cHBSS with the biotinylated ILP-TolA-AVI binders or with the ABDwt-TolA-AVI control (10 mg/ml) for 30 min at 4 C, washed with cHBSS, and the cell-bound proteins were stained with streptavidin–phycoerythrin (1:400 dilution) for 30 min at 4 C. Cells were washed, resuspended in 100 ml of HBSS and analyzed by flow cytometry in a BD LSR II instrument (BD Biosciences, San Jose, CA) in the presence of 1 mg/ml of Hoechst 33258. Data were analyzed by FlowJo software (Tree Star, Ashland, OR) and appropriate gatings were used to exclude cell aggregates and dead cells. Binding data were deduced from the mean fluorescence intensities (MFI).

Competition between DH-p19 and ILP ligands for binding to THP-1 cells

For blocking of p19 binding to the IL-23R by selected ILP variants, mixtures of the serially-diluted ILP-TolA-AVI variants, ranging from 50 to 1.6 mg/ml, were prepared in the continuous concentration 10 mg/ml of the recombinant DH-p19 protein in the total volume 50 ml of cHBSS buffer. Then, the samples were added to 2.5 10^5 THP-1 cells followed by 30 min incubation at 4 C. The cells were washed with cHBSS and the bound p19 was detected by flow cytometry using anti-IL-23(p19) polyclonal antibody in combination with Cy5-conjugated goat anti-mouse IgG, F(ab^0)2 fragment as described above.

Binding of ILP ligands to human IL-23 using ELISA

Polysorp plate (NUNC, Roskilde, Denmark) was coated with recombinant streptavidin (1 mg/ml) in coating buffer overnight at 7 C. The washed plate was blocked with PBSTB for 2 h at RT. Biotinylated ILP-TolA-AVI binders and negative control ABDwt-TolA-AVI (10 mg/ml) were immobilized in PBSTB buffer through streptavidin for 1 h at RT. Washed plate was incubated with 4 mg/ml of human IL-23 (R&D systems, Minneapolis, MN) in PBSTB buffer for 1 h at RT. Binding of IL-23 to the immobilized ILP variants was detected with mouse anti-IL-23(p19) polyclonal antibody (1:1000) sandwich with secondary goat anti-mouse-HRP conjugate (1:1000).

Modeling of ILP-p19 and p19-IL-23R interactions

The homology model of the extracellular part of human IL-23R was prepared using the MODELLER 9v14 suite of programs [30] based on the homologous structure of IL-6Rb (pdb id 1p9m, 23% and 60% sequence identity and similarity, respectively). The structure of studied ABD variants (ILP030, ILP317, ILP323 and ILP272) was modeled based on the ABDwt structure (pdb id 1gjt). The structure of p19 was obtained from the known structure of the IL-23 (pdb id 3duh), where the missing residues from the p19 loop regions were added by MODELLER. All the necessary sequence align-ments were performed employing the clustalw2 [31] program. Resulting three-dimensional structures were subjected to the flexible side chain docking performed using a local copy of the ClusPro server [32,33].

IL-23-dependent ex vivo expansion of human IL-17-producing T-cells

Functional assay was performed as described earlier [27]. Healthy donors provided written informed consent in accordance with the Declaration of Helsinki. Peripheral blood drawn into EDTA-containing tubes was used to obtain PBMCs on Ficoll-Paque gradients (Pharmacia, Uppsala, Sweden). Primary human T-cells isolated from PBMCs using Human T Cell Enrichment Kit (Stemcell Technologies, Vancouver, Canada) were washed once with PBS and resuspended in complete RPMI 1640 media (RPMI 1640 supplemented with 10% heat-inactivated FCS, 100 U/ml penicillin, 100 mg/ml streptomycin sulfate and 1.7 mM sodium glutamate). T-cells were adjusted to 2 10^6 cells/ml and activated on a 96-well

plate pre-coated with anti-CD3 (MEM-57, 10 mg/ml, Exbio Praha a.s., Praha, Czech Republic) in the presence of co-stimulatory antibodies against CD28 and CD49d (1 mg/ml, BD Biosciences, San Jose, CA), in the presence of IL-23 (10 ng/ml) and IL-2 (100 U/ml). Purified LPS-free ILP-TolA-AVI binding proteins (7 mg/ml) or control ABDwt-TolA-AVI were added into the medium and cells were incubated for three days at 37 C. Cells were re-stimulated again (as above) for 6 h at 37 C (last 4 h exocytosis was blocked with Brefeldin A (10 mg/ml, Sigma-Aldrich, St. Louis, MO)). Then, cells were stained with antibodies to CD8 Horizon V-500 (BDB) for 15 min in the dark, washed with PBS containing 0.1% sodium azide and 2% gelatin from cold fish (Sigma-Aldrich, St. Louis, MO) and fixed using FACS lysing solution/FACS Perm 2 (BDB) according to the manufacturer's instructions. After the next washing step, cells were stained for CD3 (PerCP-Cy5.5, eBioscience, San Diego, CA), for CD4 (ECD, Immunotech, Marseille, France) and with antibodies for IFN-g (PE Cy7), IL-2 (APC), IL-17 (PB) (eBioscience, San Diego, CA) and CD154 (PE, Immunotech, Quebec, Canada) and flow cytometry detection was performed using BD FACS Aria

(xxiv) flow cytometer (BDB). Absolute cell counts were obtained using BD Truecount (BDB). Viable, nucleated cells were counterstained with Syto-16 and DAPI (Invitrogen, Carlsbad, CA).

Results

Production of recombinant p19 and IL-23R proteins

The p19 protein, an alpha subunit of the IL-23 cytokine, is a molecule of 170 amino acid residues. For ribosome display selection of p19-targeted ABD-derived binding variants (ILP binders), we produced p19 in the form of a 69 kDa fusion protein. The DH-MBP-p19 fusion consists of a double His_6-tag and the MBP moiety at the N-terminus and a solubility-supporting sequence at the C-terminus of p19, respectively, as described previously [27]. The DH-MBP-p19 protein was expressed in E. coli cells and purified from the cytosolic fraction by Ni-NTA chromatography.

To explore the ability of ILP binders to inhibit p19/IL-23 binding to IL-23R-expressing cells, we constructed a 23 kDa variant of the p19 protein with an N-terminally fused double His_6-tag [27]. The DH-p19 protein was extracted from inclusion bodies of E. coli cells and affinity-purified. The purity and identity of both versions of p19 were verified on SDS-PAGE gels and Western blots using anti-IL-23(p19) antibody (data not shown).

To validate the folding and functionality of both recombinant p19 proteins using a receptor binding assay, we produced two different forms of the extracellular part of the IL-23 receptor (exIL-23R), as described previously [27]. Briefly, to produce the first form, the DNA sequence encoding exIL-23R with an N-terminally fused His_6-tag was cloned into the pET-28b vector and the exIL-23R protein was expressed in the E. coli Shuffle strain, which enabled formation of five disulphide bridges within the fibronectin type III and terminal Ig-like domains of the receptor. Then, the exIL-23R protein was extracted from inclusion bodies of bacterial cells by urea and purified by Ni-NTA chromatography. To produce the second form of exIL-23R, we cloned the same DNA sequence into the pET-26b vector containing a periplasm-targeting pelB leader sequence and exIL23R was affinity-purified from the insoluble fraction of E. coli BL21(DE3).

To verify the functionality of the recombinant p19 proteins, ELISA experiments with immobilized recombinant exIL-23R proteins were performed. The results demonstrated that both p19 proteins specifically bound to both immobilized exIL-23R forms in a saturable manner (data not shown) and thus confirmed the results obtained previously [27]. Therefore, the recombinant p19 proteins could be used as a target in ribosome display for selection of p19-specific binders and their subsequent characterization.

Ribosome display selection of ILP binders

To identify a collection of binders against the p19 subunit of IL-23, we used randomization of 11 residues in the ABD domain scaffold, generating a combinatorial ABD library of a theoretical complexity of 10^{14} protein variants, in combination with the ribosome display selection. We selected a collection of 214 ABD-TolA variants (ILP-TolA binders) that were subsequently C-terminally fused with an AviTag sequence to produce in vivo biotinylated ILP-TolA-AVI variants for further recognition by streptavidin. The ILP-TolA-AVI variants were produced as bacterial lysates and used as analytes for ELISA screening with a coated target protein DH-p19 or DH-MBP-p19, respectively. The ELISA results were correlated with Western blot analysis detecting the ILP-TolA-AVI variants with streptavidin–HRP or anti-His antibody (data not shown). After analyses, we selected a set of 53 p19-binding proteins that were sequenced, identifying 35 unique variants (Figure 2). These were purified by Ni-NTA chromatography and used to determine the binding affinity to the recombinant p19 proteins. For this purpose, the DH-p19 and DH-MBP-p19 proteins were coated on ELISA plates and serially diluted purified ILP-TolA-AVI variants were used as analytes. Alternatively, the ILP proteins were immobilized via streptavidin and both versions of the p19 proteins were used as analytes. Binding curves for the best ILP binders are shown in Figure 3.

Test of specificity of ILP binders

To verify the specificity of several selected high-affinity ILP variants, we performed a cell-surface binding test using THP-1 cells that were previously described to express significant amounts of the IL-23R and were, therefore, successfully used for the characterization of IL-23R-targeted REX binders [27]. To exclude a possible non-specificity of the ILP binders and to confirm their suitability for a p19-mediated competition binding assay, we performed the experiment using in vivo biotinylated ILP-TolA-AVI proteins. Binding of the ILP binders to THP-1 cells was monitored by streptavidin–PE conjugate. Results shown in Figure 4 demonstrate none or negligible binding of the used ILP binders to THP-1 cells except for ILP215 variant, suggesting its acquired ''dual-affinity'' or a possible non-specificity. For the test of ILP specificity, REX115-TolA-AVI, previously selected as a strong IL-23R binder, was used as a positive control, while the parental non-mutated ABDwt-TolA-AVI as a

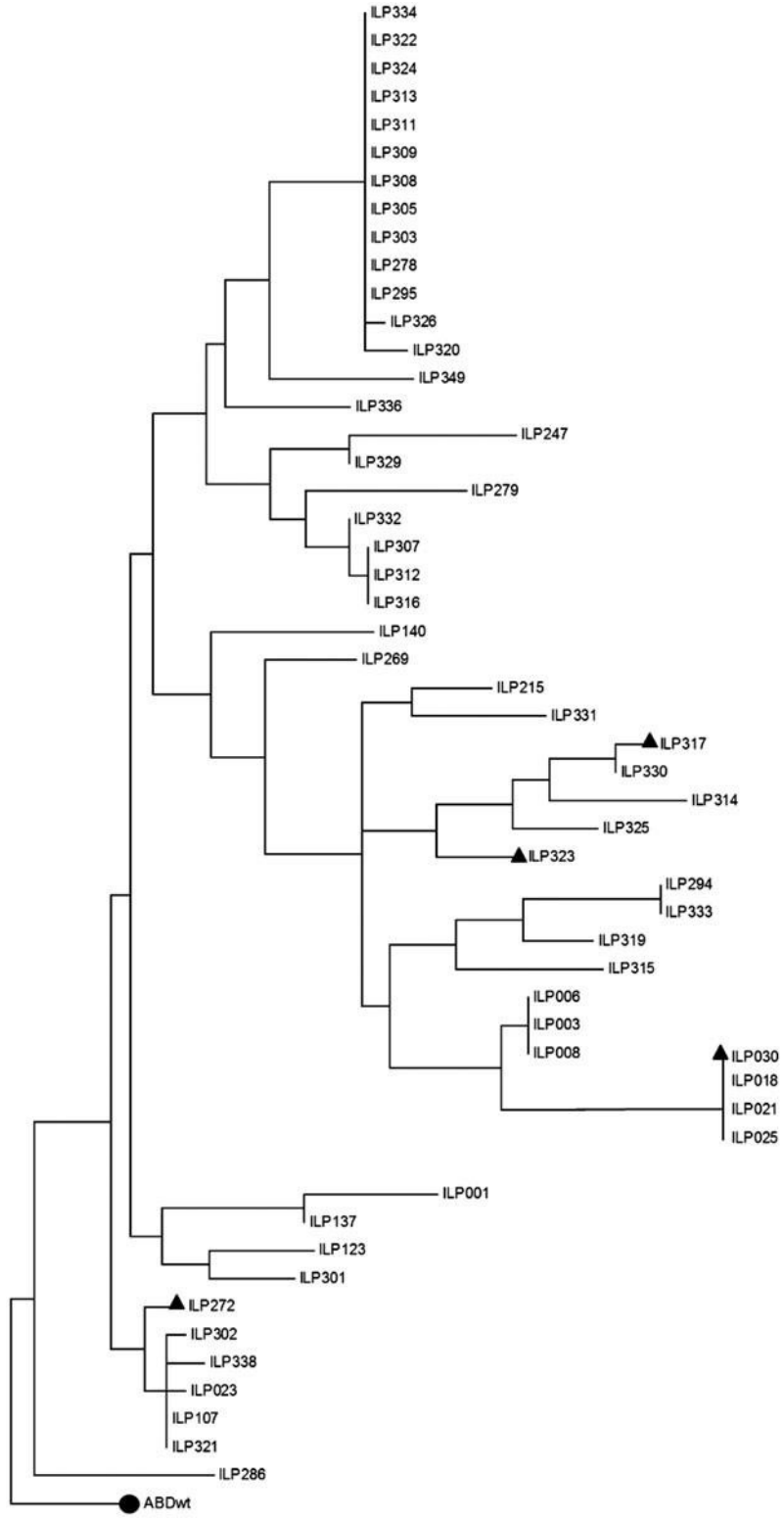

Figure 2. Comparison of sequence similarity of the selected ILP clones, targeted to the p19 protein, a-subunit of IL-23. Analysis of 53 cloned ILP binders of the p19 subunit of IL-23 obtained by ribosome display selection revealed 35 unique variants. For similarity analysis, only the sequences between residues 20 and 46 were compared, as the N-terminal amino acid positions 1–19 were non-randomized.

negative one. Based on the results of the cell-surface binding assays performed for selected high-affinity ILP variants, a group of four most promising ILP candidates was defined. The sequence similarity comparison of these binders is shown in Table 1. To further verify the specificity of the ILP clones, we performed additional ELISA test using several common proteins as targets. The ILP binders exhibited the specificity for the p19 protein in comparison with binding to lysozyme, bovine serum albumin, ovalbumin and human serum albumin, a natural partner of the ABD domain (data not shown).

Modeling of interactions of p19 with IL-23 receptor and ILP variants

Since neither the IL-23R structure nor the IL-23/IL-23R complex structure is available, we built a homology model for IL-23R using the IL-6 receptor as a template. We performed

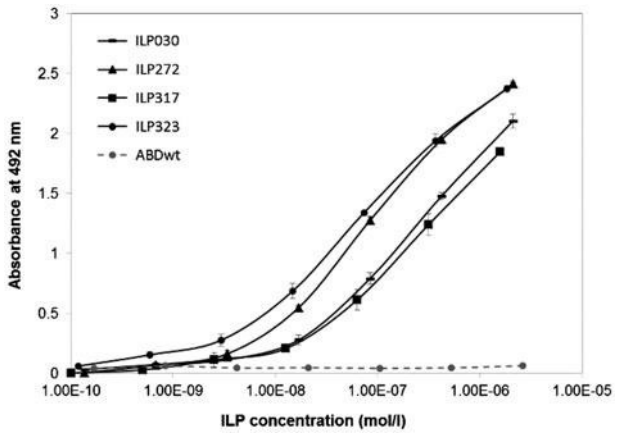

Figure 3. ILP-TolA-AVI clones bind the recombinant DH-p19 in ELISA. DH-p19 expressed in E. coli BL21(DE3), purified from inclusion bodies and refolded from 8 M urea extracts was coated on a Polysorp ELISA plate. Binding of in vivo biotinylated ILP-TolA-AVI clones was detected by streptavidin–HRP conjugate. ABDwt-TolA-AVI was used as a negative control. The results represent three individual measurements and the error bars indicate standard deviations.

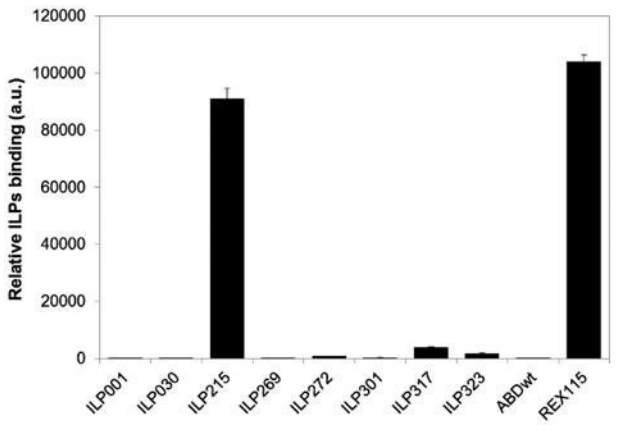

Figure 4. Test of specificity of ILP binders using THP-1 cells. For binding assay, 2.5 10^5 cells were incubated in 50 ml of cHBSS with in vivo biotinylated ILP-TolA-AVI clones or ABDwt-TolA-AVI negative control (10 mg/ml) for 30 min at 4 C. The cell-bound proteins were stained with streptavidin–PE for 30 min at 4 C and analyzed by flow cytometry. The error bars represent standard deviations.

docking of p19 as well as the IL-23 cytokine with IL-23R. The results of docking suggested the most probable binding site located at the extracellular Ig-like domain and distal domain of the fibronectin-type III of IL-23R, commonly designated as a cytokine homology region (CHR), as presented in Figure 5(a).

To investigate the most probable binding regions for the three best binding candidates of the ILP variants, we performed docking of ILP030, ILP317, ILP323 and ILP272 on the structure of the p19 protein. Our data suggested that there is no significant difference between both p19 moieties found in the crystal structure of IL-23 (pdb id 3duh, chains A and C) as well as structures of p19 with added residues originally missing in the loop regions. This indicates that a flexible loop is not involved in the ILP/p19 binding. Docking of ILP030 variant predicted (Figure 5b) that the first three most probable binding regions are located in the area where the homology model ascribed the p19/IL-23R interaction.

For the ILP317, ILP323 and ILP272 variants (Figure 5c–e), a similar binding pattern as that found for the ILP030 variant was predicted, with the most probable binding site located in the IL-23/IL-23R binding region (see Figure 5a), suggesting a probable neutralizing effect on the p19/IL-23R binding.

ILP binders compete with p19 for binding to the IL-23 receptor on THP-1 cells

To verify a predicted blocking potential of the ILP binders, we performed cell-surface competition binding assay in which the ILP-TolA-AVI binders competed with IL-23R expressed on THP-1 cells for binding to the DH-p19 protein. It is important to mention that binding of DH-p19 to THP-1 cells has already been demonstrated in our recent study, using flow cytometry

× Cells were incubated with serially-diluted ILP-TolA-AVI variants in the continuous concentration of the recombinant DH-p19 protein and its binding to IL-23R on THP-1 cells was monitored by flow cytometry using anti-IL-23(p19) poly-clonal antibody followed by a secondary IgG-Cy5-conjugate. As shown in Figure 6, increasing concentrations of ILP030, ILP272, ILP317 and ILP323 significantly decreased binding of DH-p19 to THP-1 cells. These results demonstrate that we identified a group of novel p19-specific ILP binders with a blocking potency.

ILP binders inhibit IL-23-dependent ex vivo expansion of primary human IL-17-producing T-cells

Based on the results of ELISA and cell-surface competition binding assays, we selected four most promising inhibitory variants, ILP030, ILP272, ILP317 and ILP323, that were shown to bind to recombinant DH-p19 and block it from binding to IL-23R expressed on human THP-1 cells. We first verified whether these selected ILP candidates bind also to eukaryotic product of biologically active human IL-23 using ELISA. To this goal, streptavidin was coated into 96-well plate and in vivo biotinylated ILP-TolA-AVI variants, or ABDwt-TolA-AVI control, were immobilized via binding with streptavidin. Human IL-23 was then added as an analyte and its binding was monitored by corresponding anti-IL-23 antibody conjugate. We found that the ILP variants recognize the human IL-23 cytokine (results not shown) and can be, therefore, used for tests of immunomodulation on activated primary human T-cells.

To assess ex vivo whether the selected ILP variants inhibit IL-23 signaling on primary human T-cells, we determined whether the blocking of p19/IL-23 by excess of ILP ligands would inhibit IL-23-mediated expansion of primary human Th17 lymphocytes. To this goal, we used T-cells separated from mononuclear cells of healthy donors, which were T-cell receptor stimulated in the continued presence of the Th17 conditioning cytokines IL-23 and IL-2. Over three days of ex vivo cultivation of T-cell suspensions, a significant reduction of Th17 cell expansion, detected as counts of IL-17 secreting and IFN-g non-secreting T-cells, was observed when excess of the ILP binders was present, as compared to a non-treated mock control (Figure 7a, the right bottom square with the indicated percentage). Enhancement of Th17+ cells after IL-23-mediated induction is documented as a difference between non-induced cells (sample NO IL-23, 0.463 ± 0.245, n ¼ 6,

Table 1. Sequence comparison of ILP binders. The non-mutated ABDwt was aligned with the randomized part of the ILP binders selected by ribosome display. Grey boxes indicate the 11 positions at which the residues of ABD (aa 20–46) were randomized. The non-randomized N-terminal part of ABD (aa 1–19) contains sequence LAEAKVLANRELDKYGVSD.

	20	21	22	23	24	25	26	27	28	29	30	31	32	33	34	35	36	37	38	39	40	41	42	43	44	45	46
ABDwt	Y	Y	K	N	L	I	N	N	A	K	T	V	E	G	V	K	A	L	I	D	E	I	L	A	A	L	P
ILP030	V	Y	K	N	T	I	N	P	A	A	W	V	L	A	V	K	R	M	I	D	R	I	L	A	N	L	P
ILP272	P	Y	K	N	R	I	N	T	A	S	T	V	A	L	V	K	S	W	I	D	L	I	L	A	G	L	P
ILP317	S	Y	K	N	L	I	N	M	A	G	F	V	R	Y	V	K	R	R	I	D	S	I	L	A	P	L	P
ILP323	I	Y	K	N	M	I	N	Q	A	V	L	V	R	R	V	K	R	F	I	D	V	I	L	A	R	L	P

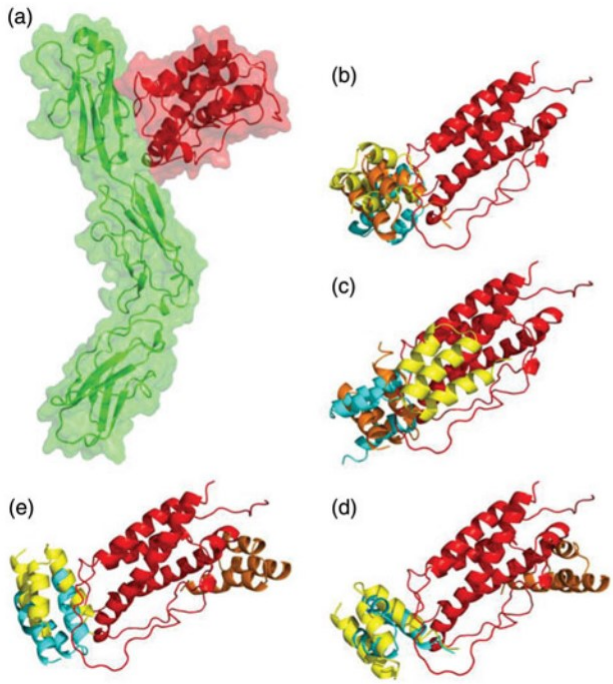

Figure 5. Modeling of p19/IL-23R and p19/ILP interactions. (a) Prediction of the interaction between alpha subunit (p19) of the human IL-23 cytokine and its cognate IL-23 receptor. For docking, a homology model based on the known IL-6/IL-6 receptor complex was used. The most probable pose of the p19 (red) docking to the IL-23R (green) is shown. (b–e) Summary of the first three poses of the ILP030 (b), ILP317
β ILP323 (d) and ILP272 (e) binding to the p19 protein (red), in decreasing predicted order of probability demonstrated in cyan (the most probable), yellow and orange, respectively.

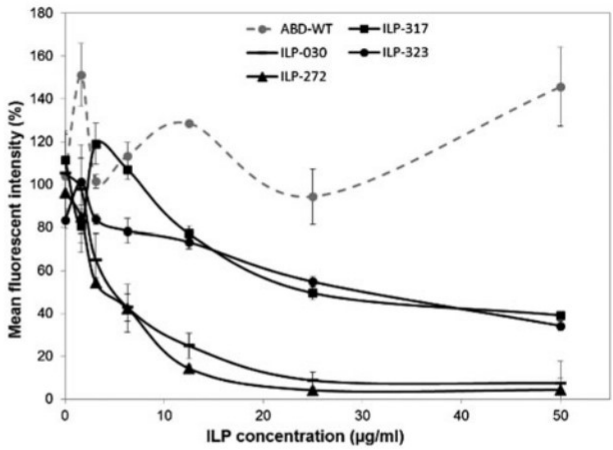

Figure 6. ILP binders inhibit p19 binding to IL-23 receptor on THP-1 cells. Serially-diluted ILP variants, ranging from 50 to 1.6 mg/ml, were prepared in the continuous concentration 10 mg/ml of the recombinant DH-p19. Then, the samples were added to THP-1 cells. After 30 min incubation on ice, the cells were washed with cHBSS and the bound p19 was detected by flow cytometry with anti-IL-23(p19) polyclonal antibody in combination with Cy5-conjugated goat anti-mouse IgG. ABDwt-TolA-AVI served as a negative control. Error bars represent standard deviations.

p ¼ 0.0030) and normalized counts of IL-23 stimulation (IL-23 only, ¼1), shown as bars in Figure 7(b). All tested ILP variants significantly inhibited Th17+ cell expansion: ILP030 (0.613 ± 0.196, n ¼ 6, p ¼ 0.0047), ILP317 (0.498 ± 0.189, n ¼ 6, p ¼ 0.0013) and ILP323 (0.456 ± 0.221, n ¼ 6, p ¼ 0.0018), as documented in Figure 7(b). In this ex vivo experiment done on activated primary human T-cells, we also verified the immunogenicity of the parental non-mutated ABDwt protein as this domain, as a part of the BB domain of the streptococcal protein G, was previously described to have an adjuvant effect and was shown to stimulate immune response. We found that there are striking differences in ABDwt-mediated T-cell reactivity among different blood donors, with the average value 0.635 ± 0.355 (n ¼ 6, p ¼ 0.0533), as compared to the IL-23-stimulated mock-treated control. In summary we conclude, that all of the used ILP variants inhibited IL-23-driven expansion of primary human T-cells to the level around IL-23 non-treated sample, thus further supporting in silico-ascribed blocking function, predicted using a built-up IL-6R/IL-23R homology model, and further confirmed by a cell-competition binding assay on IL-23R-expressing THP-1 cells.

Test of stability of selected ILP binders

To study thermal stability of the ILP binders, we used fluorescence-based thermal-shift assay and estimated temperature melting point for particular ILP variants using the evaluation of temperature melting curves (Figure 8). The melting temperature (T_m) of the ILP-TolA-AVI proteins measured in PBS solution was found to be 52 C for ILP030, 51 C for ILP272, 59 C for ILP317 and 61 C for ILP323. The T_m value of the parental non-mutated ABDwt-TolA-AVI was 58 C. These data demonstrate that random-ization of 11 amino acid residues of the ABD scaffold retained (ILP317, ILP323) or slightly decreased (ILP030, ILP272) the thermal stability of the ILP variants but particular combinations of the amino acid substitutions did not destroy a general scaffold stability.

Discussion

Generation of novel protein binders derived from non-immunoglobulin domain scaffolds represent a promising alternative to commonly used monoclonal antibodies.

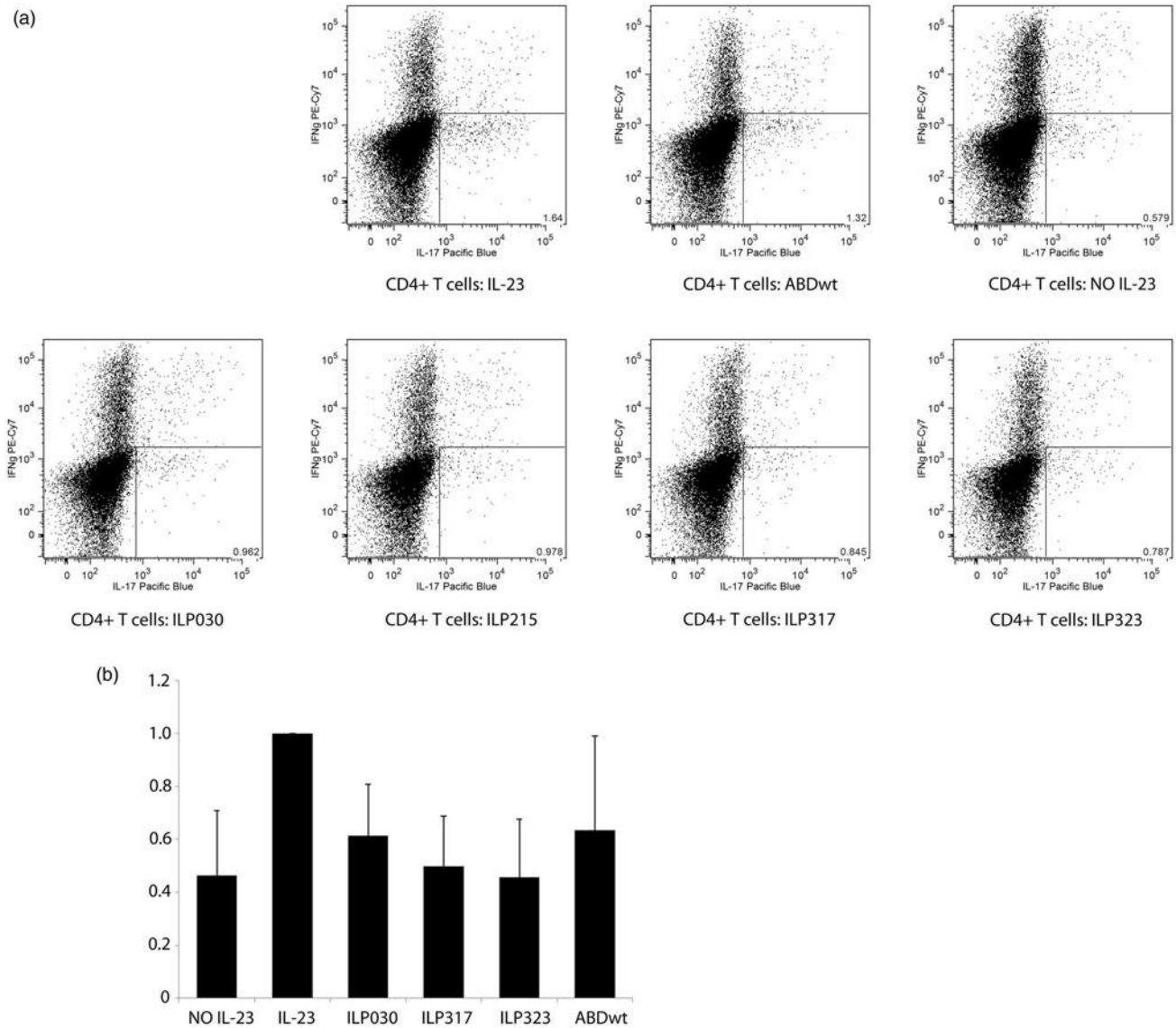

Figure 7. ILP binders inhibit IL-23-dependent ex vivo expansion of IL-17-producing CD4+ T-cells. Separated T-cells isolated from peripheral blood of six healthy volunteers, activated using anti-CD3 and co-stimulated with IL-23 and IL-2, were cultured in the presence or absence of indicated ILP binders for 3 days. (a) IL-17-producing cells were detected by flow cytometry and gated using FSC, SSC, $CD3^+$ and $CD4^+$. Representative experiment is presented. (b) The amount of IL-17-producing cells recovered from the cultured primary T-cell samples in the presence or absence of the ILP ligands are shown as bars representing the arithmetic means with standard deviations. Total cell numbers were normalized to the cell counts in IL-23/IL-2-treated samples.

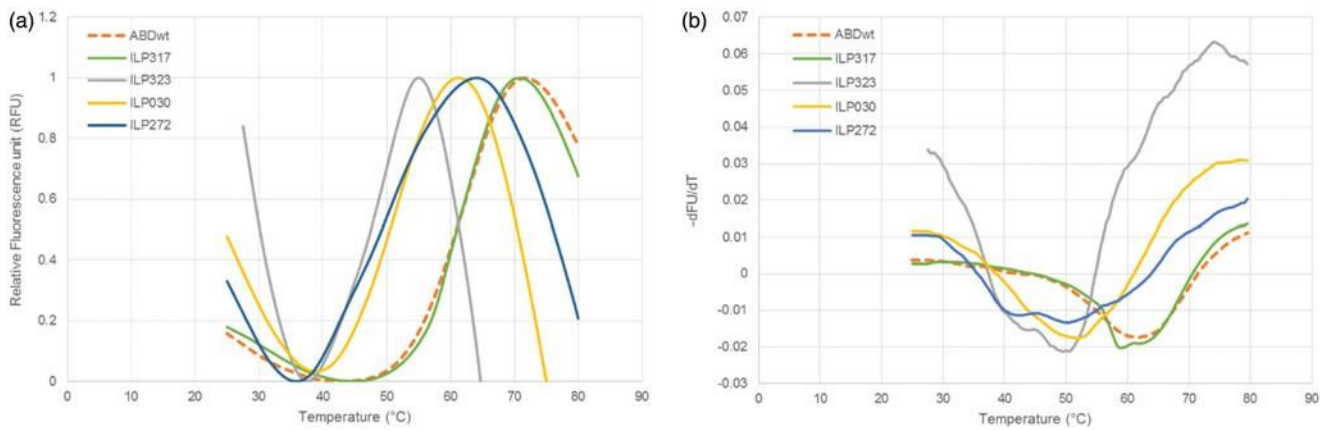

Figure 8. Analysis of thermal stability of selected ILP binders. (a) Normalized thermal melting fluorescence curves of the ILP-TolA-AVI binders and parental non-mutated ABDwt-TolA-AVI control. (b) First derivative of fluorescence versus temperature of curves is shown in the panel A. The melting point is given as the lowest point of the curve. All measurements were done in duplicate and averaged.

Currently, more than 130 protein binders derived from 20 different non-Ig scaffolds have been developed to target more than 100 proteins, including cytokines and cytokine receptors 5. Among them, IL-23-specific p19-targeted Adnectin [35] and Alphabody-derived IL-23 binders [36] were developed. Besides monoclonal antibody-based anti-IL-23 therapeutics and developed non-Ig binding proteins, a soluble form of human IL-23R has also been recently demonstrated to efficiently eliminate IL-23 function in vivo by inhibition of murine Th17 cell development, and to suppress brain inflammation in model of experimentally-induced auto-immune encephalomyelitis [37].

Three-helical bundle of the ABD scaffold has recently been convincingly demonstrated as a suitable structure model for generating of high-complex combinatorial libraries. With two quite different conceptual approaches, two groups have recently presented collections of high-affinity ABD-derived binders targeted to human cytokines, TNF-a and IFN-g [29,38]. Binders of TNF-a were selected as dual-affinity binders with the installation of desired specificity using randomization of 11 residues located in helices one and three of the ABD scaffold, thus preserving the original affinity for human serum albumin [38]. In contrast to that, our group randomized another part of the ABD surface between helices 2 and 3, where critical amino acid residues for binding to HSA are located, and selected 11 mutable residues of the ABD scaffold to engineer a novel selectivity for the targeted protein, while suppressing binding of natural HSA. We have recently introduced this model of combinatorial library in combination with efficient ribosome display selection approach by generation of binders of human IFN-g with sub-to-nanomolar range of affinity [29].

Inspired by our recent outcome describing a unique collection of REX antagonists blocking the IL-23R [27], we generated a novel set of ABD-derived binding proteins, called ILP binders, targeted to the alpha-subunit of IL-23. As a crystal structure of the IL-23/IL-23R complex remains unavailable, we built up an IL-6R-based homology model for in silico modeling of ILP-versus-p19 and p19-versus-IL23R interactions. Several ILP candidates were predicted to have a blocking potential based on the prediction of the most probable binding sites located at exposed surface of the p19 protein, ascribed to be responsible for binding to a CHR of the IL-23R, and this prediction was further confirmed by cell-competition binding assay using THP-1 cells. While majority of the ILP variants did not substantially bind to THP-1 cells, one of the tested variants called ILP215 demonstrated a strong binding to these cells, similar to binding of the best IL-23R-targeted REX115 ligand described previously [27]. As this ILP215 also strongly inhibited p19-binding to THP-1 cells (not shown), we cannot exclude that this binder represents a ‘‘dual affinity-binder’’. It is of interest that this variant also inhibited IL-23-stimulated expansion of primary human T-cells. Four blocking ILP variants do not contain any cysteine residues and variants ILP317 and ILP323 share a sequence motif of three arginine residues found in positions 32, 33, 36 and 37. Moreover, arginine residues 32 and 36 in these binders do match with those found also in the ILP215 variant and ILP030 also contains randomized arginine in residue 36, strongly suggesting that these two residues can be essential for high-affinity interactions and might also contribute to the blocking potential of all these variants. Contrary that, no substantial sequence similarity between these ILPs and another blocking variant, ILP272, could be identified.

For tests of the immunomodulatory function of the selected inhibitory ILP variants, we used long versions of the ILP binders produced in the form of the ILP-TolA fusion proteins. In our previous studies, we demonstrated that the TolA moiety of protein binders does not affect specificity nor affinity of the REX ligands and rather contributes to the improved protein stability [27]. We also demonstrated that the deletion of the TolA moiety of the REX009-TolA binder did not change the immunosuppressive function of this ligand, while a variant called DABD-TolA, harboring the TolA moiety but lacking the entire ABD domain, lost the binding properties as well as the immunosuppressive function [27]. To avoid any unintended stimulation of the lymphocytes during ex vivo experiments, we removed bacterial LPS from highly purified ILP-TolA-AVI protein samples.

Several variants of ILP binders exhibited the ability to inhibit IL-23-mediated expansion of primary human IL-17-producing CD4+ T-cells, as demonstrated on counts of purified peripheral blood T-cells cultured for three days ex vivo. The selected ILP binders were able to suppress expansion of Th17 cells around the level of control unstimulated Th17 cell population. This significant decrease in the range between 46 and 61% compared to the level of IL-23-stimulated cells was also confirmed using a statistical evaluation by ANOVA in which p values for all tested ILP variants were found to be between 0.026 and 0.001. This neutralizing potential of the ILP variants resembles features of previously generated ABD-derived REX antagonists, efficiently blocking IL-23R binding as well as Th17+ expansion of ex vivo cultured PBMCs or separated T-cells 14. In addition, in vivo immunosuppressive potential has been recently confirmed for REX125 in our separate study, using IMQ-stimulated mouse model of psoriasis where significant decrease of CD3 + RORgT + cells as well as lower secretion of IL-17 cytokine after PMA/ionomycin stimulation in splenocytes was found (Jira´skova´-Za´kostelska´, Hlavnic˘kova´ and Maly´, unpublished data).

Following our previous experiments with the REX binders, we used the original parental non-mutated ABD domain (ABDwt), in the form of the TolA fusion protein, in our ex vivo studies. However, the ABD scaffold, as a part of the larger BB domain of the streptococcal G protein, was previously described to exhibit immunogenic properties in several mouse strains [39]. Therefore, it was used not only as an affinity tag but also as a carrier to potentiate the immunogenicity for weak immunogens, and as a suitable fusion candidate for vaccine development [40]. More detailed study with the BB domain, containing three independently folded ABDs, indicated that the immunogenicity in mouse can be attributed to seven linear and one conformational B-cell epitopes, and that two of these B-cell epitopes are shared with human epitopes [41], yet their real function remains questionable. In addition, Pepscan analysis revealed presence of two murine T-cell epitopes, each of them repeated twice in the BB domain. Thus, the immunogenicity of the ABDwt scaffold can be related to the presence of these B- and T-cell

epitopes in mouse. When PBMCs from 24 healthy donors were incubated in the presence of the BB domain, 12 of them proliferated [41]. This is in correlation with our current data showing a large range of immunoreactivity of the ABDwt in samples of six human donors, further confirming our former data with a significant variability in PBMC samples of seven other human donors [27]. In addition, we confirmed ABDwt-mediated immunogenicity in balb/c mouse model of IMQ-induced psoriasis (not shown).

We conclude that our developed ILP binders, in contrast to the parental non-mutated ABD scaffold, have abolished original high-affinity binding site for HSA, due to the randomization of critical residues in positions 20, 24, 27, 29, 30, 32 and 33 located in the second helix and the adjacent loop. This leads to inevitable loss of binding affinity of the ILP binders to HSA, decreased by several orders of magnitude. Indeed, the substitution Y20A in the ABD domain was previously shown to have most influence on the HSA binding and substitutions of residues located in the vicinity of the Y20 residue, including L24A, K29A and E32A, significantly decreased the affinity of the ABD variants to HSA, while their particular combinations even amplified this effect [42]. Randomization of these critical residues also leads to damage of a human T-cell epitope (with sequence VSDYYKNLIN NAKTVE) located between residues 17–32 of the second a-helix of the ABD domain [41]. Interestingly, this T helper epitope overlaps with a B-cell epitope and HSA binding. Therefore, ABDwt-mediated immunogenicity cannot be simply attributed to the randomized ILP variants and ABDwt is not a proper control for human ex vivo nor mouse in vivo experiments. Nevertheless, further improvement of the 46-amino acid ILP-scaffold leading to minimizing possible immunogenic effects will be most likely necessary. This includes the substitution Y21H completely abolishing T helper activity as shown previously [41] as well as mutagenesis or masking of the N-terminal LAEAKVLA sequence which forms a part of another human T-cell epitope (with sequence AEDTVKSIELAEAKVLA) located in the BB domain, yet this fragment of the found T-cell epitope is believed to be nonfunctional.

In summary, we present here a novel collection of the p19-targeted IL-23 binders with an inhibitory effect on IL-23R-mediated binding and possible therapeutic potential. The ILP binders can be useful not only as unique IL-23-specific probes for epitope-mapping studies but also as important low-molecular weight and self-refolding tools for development of skin-penetrating drugs for topical treatment of psoriasis.

Acknowledgements

The authors thank Michal Maly´ and Petra Kadlc˘a´kova´ for excellent experimental assistance and Prof. Peter Sebo for helpful discussion.

Declaration of interest

The authors report no conflicts of interest.

Funding

This work was supported by the Czech Health Research Council [AZV 16-27676A]; Czech Science Foundation [grant Nos. GAP303/10/1849 to P.M. and GA15-09157S to R.O.]; Institutional Research Concepts [RVO 86652036, RVO 61388971]; European Regional Development Fund [BIOCEV CZ.1.05/1.1.00/02.0109]; Ministry of Health and University Hospital Motol [00064203]; EU [Prague project CZ.2.16/3.1.00/24022].

References

17. Cua, D. J., J. Sherlock, Y. Chen, et al. 2003. Interleukin-23 rather than interleukin-12 is the critical cytokine for autoimmune inflammation of the brain. Nature. 421: 744–748.
18. Langrish, C. L., Y. Chen, W. M. Blumenschein, et al. 2005. IL-23 drives a pathogenic T cell population that induces autoimmune inflammation. J. Exp. Med. 201: 233–240.
19. Langrish, C. L., B. S. McKenzie, N. J. Wilson, et al. 2004. IL-12 and IL-23: master regulators of innate and adaptive immunity. Immunol. Rev. 202: 96–105.
20. Oppmann, B., R. Lesley, B. Blom, et al. 2000. Novel p19 protein engages IL-12p40 to form a cytokine, IL-23, with biological activities similar as well as distinct from IL-12. Immunity. 13: 715–725.
21. Duerr, R. H., K. D. Taylor, S. R. Brant, et al. 2006. A genome-wide association study identifies IL23R as an inflammatory bowel disease gene. Science. 314: 1461–1463.
22. Beyer, B. M., R. Ingram, L. Ramanathan, et al. 2008. Crystal structures of the pro-inflammatory cytokine interleukin-23 and its complex with a high-affinity neutralizing antibody. J. Mol. Biol. 382: 942–955.
23. Kastelein, R. A., C. A. Hunter, and D. J. Cua. 2007. Discovery and biology of IL-23 and IL-27: related but functionally distinct regulators of inflammation. Annu. Rev. Immunol. 25: 221–242.
24. Parham, C., M. Chirica, J. Timans, et al. 2002. A receptor for the heterodimeric cytokine IL-23 is composed of IL-12Rbeta1 and a novel cytokine receptor subunit, IL-23R. J. Immunol. 168: 5699–5708.
25. Yao, Z., M. K. Spriggs, J. M. Derry, et al. 1997. Molecular characterization of the human interleukin (IL)-17 receptor. Cytokine. 9: 794–800.
26. Boniface, K., B. Blom, Y. J. Liu, and R. de Waal Malefyt. 2008. From interleukin-23 to T-helper 17 cells: human T-helper cell differentiation revisited. Immunol. Rev. 226: 132–146.
27. Gu, C., L. Wu, and X. Li. 2013. IL-17 family: cytokines, receptors and signaling. Cytokine. 64: 477–485.
28. Lowes, M. A., C. B. Russell, D. A. Martin, et al. 2013. The IL-23/T17 pathogenic axis in psoriasis is amplified by keratinocyte responses. Trends Immunol. 34: 174–181.
29. Mabuchi, T., T. W. Chang, S. Quinter, and S. T. Hwang. 2012. Chemokine receptors in the pathogenesis and therapy of psoriasis. J. Dermatol. Sci. 65: 4–11.
30. Song, X., and Y. Qian. 2013. The activation and regulation of IL-17 receptor mediated signaling. Cytokine. 62: 175–182.
31. Fitch, E., E. Harper, I. Skorcheva, et al. 2007. Pathophysiology of psoriasis: recent advances on IL-23 and Th17 cytokines. Curr. Rheumatol. Rep. 9: 461–467.
32. Chan, J. R., W. Blumenschein, E. Murphy, et al. 2006. IL-23 stimulates epidermal hyperplasia via TNF and IL-20R2-dependent mechanisms with implications for psoriasis pathogenesis. J. Exp. Med. 203: 2577–2587.
33. Hedrick, M. N., A. S. Lonsdorf, A. K. Shirakawa, et al. 2009. CCR6 is required for IL-23-induced psoriasis-like inflammation in mice. J. Clin. Invest. 119: 2317–2329.
34. Zheng, Y., D. M. Danilenko, P. Valdez, et al. 2007. Interleukin-22, a T(H)17 cytokine, mediates IL-23-induced dermal inflammation and acanthosis. Nature. 445: 648–651.
35. Yao, J., L. Liu, and M. Yang. 2014. Interleukin-23 receptor genetic variants contribute to susceptibility of multiple cancers. Gene. 533: 21–25.
36. Gottlieb, A. B., K. D. Cooper, T. S. McCormick, et al. 2007. A phase 1, double-blind, placebo-controlled study evaluating single subcutaneous administrations of a human interleukin-12/23 monoclonal antibody in subjects with plaque psoriasis. Curr. Med. Res. Opin. 23: 1081–1092.

33. Krueger, G. G., R. G. Langley, C. Leonardi, et al. 2007. A human interleukin-12/23 monoclonal antibody for the treatment of psoriasis. N. Engl. J. Med. 356: 580–592.
34. Toichi, E., G. Torres, T. S. McCormick, et al. 2006. An anti-IL-12p40 antibody down-regulates type 1 cytokines, chemokines, and IL-12/IL-23 in psoriasis. J. Immunol. 177: 4917–4926.
35. Leonardi, C. L., A. B. Kimball, K. A. Papp, et al. 2008. Efficacy and safety of ustekinumab, a human interleukin-12/23 monoclonal antibody, in patients with psoriasis: 76-week results from a randomised, double-blind, placebo-controlled trial (PHOENIX 1). Lancet. 371: 1665–1674.
36. Papp, K. A., R. G. Langley, M. Lebwohl, et al. 2008. Efficacy and safety of ustekinumab, a human interleukin-12/23 monoclonal antibody, in patients with psoriasis: 52-week results from a randomised, double-blind, placebo-controlled trial (PHOENIX 2). Lancet. 371: 1675–1684.
37. Garber, K. 2012. Anti-IL-17 mAbs herald new options in psoriasis. Nat. Biotechnol. 30: 475–477.
38. Kopp, T., E. Riedl, C. Bangert, et al. 2015. Clinical improvement in psoriasis with specific targeting of interleukin-23. Nature. 521: 222–226.
39. Kuchar, M., L. Vankova, H. Petrokova, et al. 2014. Human interleukin-23 receptor antagonists derived from an albumin-binding domain scaffold inhibit IL-23-dependent ex vivo expansion of IL-17-producing T-cells. Proteins. 82: 975–989.
40. Schroder, J., J. M. Moll, P. Baran, et al. 2015. Non-canonical interleukin 23 receptor complex assembly: p40 protein recruits interleukin 12 receptor beta1 via site II and induces p19/interleukin 23 receptor interaction via site III. J. Biol. Chem. 290: 359–370.
41. Ahmad, J. N., J. Li, L. Biedermannova, et al. 2012. Novel high-affinity binders of human interferon gamma derived from albumin-binding domain of protein G. Proteins: Struct. Funct. Bioinform. 80: 774–789.
42. Sali, A., and T. L. Blundell. 1993. Comparative protein modelling by satisfaction of spatial restraints. J. Mol. Biol. 234: 779–815.
43. Larkin, M. A., G. Blackshields, N. P. Brown, et al. 2007. Clustal W and clustal X version 2.0. Bioinformatics. 23: 2947–2948.
38. Kozakov, D., D. Beglov, T. Bohnuud, et al. 2013. How good is automated protein docking? Proteins. 81: 2159–2166.
39. Kozakov, D., R. Brenke, S. R. Comeau, and S. Vajda. 2006. PIPER: an FFT-based protein docking program with pairwise potentials. Proteins. 65: 392–406.
40. Skrlec, K., B. Strukelj, and A. Berlec. 2015. Non-immunoglobu-lin scaffolds: a focus on their targets. Trends Biotechnol. 33: 408–418.
41. Ramamurthy, V., S. R. Krystek, Jr., A. Bush, et al. 2012. Structures of adnectin/protein complexes reveal an expanded binding footprint. Structure. 20: 259–269.
42. Desmet, J., K. Verstraete, Y. Bloch, et al. 2014. Structural basis of IL-23 antagonism by an Alphabody protein scaffold. Nat. Commun. 5237.
43. Guo, W., C. Luo, C. Wang, et al. 2014. Suppression of human and mouse Th17 differentiation and autoimmunity by an endogenous Interleukin 23 receptor cytokine-binding homology region. Int. J. Biochem. Cell Biol. 55: 304–310.
44. Nilvebrant, J., T. Alm, S. Hober, and J. Lofblom. 2011. Engineering bispecificity into a single albumin-binding domain. PLoS One. 6: e25791.
45. Sjolander, A., P. A. Nygren, S. Stahl, et al. 1997. The serum albumin-binding region of streptococcal protein G: a bacterial fusion partner with carrier-related properties. J. Immunol. Methods. 201: 115–123.
40. Libon, C., N. Corvaia, J. F. Haeuw, et al. 1999. The serum albumin-binding region of streptococcal protein G (BB) potentiates the immunogenicity of the G130-230 RSV-A protein. Vaccine. 17: 406–414.
41. Goetsch, L., J. F. Haeuw, T. Champion, et al. 2003. Identification of B- and T-cell epitopes of BB, a carrier protein derived from the G protein of Streptococcus strain G148. Clin. Diagn. Lab. Immunol. 10: 125–132.
42. Linhult, M., H. K. Binz, M. Uhlen, and S. Hober. 2002. Mutational analysis of the interaction between albumin-binding domain from streptococcal protein G and human serum albumin. Protein Sci. 11: 206–213.